Active Brownian Dynamics

Der Fakultät für Physik und Geowissenschaften

der Universität Leipzig

eingereichte

D I S S E R T A T I O N

zur Erlangung des akademischen Grades

doctor rerum naturalium

Dr. rer. nat.,

vorgelegt

von M.Sc. Stefano Steffenoni

geboren am 09.10.1990 in Venedig, Italien.

Leipzig, den December 14, 2018

Datum der Verteidigung: May, 21 2019

Abstract

This thesis collects the results (already published and yet to publish) obtained during my PhD on the subject of classical nonequilibrium statistical mechanics. Mainly stochastic systems are considered, with special regard to applications in soft matter physics. First, we study the dynamics of two colloidal particles embedded in a environment driven far from equilibrium. Performing a systematic coarse-graining over the environment degrees of freedom, we derive the generalised Langevin description and extended fluctuation-dissipation relation. In particular we focus on an active matter environment and we derive the generalised Langevin equation for a colloid with a mean-field linear coupling to a bath of noninteracting active particles. In order to account for typical active effects, such as clustering, we include nonlinear interactions effects in the Langevin equation in the form of effective coefficients. This is done by means of perturbation theory and Brownian dynamics simulations. We show that the so-obtain effective minimal model well reproduces actual colloid statistics observed in experiments. Then, we investigate a heat engine based on an active Brownian particle confined in a parabolic potential and immersed in a thermal bath. Given that the potential is harmonic, the average energetics of the engine is determined by the second moment of the particle position. We map the model to a passive engine in a bath with a suitable time-dependent effective temperature. The performance of both the active and the passive engine including maximum efficiency, efficiency at maximum power and maximum efficiency at a fixed power thus obeys the same formal limitations. Finally, we investigate the pressure exerted by a fluid of active particles deriving the hydrodynamic equations of motion for the fluid described by underdamped Langevin equations. The contraction into the hydrodynamic description is performed by locally averaging the particle dynamics with the non-equilibrium many-particle probability density, whose formal expression is found in the physically relevant limit of high-friction through a multiple-time-scale analysis. This approach permits to identify the conditions under which self-propulsion can be subsumed into the fluid stress tensor and thus to define systematically and unambiguously the local pressure of the active fluid.

Contents

Chapter 1

Introduction

One of the most important achievements of modern physics is the atomistic hypothesis, according to which any macroscopic object has a microscopic structure, made by an enormous amount of small elements called atoms[1]. The different ways they interact constitute matter as we know it. This hypothesis encouraged physicists to study systems through particles-based theories, aiming to explain their macroscopic behaviour, but it became immediately a very challenging task. Indeed, systems made by many interacting degrees of freedom, either classic or quantum, are typically intractable in full detail. Namely, the dynamical equations that characterise them usually cannot be explicitly solved neither analytically nor computationally. But, even if a solution could be obtained, we would still not easily grasp the phenomenology at the macroscopic scale. As a matter of fact, many features of any physical system are collective, emerging phenomena from a coherent behaviour of the underlying degrees of freedom, which in principle cannot be deduced by the microscopic laws and it creates a gap between the microscopic and the macroscopic level.

As disarming this situation can be, a substantial help is given, if the degrees of freedom under survey are not too strongly correlated across well-separated scales, e.g. spatial, temporal etc. This separation implies that most of the information stored at a certain scale is superfluous to characterise the bigger scales and should not be inherited. This suggests to perform a systematic coarse-graining of the systems, such that their description relies only on certain relevant observables [1]. The physical interpretation of whom, in agreement with the (macroscopic) laws of Thermodynamics, is then provided by Statistical Mechanics, responsible for bridging the gap. Indeed, it gives the recipe for the coarse-graining performed through the elimination of a large subset of the whole degrees of freedom. The latter are discerned according to well-apart dynamical features, e.g. characteristic times, which classify the entire set into fast and slow subsets. In this direction, probably the most famous example is Brownian Motion, regarding a particle embedded in a fluid made by countless molecules, which is small enough to jiggle perceptibly, but large enough to be visible

---

[1]We neglect here and through all the thesis their subdivision into quarks and so on.

in the microscope[2]. We are not interested in the individual interaction between the fluid molecules and the Brownian particle (BP). Indeed each collision has a negligible effect, but only the superposition of many small interactions produces an observable effect. Assuming the BP weakly-coupled and much bigger than the fluid molecules, a time-scale separation naturally emerges such that the fluid can be treated as a homogeneous thermal environment with infinite heat capacity and a fast relaxation time compared to the BP. This allows to replace the microscopic coupling with a hydrodynamic one. It is conveniently decomposed into a random and a friction term accounting for the random aspects of the collisions and their systematic part, respectively. This leads, for the BP alone, to an effective description, belonging to a scale intermediate between the micro and macro and thus called mesoscopic [2]. The distinction between the macroscopic, mesoscopic and microscopic levels is not unambiguous. It is common to make the following distinction: the macroscopic level is described using deterministic, irreversible laws like hydrodynamics. For the mesoscopic level, thermal noise plays a major role and stochastic models are used. The microscopic level refers to any underlying deterministic and reversible description, i.e. atomistic Hamiltonian dynamics.

The explicit derivation of the mesoscopic equations relies on the solution of the eliminated microscopic degrees of freedom and typically it is as difficult as the solution of the entire system. Remarkably, this derivation is unnecessary for systems in thermodynamic equilibrium, i.e. without any macroscopic current (of mass, energy etc.), through the employ of equilibrium statistical mechanics [3, 4]. The latter recurs to minimal assumptions, namely, the micro-states of constant energy are equally probable and the existence at the macroscopic level of thermodynamic potentials, whose minimisation characterises univocally the system features, thus addressing the coarse-graining towards a reliable physical interpretation. For Brownian Motion, the coarse-graining is steered by equilibrium principles from classical statistical mechanics and kinetic theory, e.g. the Gibbs distribution and the equipartition theorem, to a clear physical interpretation for the obtained effective equation, e.g. the fluctuation-dissipation theorem we will introduce in Sec. 2.1.

On the contrary, for nonequilibrium systems, i.e. those traversed by macroscopic currents, a unifying theoretical framework is still to be established, since thermodynamic potentials do not admit straightforward extension to nonequilibrium. Such accomplishment is likely to have far reaching impacts, as nonequilibrium conditions are ubiquitous in Nature, much more than equilibrium's. Nonequilibrium statistical mechanics is still a wide open field, but despite the disarming complexity, general results have been obtained that are valid far-from-equilibrium. To name a few, fluctuation theorems [5–7], Jarzinsky relation [8], and stochastic entropy production related to fluctuations of heat, work [9, 10]. Some assumptions adopted for equilibrium systems are no longer applicable. Therefore, coarse-graining must start from first principles and be explicitly carried out. To bypass it, approaches independent

---

[2]Any quantum effect is therefore neglected.

of the equilibrium constraints must be developed and employed. An example is the large deviation theory [11, 12], which gives insight about fluctuations regardless of the magnitude of the nonequilibrium source. Remarkably, the general framework for dealing with Brownian Motion by elimination of "fast" degrees of freedom is independent of equilibrium constraints. Nevertheless, while the mathematical derivation is the same, the physical interpretation of the coarse-grained equation must be carefully carried out. Assuming that the nonequilibrium source is affecting only the BP and not the thermal environment, the extension is physically reliable and not limited to close-to-equilibrium systems. Nevertheless, the symmetries that characterise Brownian Motion at equilibrium are not satisfied a priori, but depend on the nature of the eliminated degrees of freedom. Examples recurring in the thesis are driven and active matter. Both are characterised by the presence of a nonequilibrium source, responsible for a continuous production of entropy and thus for time reversal symmetry [13]. While, in the former this source is "external" and impose coherent shear flows on the whole system particles, in the latter it comes from hidden degrees of freedom and acts at the level of the individual particle[3].

The thesis aims to give a contribution in this direction and it is structured as follows. In Chapter 2 we introduce more precisely Brownian Motion through two equivalent formalisms: the Langevin and the Fokker-Planck equations for a generic many-body system and, especially, for active particles. Later in the same Chapter we present some other important tools based on those equations and to be employed in the following, namely path integral formulation and linear response theory. In Chapter 3 we set up a theory for interacting Brownian particles embedded in a nonequilibrium environment, starting from the microscopic interacting many-body theory. Using nonequilibrium linear response theory, we perform a coarse-graining and we characterise the effective dynamical interactions at the colloid scale and the statistics of the nonequilibrium environmental noise, arising upon integrating out the fast degrees of freedom. As hallmarks of nonequilibrium, the breakdown of the fluctuation-dissipation and action-reaction relations for Brownian degrees of freedom is exemplified with two prototypical models for the environment, namely Brownian particles driven by an external vortex and stirred colloids [15, 16]. In Chapter 4 we focus on a specific nonequilibrium environment, i.e. a fluid of active particles. The colloid is described by a Newton equation, while the active particles by a set of overdamped Langevin equations. If their coupling to the colloid is linear, the elimination of fast degrees of freedom can be analytically done and leads to a non-Markovian underdamped Langevin equation for the colloid alone. The latter is in the overdamped and Markovian limit formally equivalent to the equation employed to model the active particles. In other words, under those approximations, the colloid behaves like an active particle itself. We investigated the contribution of non-linearities both analytically and with simulations. First we introduce a small non-linear force in the

---

[3]For more details about the differences between active and driven matter see the remarkable review by Menzel [14].

linear equation and we calculate the first correction to the variance in the framework of the perturbation theory. Then, to confirm the analytical prediction, we simulate the entire dynamics of the colloid coupled to the active particles investigating the variance and the displacement distribution of the colloid [17]. In Chapter 5, we start from the linear model and, introducing time-dependent parameters, we induce a periodic dynamics on the colloid, to be treated as a Stirling cycle affected by thermal and non-thermal fluctuations, thus describable within the Stochastic Thermodynamics framework. We investigate the characteristics of its, work, heat and efficiency, in comparison with the same cycle run with a colloid embedded in an equilibrium environment. In particular we established a mapping to the equilibrium result provided that an active effective temperature is defined [18]. We investigate the cycle both in the quasi-static limit, which allows for an exact analytic solution, and in the finite-time regime. The latter has been studied both via simulation of Brownian dynamics and numerical solution of the Fokker-Planck equation employing the method presented in [19]. In Chapter 6, we derive the hydrodynamic equations of motion for a fluid of active particles described by underdamped Langevin equations that reduce to the active Brownian particle model, in the overdamped limit. The contraction into the hydrodynamic description is performed by locally averaging the particle dynamics with the nonequilibrium many-particle probability density, whose formal expression is found in the physically relevant limit of high friction through a multiple-time-scale analysis. This approach permits us to identify the conditions under which self-propulsion can be subsumed into the fluid stress tensor and thus to define systematically and unambiguously the local pressure of the active fluid [20], subject previously highly debated in the community [21–24]. In particular we discuss our result within the dilute limit for the fluid, in which the introduced observables have a simpler and more intuitive form.

Chapter 2

Preliminary material

2.1   Langevin equation

Consider a sphere immersed in a tube filled with water. As long as the sphere is macroscopic, its dynamics is perfectly described by classical mechanics, predictable at later times given the initial conditions. The water, assuming an equilibrium coarse-graining over its microscopic degrees of freedom (molecules), is described as a uniform and inert continuum, such that any interactions with the sphere can be modelled with macroscopic forces, e.g. gravity and friction. If we reduce the radius to the order of micrometers, the motion becomes unpredictable and erratic. This was the surprising conclusion of Robert Brown in 1827 from observation of small pollen grains suspended in water, later called Brownian particles (BPs). The source of this motion was not attributed to some features of the pollen, rather to the water, to be treated as a never-resting environment made by a huge number of fluctuating, upsetting the inert medium obtained via the previous coarse-graining at this scale. For long time, the surprising observation by Robert Brown was left without a mathematical explanation. The first detailed explanation of Brownian Motion had to wait almost eighty years for Einstein [25], to provide the link between the theory of heat and the statistical motion of particles in suspensions, thereby relating diffusion and osmotic pressure, in a way not expected from equilibrium thermodynamics. This work was a breakthrough showing the limit of classical macroscopic theories when dealing with smaller and smaller systems and providing an atomistic link between previously (seemingly) unrelated macroscopic notions. Few years before, another formulation of Brownian Motion aiming to model the stocks market behaviour was accomplished by Louis Bachelier [26], but for long time ignored by the physics community. Extensive systematic tests of the new theory of Brownian Motion were conducted by Jean Perrin in 1909 [27], which confirmed the prediction by Einstein, crowning him as founder of the theory of Brownian Motion and established the foundation of the atomic theory of matter. The first modern mathematical formulation of Brownian Motion is attributed to Paul Langevin [28] (although a more complete and rigorous formulation has been done by Ornstein [29, 30]), in 1908, wrote down

an equation for the BP, named after him, based on two assumptions: weak-coupling and big mass difference between the BP and the fluid molecules. If the BP is much heavier a time-scale separation between the two dynamics naturally appears implying that the water molecules can be regarded as fast degrees of freedom with respect to the BP [31]. The former are assumed to be much more numerous and cumulatively massive than the latter, so to be treated in a coarse-grained description, as a homogeneous thermal environment for the BP, with instantaneous relaxation time and infinite heat capacity characterised by a temperature T and a viscosity η. The environment-BP coupling, no longer negligible at this scale, is assumed weak so to be treated as a small perturbation to the fast degrees of freedom in the framework of the linear response theory. The response function is by definition a coarse-grained observable averaged over the fast degrees of freedom. Accordingly, the coupling with the BP can be written as the sum of two separate forces: the random force or noise, $\xi(t)$, which through random kicks due to the countless collisions with the fluid particles, pumps energy into the system and the friction [32], that extracts excess energy from the system and it gives back to the environment producing the never-resting motion of the BP. Thus, the Langevin equation for a free BP with mass M and radius R in one dimension[1] reads

$$M\dot{v}(t) = -\gamma v(t) + \xi(t) \tag{2.1}$$

with γ the friction coefficient. For an isolated sphere $\gamma \equiv 6\pi\eta R$. The noise is a random variable and it is formally (although not mathematically rigorously[2]) defined as

$$\xi(t) = \lim_{dt\to 0} \frac{dW(t)}{dt}, \tag{2.2}$$

with $W(t)$ a Wiener process. Therefore, ξ is a Gaussian variable, completely characterised by its first two moments:

$$\langle \xi(t) \rangle = 0, \, \forall \, t \in \mathbb{R} \qquad \langle \xi(t)\xi(t') \rangle = \Lambda \, \delta(t - t'), \quad \Lambda = 2\gamma k_{\mathrm{B}} T \tag{2.3}$$

with k_B the Boltzmann constant, as stated by the equipartition theorem and consistent with the equilibrium canonical ensemble distribution [35]. A noise with such properties is called Markovian, or memoryless. The noise as a Gaussian variable can be physically understood as the result of the employ of the central limit theorem in the limit of infinite number of fast degrees of freedom and, thus, infinite collisions with the BP. The systematic friction, in the framework of linear response theory, is proportional to the velocity and it describes the natural deceleration a macroscopic

---

[1]for the sake of simplicity. The extension to more dimensions is straightforward.

[2]The white noise in the Langevin equation (2.1) is thus defined as a gaussian random variable with zero mean and infinite variance. Nevertheless, it is widely used keeping in mind it is ill-defined. A discussion of this issue is beyond our scope, so we address the interested reader to [33, 34]

system is subjected to when it is moving in a fluid. Absent in the initial microscopic equation it emerges from the coarse-graining. The dynamics of the BP is now given by a Markovian stochastic differential equation characterised by a random term responsible for the diffusion and a deterministic one, from the underlying Newton equation, responsible for the advection (in (2.1) there is only the friction but any force can be similarly included).

Given the simple properties of the noise, (2.1) can easily be solved providing for the (average) moments of velocity and position, both during the initial transient and in the steady state. Note that the average values are defined from an ensemble of realisation of the stochastic process along a time interval $[0, t]$, called trajectories. Regardless of the initial conditions, the first moment of position and velocity in the steady state is zero, due to the relaxation of the BP in the environment. The velocity second moment in the steady state $\langle v^2 \rangle = k_{\mathrm{B}}T/M$ in agreement with the equipartition theorem, while for position $\langle x^2 \rangle /t = 2k_{\mathrm{B}}T/\gamma$. Namely, the mean square position for a free BP does not grow quadratically as for a ballistic Newtonian system, but linearly. Due to the collisions with the solvent molecule the dynamics is in the long time limit diffusive, ruled by the diffusion coefficient, defined here as $D \equiv \int_0^\infty \langle v(t)v(0) \rangle \, dt = k_{\mathrm{B}}T/\gamma$. D gives the magnitude of the system fluctuations and is related to friction and temperature via the Einstein-Smoluchowski relation, also known as fluctuation-dissipation theorem (FDT) [36], where the diffusion provides for the fluctuation and the friction for the dissipation. Equilibrium at this level is no longer associated to a static condition, rather to a dynamical balance of noise and friction ruled by one parameter: the temperature T of the fluid. This result is not to be taken for granted, indeed it is valid only for equilibrium classical systems[3]. In the following we discuss the extension to nonequilibrium systems.

In many physical situation the system is embedded in a highly viscous environment. This means that the friction γ is very big. If on top of that the mass of the system is very small, one enters the overdamped region, in which the system after each random kick relaxes quickly (on the time scale M/γ) to the average velocity, determined by the equipartition theorem. Therefore inertia can be neglected leading to the overdamped version of (2.1),

$$\dot{x}(t) = \xi(t), \qquad \langle \xi(t)\xi(t') \rangle = 2\mu k_{\mathrm{B}}T \, \delta(t - t') = 2D \, \delta(t - t') \qquad (2.4)$$

where $\mu \equiv \gamma^{-1}$ is the mobility. The velocity $\dot{x}(t)$ is now discontinuous in time, as the noise itself. Indeed overdamped trajectories appear less smooth than underdamped ones. (2.1) and (2.4) accounts for the simplest Brownian motion, namely free BPs in homogeneous environment, but an external force can be included in the deterministic part of the Langevin equation without changing the properties of the stochastic one [37]. Non-homogeneities, e.g. space dependent friction, can also be treated, provided that the noise is no longer additive (with respect to the process), but

---

[3]For quantum systems, i.e. the harmonic oscillator, the energy levels are parameterising by the frequency and not just by a univocal temperature.

multiplicative [38], whose intensity depends on the process itself. This introduces a formal complexity concerning the time at which the pre-factor of the noise must be evaluated, called the Itô/Stratonovitch dilemma [1, 39]. It states that before we choose the time the pre-factor of the noise is evaluated at, the associated Langevin equation is meaningless and cannot be even called an equation, but a mere string of symbols [40]. If we discretise the Langevin (2.4) equation with multiplicative noise represented by the process-dependent pre-factor $\alpha(x)$ in intervals with small width dt as $[t, t + dt]$,

$$x(t + dt) = x(t) + \int_t^{t+dt} \alpha(x(t'))\xi(t')dt' \tag{2.5}$$

For any small dt the noise can be represented as a sequence of delta peaks arriving at random times (for the sake of clarity this representation is general and so valid for additive noise too). Each delta function in ξ produces a jump in the process. Therefore the value of the process at the time the delta peaks arrive is undetermined and so the value of the pre-factor. In the equation it is not specified which value should be inserted. The choice is ruled by the introduction of a well-accepted convention. The Langevin equation is interpreted a là Itô, if the pre-factor is evaluated before the arrival of the delta peaks,

$$x(t + dt) = x(t) + \alpha(x(t)) \int_t^{t+dt} \xi(t')dt' \tag{2.6}$$

and a là Stratonovitch if the value of the pre-factor is the average of the values before and after the delta peak (defined as half the sum of the values before and after the jump),

$$x(t + dt) = x(t) + \alpha \left(\frac{x(t) + x(t + dt)}{2} \right) \int_t^{t+dt} \xi(t')dt', \tag{2.7}$$

although other infinite choices are well-defined too. A detailed discussion of this technical aspect is beyond the purpose of this thesis. We conclude stressing that it has many consequences, among which the fact that the simple neglect of inertia does not lead to the correct overdamped limit, but more sophisticated technique must be pursed [41–43]. Indeed a process-dependent pre-factor produces in the overdamped limit extra advective terms, which are typically different if interpreted a là Itô or a là Stratonovitch [44]. Typically mathematicians and economists use Itô convention, while physicists prefer Stratonovitch. The reason is twofold: Stratonovitch allows to use ordinary calculus and the trajectories under this convention are exactly the same if run backward, since the middle point of the interval discretisation is not changing.

2.2   Fokker-Planck equation

Let us now change point of view, and consider the system rather than from the point of view of individual trajectories with particular noise realisations, as a 'probability

cloud' evolving in space [45]. The equation describing the evolution of probability $\rho = \rho(x, v, t)$ in time is called Fokker-Planck equation (FPE) and for the Langevin equation (2.1) subjected to the external potential $U = U(x)$, is:

$$\frac{\partial \rho}{\partial t} + v \frac{\partial \rho}{\partial x} - \frac{1}{M} \frac{\partial U}{\partial x} \frac{\partial \rho}{\partial v} = \gamma \frac{\partial}{\partial v} \left(v\rho + \frac{k_B T}{M} \frac{\partial \rho}{\partial v} \right) \tag{2.8}$$

Its physical interpretation is glaring: on the left hand side there is the Liouville equation for the colloid, while on the right hand side the coupling with the environment providing for noise (diffusion) and friction. The FPE is a linear equation for the probability, i.e. $\partial_t \rho = \mathcal{L}^+ \rho$ with the forward generator

$$\mathcal{L}^+ = -v \frac{\partial}{\partial x} + \frac{1}{M} \frac{\partial U}{\partial x} \frac{\partial}{\partial v} + \gamma \frac{\partial}{\partial v} v + \frac{\gamma k_B T}{M} \frac{\partial^2}{\partial v^2}, \tag{2.9}$$

and assures probability conservation since it can be written as a continuity equation, i.e. $\partial_t \rho + \nabla \cdot J = 0$, with $J = J(x, v)$ the probability current and $\nabla = (\partial_x, \partial_v)$. If the force, $-\partial_x U(x)$, is time-independent, we assume that there is a stationary distribution ρ_s, (which solves the FPE with zero left-hand side, i.e. $\mathcal{L}^+ \rho_s = 0$). The conservative-force FPE is one of the few cases in which (2.8) can be analytically solved [46]. The solution, in agreement with the canonical ensemble, is the Maxwell-Boltzmann distribution

$$\rho_s(x, v) = \frac{1}{Z} e^{-\beta \left(U(x) + \frac{mv^2}{2} \right)} \tag{2.10}$$

where Z is the usual partition function [4] and $\beta = (k_B T)^{-1}$. Due to its linear structure the solution of the FPE is equivalent to an eigenvalue problem for the operator $\mathcal{L}^+$. Indeed ρ_s is the eigenfunction associated to eigenvalue 0. This observation connects the FPE to quantum mechanics and the Schrödinger equation for which the Hamiltonian plays the role of the forward generator [47]. The main difference is that, unlike the Hamiltonian of closed quantum systems, the generator of the FPE is not always self-adjoint or hermitian, a property deeply related to whether we are dealing with an equilibrium or nonequilibrium process. This means, in practice, that we have to be careful when diagonalising matrices or operators and dealing, in general, with eigenvectors or eigenfunctions: if the spectrum is real it is possible to symmetrise the operator $\mathcal{L}^+$ through a unitary transformation. In the overdamped limit the FPE, or Smoluchowski equation, for the density $\rho = \rho(x, t)$ is

$$\frac{\partial \rho}{\partial t} = -\frac{\partial}{\partial x} \left(\mu \frac{\partial U(x)}{\partial x} \rho - D \frac{\partial \rho}{\partial x} \right) \tag{2.11}$$

This can indeed be intuitively understood, if the friction is high, the velocity relaxes after a short time γ^{-1}, and the evolution on larger time scales is only determined by the spatial distribution. Eq. (2.15) can be directly derived from (2.8) with a systematic expansion in powers of γ^{-1}, assumed to be small. This approach is thus

called multiple-time-scale theory [1,42], since the overdamped density is obtained by comparing the FPE terms (2.8) at different orders of γ^{-1}, to whom different time scales are associated. We are going to use this approach in Chapter 6 and more details can be found in Appendix C.1. The steady solution of (2.15) is obtained imposing,

$$J = 0 \quad \iff \quad \mu \frac{\partial U(x)}{\partial x} \rho_s = D \frac{\partial \rho_s}{\partial x} \tag{2.12}$$

and it is the Maxwell-Boltzmann distribution for the position alone if $\mu = \beta D$ according to the Einstein-Smoluchowski relation. Interestingly (2.12) is called detailed balance and it is a necessary and sufficient condition for equilibrium. The absence of current from the balance of two forces, advection and diffusion, guarantees the validity of time reversal symmetry and therefore thermodynamic equilibrium. An equivalent condition appears in the framework of the Markov chains [48].

In conclusion we stress that the FPE and Langevin equations are two faces of the same medal. A similar role is played in quantum mechanics by the Schrödinger and the Heisenberg equation for the probability and for the observable respectively. Nonetheless, while deriving the Langevin from the FPE is usually straightforward (some complications can come out for multiplicative noise due to the choice of the convention Itô/Stratonovitch), the other direction is not and it leads to closure problem both for additive [49] and multiplicative noise [50].

2.3 Nonequilibrium

Nonequilibrium and irreversibility are the rule in Nature while equilibrium is the exception [51]. From the terrestrial magnetic field to the extraction of energy from ATP-molecules, basis of each living being, natural phenomena are controlled by currents at every length scale. Despite of the lack of a universal theory for nonequilibrium, some common features allow to introduce a classification of nonequilibrium phenomena into three categories[4]. The first deals with nonequilibrium as a relaxation process to equilibrium. Examples are the diffusion and the Fick equations, that describe how a macroscopic system, provided with inhomogeneous initial conditions, e.g. of density, converges to a homogeneous and stable configuration. For microscopic systems the canonical example is the Boltzmann equation. If the inhomogeneity is provided by an external source which continuously produces entropy, the system cannot reach equilibrium. If conveniently manoeuvred, e.g. external temperature or chemical potential gradient, the dynamics converges to a time-independent regime, i.e. the nonequilibrium steady state. This second category is visibly wider than the first. Different forces induce different nonequilibrium phenomena, that share similar properties as long as the external force is not acting the environment the system is

---

[4]From "What is (non)equilibrium, static and dynamical aspects, and their problems." Christian Maes. 2018 Leuven Summer school on nonequilibrium physics.

embedded in. If the environment itself is driven out of equilibrium the third category is involved, for which there is entropy production associated to the system, to the environment (to keep it out of equilibrium) and to the mutual interaction. None of the results known from equilibrium can be a priori relied on. The disarming complexity of this category is indeed rewarded, since this category is by far the most vast and interesting. Adopting some approximations, unfortunately not valid for every system, many interesting problems can be investigated.

Now we provide a more rigorous characterisation of nonequilibrium through the tools we just introduced. The Langevin equation describes an equilibrium system, with probability distribution given by the usual canonical weight [4] as long as the deterministic force is conservative or the (multiplicative) noise is not effecting the temperature of the environment. Otherwise, a nonequilibrium state is induced by a continuous production of entropy which breaks the time-reversal symmetry and, equivalently the detailed balance (2.12). Due to the presence of dissipation and currents in the systems, neither the Maxwell-Boltzmann distribution is the steady solution, nor FDT as the relation between diffusion and friction is satisfied. Nonetheless, we can still treat the environment as a fast degree of freedom and reduce its effect to a Gaussian noise if the nonequilibrium condition imposed on the system does not directly affect the environment [52], which is assumed to be at equilibrium at each time. Namely, since assumed big and weakly coupled to the system, it is not influenced by any energy exchange with the system. This condition is called local detailed balance [53, 54], weaker than detailed balance, and formally restores FDT guaranteeing the validity of Einstein-Smoluchowski relation for diffusion and mobility, but here comes the subtlety. The mobility involved in the Einstein-Smoluchowski relation is not equal to the susceptibility under an applied external field [55,56]. And $\mu = \beta D$ must be thought as a generalised Einstein-Smoluchowski relation. We will come back to it in Sec. 2.6. The name local detailed balance derives from nonequilibrium thermodynamics according to which a nonequilibrium system can be thought as coupled to many reservoirs locally at equilibrium at certain conditions of temperature, chemical potential, pressure [57]. The reservoirs only interact with the system, not with each other and the system is allowed to interact only with one reservoir at a time, such that the entropy production can be easily defined for each time. Reservoirs with different features induce currents and forces on the system keeping it out of equilibrium. Similarly, in the Langevin equation framework, external forces are added to the advective part of the equation.

Currents make the solution of the FPE much more complicate. There are very few systems it can be solved for. One of them is the one-dimensional diffusion on a circle with periodic boundary condition, introduced as an example in Sec. 3. For a nonequilibrium system the FPE is still linear for the probability and thus can still be related to an eigenvalue problem, but the problems come at the first attempt to solve it. Namely, for an equilibrium system the eigenvalue are by definition all real and negative according to the Perron-Frobenius theorem [45], while for a nonequilibrium system they can be complex as well. If the spectrum is complex there is no unitary

map that allows to map the operator $\mathcal{L}^+$ to a hermitian one, making necessary the calculation of both left and right $\mathcal{L}^+$-eigenvalues to characterise its spectrum.

2.4 Active particles

In the introduction we mentioned two examples of nonequilibrium systems, driven and active matter. In this section we focus on the latter discussing more features of it and providing a simple modelisation. The word "active" derives from the ability, peculiarity of certain systems, to convert internal energy, e.g. chemical, into persistent motion. This supply of energy, at the level of the individual particle, breaks the conservation of kinetic and potential energy and the time-reversal symmetry since entropy is continuously produced. Due to this self-propulsion mechanism, the interaction with each others and with the medium they live in is no longer elastic and then in general not instantaneous, as commonly assumed by equilibrium kinetic theory. Those features lead to collective behaviours absent in equilibrium, like wall accumulation proportional to the local spatial curvature [58–60] and spontaneous phase separation due to clustering formation [61,62] without attractive interaction[5]. Those are only few of the surprising results observed for active particles, to name few others: active particles are ratchet systems since, provided the spatial asymmetry, they can spontaneously create non-homogeneous density profile and currents [65], they can exhibit repulsive as well as attractive depletion interaction between two obstacles, e.g. walls [66], two bigger passive particles [67]. Many other examples can be found in these remarkable reviews [68–70].

In Nature there are many examples of active particles systems at every length scale, from flock of birds and school of fishes [71,72], to bacteria [73] and sperm cells [74]. As for equilibrium, the smaller the system the more important the thermal fluctuations of the environment surrounding the active particles becomes. Therefore, the dynamics is the interplay of standard diffusion and persistent self-propulsion exhibiting a crossover from diffusive short-time motion to super-diffusive motion at intermediate times and again to (enhanced) diffusion in the long time limit [75]. Provided that the self-propulsion is not affecting the solvent's thermal fluctuations, an active particle can be treated as a BP described by a Langevin equation like (2.4), equipped with an extra term accounting for the activity. In the simplest model, called active Brownian particle (ABP), the term is a force assumed to have constant magnitude and stochastic direction, due to the collisions with the solvent particles that tend to randomise the direction of propulsion. In two dimensions[6] the Langevin equation

---

[5]Noteworthy equilibrium hard spheres exhibit entropy-driven phase transition without attraction [63,64] as well, but it is constrained to excluded volume interaction such that the internal energy is not depending on the density. Active particles con create clusters with any repulsive potential.

[6]Extension to three dimensions involves many technical aspects, not relevant for the characterisation, see e.g. [76].

reads

$$\dot{\mathbf{x}} = \mu F^{\mathrm{a}}\,\mathbf{n}(\theta) + \sqrt{2\mu T}\boldsymbol{\xi}, \qquad \dot{\theta} = \sqrt{2D_{\mathrm{r}}}\eta. \tag{2.13}$$

where F^{a} is the active force, often expressed through the velocity $v_0 \equiv \mu F^{\mathrm{a}}$, $\mathbf{n}^T(\theta) = (\cos(\theta), \sin(\theta))$ is the direction of propulsion which evolves with an ordinary Brownian Motion whose intensity is ruled by the rotational diffusion coefficient D_{r}. Its inverse is the characteristic time the particle need to lose memory of its initial orientation and $v_0 D_{\mathrm{r}}^{-1}$ is the persistence length, similarly defined for the worm-like-chain in polymer physics. Note that from now on $k_{\mathrm{B}} = 1$. An explicit solution of (2.13) shows that activity not only introduces memory into the dynamics, namely $\langle \dot{\mathbf{x}}(t)\dot{\mathbf{x}}(s)\rangle$ is no longer delta-correlated due to $\langle \mathbf{n}(t)\mathbf{n}(0)\rangle = 0.5 \exp\left(-D_{\mathrm{r}}t\right)$, but non-Gaussian fluctuations as well[7]. It is confirmed by a negative kurtosis of the displacement distribution [77], which exhibits a broadened peak and steep tails on the time scales in which activity dominates entailing super-diffusive dynamics, while converges to a Gaussian in the long-time limit. Increasing the activity, non-Gaussian deviations become even more evident due to the formation of two well-separated peaks whose distance is ruled by the persistence length, meaning that, if we consider the distribution as a result of many independent particles displacement only few of them stay close to their initial position. For the sake of completeness we introduce a simplified version of the ABP model, although not used in the thesis, that considers the active velocity as a variable, but neglects any non-Gaussian fluctuation [78],

$$\dot{\mathbf{x}} = \mathbf{v} + \sqrt{2\mu T}\boldsymbol{\xi}, \qquad \dot{\mathbf{v}} = -D_{\mathrm{r}}\mathbf{v} + v_0\sqrt{D_{\mathrm{r}}}\boldsymbol{\eta}. \tag{2.14}$$

Using the nomenclature introduced in [79], both models describe "dry" active matter, in contrast with "wet" models, in which the momentum exchanged among the active particles and their solvent is taken more seriously. Another model frequently used for active particles is called run and tumble [80]. The dynamics, consisting of periods of straight-line swimming whose duration is Poisson distributed interrupted by brief bursts of rotational motion, exhibits discrete angular relaxation differently from ABP for which is continuum [81]. The FPE associated to (2.13) for the density $\rho = \rho(\mathbf{x}, \theta, t)$ involves two diffusion terms,

$$\frac{\partial \rho}{\partial t} = -\left(v_0\mathbf{n}(\theta)\cdot\frac{\partial}{\partial \mathbf{x}} - D\frac{\partial^2}{\partial x^2} - D_{\mathrm{r}}\frac{\partial^2}{\partial \theta^2}\right)\rho \tag{2.15}$$

Eq. (2.15) is analytically unsolvable even in the steady state since the variable $(\mathbf{x}, \theta)$ cannot be easily separated. Some approximated solution can be found in the literature for the steady state under the assumption $\rho_s(\mathbf{x}, \theta) = \rho_s^x(\mathbf{x})\rho_s^\theta(\theta)$, namely through

---

[7]The exponential decay for the angular decorrelation is responsible for the violation of detailed balance since different from the time scale over which position decorrelates. The latter becomes self-evident if we write the process $\dot{x}$ as a convolution, $\dot{x}(t) = \int_{-\infty}^{t} dt'\, \delta\left(t - t'\right)\dot{x}(t')$, with a memory-less kernel, given by a δ-function. Remarkably, if the position presents a finite time decay, comparable with D_{r}, detailed balance must be valid, see e.g. non-spherical brownian particles.

Mathieu functions [82] and from (2.14) subjected to a generic external potential but with $\boldsymbol{\xi} = 0$ through an expansion in powers on v_0 reliable for small activity [83]. Nonetheless their simplicity (2.13) and (2.14) are able to predict all the mentioned features of active particles dynamics, therefore have been used to investigate many open problems.

2.5 Path integral derivation

In the Langevin framework average values are over an ensemble of trajectories, i.e. realisations of the stochastic process. Therefore it is natural to wonder what is the probability of a single trajectory and if there are some trajectories that are more probable than others. The Path integral theory gives an answer to that, firstly formulated by Wiener for classical stochastic process [84] and later applied to quantum electrodynamics by Richard Feynman [85]. Since then, the applications and the developments have been uncountable and a report of them would be beyond our purpose, but can be found in the remarkable review [86]. The standard way to derive the path integral is to discretise the trajectories $\omega = \{x_s \colon 0 \leq s \leq t\}$ of the stochastic process x_t in a finite number of steps of length dt and then to calculate the probability of crossing all the steps at the particular time given the initial state x_0. For simplicity we use a one-dimensional notation, but the extension is straightforward. Namely,

$$\mathcal{P}(\omega) = \lim_{n \to \infty,\, dt \to 0} \mathcal{P}\left(x_1, t_1; \ldots; x_n, t_n | x_0, t_0\right). \tag{2.16}$$

The probability is expressed as evolution of the noise through a change of variable,

$$\mathcal{P}\left(x_1, t_1; \ldots; x_n, t_n | x_0, t_0\right) = \mathcal{P}\left(\xi_1, \xi_2, \ldots \xi_n\right) \cdot \det J, \qquad J = \frac{\partial \xi}{\partial x} \tag{2.17}$$

with J the Jacobian. Here ξ is treated as function of the process x as established by the Langevin equation. For the derivation we will refer to the overdamped Langevin equation $\dot{x} = \mu F(x) + \sqrt{2D}\,\xi$ where F is a generic force, non-conservative too and D is diffusion coefficient. Here we consider white and additive noise, but extension to non-Markovian or multiplicative noise can be found in [87–91]. If we assume that the process is Markovian, (2.17) becomes the product of the probabilities of each single discrete transition. Namely

$$\mathcal{P}\left(x_1, t_1; \ldots; x_n, t_n | x_0, t_0\right) = \prod_{i=1}^{n} \mathcal{P}\left(\xi_i \mid \xi_{i-1}\right) \det J \tag{2.18}$$

Since the noise is Gaussian, the propagator of the noise is

$$\mathcal{P}\left(\xi_i \mid \xi_{i-1}\right) = \frac{1}{\sqrt{2\pi dt}} e^{-\frac{dt}{2}\xi_i^2}, \quad \xi_i = \frac{(x_i - x_{i-1})/dt - \mu F(x_i)}{\sqrt{2D}} \tag{2.19}$$

Although the noise is additive, for $F(x_i)$ we have to choose either Itô or Stratonovitch as convention. The final result is, unless multiplicative noise is considered, the same, but the derivation must be consistent. We choose Stratonovitch. If we plug (2.19) into (2.18) and we take the limit $n \to \infty, dt \to 0$ we obtain the path integral (2.16),

$$\mathcal{P}(\omega) \propto e^{-\mathcal{A}(\omega)}, \quad \mathcal{A}(\omega) = \frac{1}{4D} \int_0^t ds \; (\dot{x}_s - \mu F(x_s))^2 + \frac{\mu}{2} \int_0^t ds \; F'(x_s) \qquad (2.20)$$

where $\mathcal{A}(\omega)$ is the action, also called Onsager-Machlup functional [92]. The last term is given by the Jacobian of the change of variable in the Stratonovitch convention. Note that in general the action has not a well-defined parity with respect to time reversal, therefore it is common to decompose it into a time-symmetric and a time-antisymmetric part [93], i.e. $\mathcal{A} = (\mathcal{T} - \mathcal{S})/2$ with:

$$\mathcal{T}(\omega) = \mathcal{A}(\theta\omega) + \mathcal{A}(\omega), \quad \mathcal{S}(\omega) = \mathcal{A}(\theta\omega) - \mathcal{A}(\omega) \qquad (2.21)$$

Note that the probability defined through the action can be interpreted as a large deviation principle [11] with $\mathcal{A}D$ the large deviation rate. It gives the magnitude and the behaviour of the fluctuations around the deterministic and most probable dynamics, approached exponentially fast as long as $D \to 0$. This parallelism to the framework of the large deviations theory is very powerful. Interesting questions like the probability the process reaches a point x at time t given certain initial condition that would require to integrate (2.20) over the trajectories with given initial and final points can be approached throughout the contraction principle [94].

2.5.1 Entropy flux and local detailed balance

Eq. (2.20) relates explicitly the probability of a trajectory to the dynamics of the Langevin equation. Thus it is very helpful to compare and relate different dynamics at the level of the single trajectory. For example, how the introduction of a particular force into the Langevin equation can affect the probability of performing a certain trajectory. Interestingly, if we define the probability of a trajectory covered backward in time $\mathcal{P}(\Theta\omega)$, with Θ the time-reversal operator that reverts all the velocities, i.e. $\Theta\omega = \{x_{t-s}, -\dot{x}_{t-s}, 0 \le s \le t\}$, we can investigate the symmetry for time reversal of the dynamics. Namely,

$$\mathcal{S}(\omega) \equiv \ln \frac{\mathcal{P}(\omega)}{\mathcal{P}(\Theta\omega)} = \frac{\mu}{D} \int_0^t ds \; F(x_s) \dot{x}_s = \frac{\mu}{D} \int dx_s \circ F(x_s) \qquad (2.22)$$

where $\circ$ is referring to the Stratonovitch convention. Noteworthy, if the Einstein-Smoluchowski relation $\mu = D\beta$ holds the integral in (2.22), i.e. the time anti-symmetric part of the action, assumes a clear physical meaning, namely, the entropy dissipated into the environment by the nonequilibrium driving during $[0, t]$. This condition, that relies on the assumption that the Einstein-Smoluchowski relation is not violated by the nonequilibrium source, is another way to define the local detailed

balance [13,95–97]. Note that if the system is at equilibrium, i.e. $F(x) = -U'(x)$, the entropy production equals the energy change of the environment over its temperature $\beta \int_0^t dx_s \circ F(x_s) = \beta(U(x_t) - U(x_0))$, which does not depend on the whole trajectory, but only on the initial and final point, and is zero in average.

For example, we substitute (2.13) assuming that active force and thermal noise are not correlated, the average entropy flux is found to be linearly increasing, $\langle \mathcal{S} \rangle / t = v_0^2 / 2\mu T$ since the active particles continuously dissipate energy in the heat bath, coming from the hidden degrees of freedom and, therefore, not included in the balance of energy at the level of the Langevin equation.

2.5.2 Entropy production

A stronger connection with entropy can be made. Note that (2.20) is the probability given the initial state x_0, one can consider the path probability given the initial distribution. Namely, $\mathcal{P}_{\rho_0(x_0)}(\omega) = \rho_0(x_0)\mathcal{P}(\omega)$, where ρ_t is a time-dependent distribution. If we define the quantity $\mathcal{S}_\rho$

$$\mathcal{S}_\rho(\omega) \equiv \ln \frac{\mathcal{P}_{\rho_0(x_0)}(\omega)}{\mathcal{P}_{\rho_t(x_t)}(\Theta\omega)} = \ln \frac{\rho_0(x_0)}{\rho_t(x_t)} + \mathcal{S}(\omega) \tag{2.23}$$

where $\mathcal{S}(\omega)$ is (2.22), independent of the initial distribution. $\mathcal{S}_\rho(\omega)$ is a measure of irreversibility and is therefore equal to zero for every trajectory at equilibrium where $\rho_0 = \rho_t = \rho_{eq}$. If we average over the trajectories with the weight given by $\mathcal{P}_{\rho_0}$ we obtain a physical interpretation for the terms in (2.23). Namely, the left-hand side

$$\langle e^{-\mathcal{S}_\rho} \rangle = \int d\mathcal{P}_{\rho_0}(\omega) \frac{\mathcal{P}_{\rho_t}(\Theta\omega)}{\mathcal{P}_{\rho_0}(\omega)} = 1, \tag{2.24}$$

using Jensen's inequality, is the total entropy production in the system, given that $\langle \mathcal{S}_\rho \rangle > 0$ [98], while the first term on the right hand side is the Shannon entropy associated to the entropy of the system, if the average is meant as a sequence of independent copies of the system and ρ as the relative occupation of the space. It depends only on the initial and steps of the trajectories, i.e. it is a state function of the system. For consistency and in agreement with the definition of local detailed balance the last term must be interpreted as the entropy flux from the system to the environment [96] and it depends on the whole trajectory, if not at equilibrium.

2.6 Linear response theory

Understanding the dynamical properties of a many-body problem is very complicated, therefore approximated methods are usually employed. One of them is called response theory, whose intuitive idea is to apply a perturbation on a system and

observe its (average) reaction, being very instructive about the dynamical properties of the system itself. An example is the mobility of a BP defined as,

$$\mu = \lim_{t \to \infty} \frac{1}{t} \frac{\partial}{\partial f} \langle x(t) \rangle^f \bigg|_{f=0} \qquad (2.25)$$

where f is a constant external force applied on the BP and $\langle \cdot \rangle^f$ means the average to be taken in the dynamics with the extra force f, which is often unknown. On the other hand, if the perturbation is small, e.g. modulated by a function $h(t) \ll 1$, the dynamics does not radically change, at least during a certain time span. Therefore, assuming the existence of a Taylor-expansion in h, one can relate the response defined through the perturbed dynamics to correlations over the unperturbed one. If the initial dynamics is at equilibrium satisfying time-reversal symmetry, the Taylor-expansion can be done at the level of the probability distribution, whose fluctuations are subjected to the Onsager's regression principle [99]. Namely the relaxation to equilibrium due to an external perturbation behaves like a spontaneous fluctuation of the system and, therefore, the response relies on equilibrium correlations only. Given an observable $\mathcal{O}(t)$ of a system subjected to an energetic perturbation, $U \to U - hV$, the change in average value, i.e. the susceptibility $\chi_{\mathcal{O}V}(t) \equiv \langle \mathcal{O} \rangle^h - \langle \mathcal{O} \rangle$ is given by the Green-Kubo formula [100],

$$\chi_{\mathcal{O}V}(t) = \int ds\, R_{\mathcal{O}V}(t,s), \quad R_{\mathcal{O}V}(t,s) = \beta \frac{d}{ds} \langle \mathcal{O}(t)V(s) \rangle_{\text{eq}} \qquad (2.26)$$

which relates the response of the observable to the entropy flux from the system to the environment, kept at temperature β^{-1}, caused by the perturbation. Green-Kubo equation is also called fluctuation-response relation [35], similarly to FDT. Besides some initial concerns [101], linear response theory has proved itself to be a strong theory and suitable to calculate e.g. thermodynamic or electromagnetic suscepti-bilities [102–104]. Feared but expected, if the system is out of equilibrium most of the mentioned symmetries are broken, along with Onsager's regression hypothesis which relies on the time-reversal symmetry of the fluctuations. Since nonequilibrium probability distributions are unknown, the standard derivation leads to a dead end. Therefore Taylor-expansion must be shifted from phase-space probabilities to prob-abilities defined on the functional-space of trajectories for a Langevin or a Markov jumps dynamics. Namely, since the perturbation influences the probability of cer-tain trajectories, one can write the perturbed path probability with respect to the unperturbed one, $\mathcal{P}^h(\omega) = e^{-\mathcal{A}^h(\omega)}\mathcal{P}(\omega)$, with $\mathcal{A}^h$ the "excess" action, whose anti-symmetric part describes the entropy flux due to the perturbation as assured by local detailed balance assumption. Therefore the perturbed average value,

$$\langle \mathcal{O} \rangle^h = \int d\mathcal{P}(\omega) \frac{\mathcal{P}^h(\omega)}{\mathcal{P}(\omega)} \mathcal{O}(\omega) = \left\langle \mathcal{O}e^{-\mathcal{A}^h(\omega)} \right\rangle \approx \langle \mathcal{O} \rangle - \langle \mathcal{O}\mathcal{A}^h(\omega) \rangle \qquad (2.27)$$

neglecting contribution of order h^2, in the excess action too. Note that (2.27) va-lidity is not limited to a steady state. As we have seen in Sec. 2.5 the action can

be decomposed according to its time-reversal symmetry. At equilibrium only the anti-symmetric part, i.e. the entropy production, contributes to the response. Indeed, detailed balance condition allows to write the symmetric part as minus the anti-symmetric one, its effect absorbed by the entropy production. Such a peculiar symmetry is broken out of equilibrium and the symmetric part is expected to influence the response as well. Remarkably, the symmetric part becomes crucial for non-linear response around equilibrium too [105]. If we consider again a potential perturbation acting on an overdamped Langevin dynamics, i.e. $\dot{x} \to \dot{x} - \mu h_t \partial_x V(x)$, the response function can be written in an elegant form [106],

$$R_{\mathcal{O}V}(t, s) = \frac{\beta}{2} \left(\frac{d}{ds} \langle \mathcal{O}(t)V(s) \rangle - \langle \mathcal{O}(t)\mathcal{L}V(s) \rangle \right) \tag{2.28}$$

where $\mathcal{L}$ is called backward generator and it is the adjoint of the FP linear operator defined in Sec. 2.2. The backward generator depends on the features of the Langevin dynamics and so the susceptibility, differently from the Green-Kubo formula whose structure relies only on the entropy production. The symmetric part $\mathcal{T}$ of the action is also called dynamical activity, traffic or frenesy [107], and highlights the violation of the fluctuation-response theorem. The latter is related to the average rate of dissipation energy as stated by the Harada-Sasa relation which expresses the stationary heat dissipated in terms of the violations of the equilibrium FDT in the frequency domain [108, 109]. FDT can be formally restored introducing an effective temperature, nonetheless this temperature has in general not a straightforward thermodynamic explanation since sensitive, through the backward generator, to the particular microscopic features. Note that a response function as elegantly written through the backward generator as (2.28) is possible only for overdamped Markovian Langevin equation with additive noise perturbed by potential perturbations. Extension of (2.28) for non-Markovian, underdamped systems or time-dependent perturbation can be found in [110], [111] and [15] respectively. Several applications can be found for many systems, e.g. in [112, 113]. Most of the results in Chapter 3 are based on (2.28). We conclude this section employing (2.28) to stress the consequence of local detailed balance on the mobility mentioned in Sec. 2.3. The mobility as defined in (2.25) is given by (2.28) with potential perturbation $V(x) = fx$,

$$\mu = \lim_{t \to \infty} \frac{\beta}{2t} \left(\langle x^2(t) \rangle - \int_0^t ds \, \langle \mathcal{L}x(s) \, x(t) \rangle \right) = \beta D - \lim_{t \to \infty} \frac{\beta}{2t} \int_0^t \langle \mathcal{L}x(s) \, x(t) \rangle \tag{2.29}$$

where D is the diffusion coefficient, measured from the mean square displacement. If the system is driven by a nonequilibrium source the mobility is not directly proportional to the diffusion, but depends on additional dynamical features of the system. Namely, the mobility μ that appears in the local detailed balance relation is called generalised mobility and it is different from (2.29). To sum up, $\mu = \beta D$ for nonequilibrium systems is an expression of local detailed balance assuring the proper physical identification of the various terms in the Langevin equation [55, 112]. It is also

called generalised Einstein-Smoluchowski relation and must not be confused with fluctuation-dissipation theorem as defined in Sec. 2.1 where mobility is defined as (2.25). Clearly, they coincide at equilibrium.

Chapter 3

Colloids in nonequilibrium environment

3.1 Introduction

The notion of Brownian Motion refers to the thermal fluctuations of some mesoscopic particles in contact with a bath of smaller particles. The essential feature is a scale separation between the Brownian and the bath degrees of freedom that allows for a systematic coarse-graining of an otherwise intractable many-body system. It leads to an effective description for the BPs alone, via some stochastic differential equations, (typically not Markovian generalised) Langevin equation, GLE. Although there exist systematic derivations of such mesoscopic equations of motion from an underlying microscopic many-body Hamiltonian through the elimination of the fast degrees of freedom [31, 114, 115], easier approach are available, if the system under survey is at equilibrium. Indeed, one typically appeals to equilibrium Statistical Mechanics in order to make the formal expressions practically useful. Namely, to bypass the explicit solution of the microscopic dynamic equations, the "noise" fluctuations that agitate the mesoscopic degrees of freedom are assigned a weight in agreement with Boltzmann's principle [92]. By construction, their correlations then satisfy detailed balance in the form of a fluctuation-dissipation theorem [36]. This implies, in particular, that they induce mesoscopic correlations in accord with the equipartition theorem. Moreover, the average mesoscopic dynamics is found to be a gradient flow in a convex free energy landscape. Being derived by such a (thermodynamic) potential, the mean effective interactions of the Brownian degrees of freedom themselves obey the action-reaction principle. In other words, for systems in thermodynamic equilibrium, the symmetries holding on the microscopic level can essentially be lifted up to the mesoscopic scale.

The theory remains valid even when some of these mesoscopic degrees of freedom are externally driven out of equilibrium, as long as local detailed balance persists [52,54], i.e., under the assumption that the source of non-equilibrium does not appreciably affect the (many) bath degrees of freedom. For this reason, the concept of a Brow-

nian scale separation, as embodied in the Langevin equation, has played a central role in the development of a framework of stochastic thermodynamics that reaches out to conditions far from equilibrium [10, 32] and in the study of nonequilibrium fluctuation and work relations [6].

In contrast, none of the above symmetry properties generally survives on the Brownian scale if the bath itself is driven out of equilibrium. Not only is the detailed balance of the Brownian degrees of freedom then lost, but also equipartition gives way to a more complex energy partition rule [116], stochastic forces are no longer of gradient-type [117], and the action-reaction principle is violated [118]. In soft matter physics, one finds many examples for interacting probes in non-equilibrium baths. One may naturally think of a suspension of colloids immersed in a non-equilibrium solvent, such as a sheared fluid [119], a granular [120], glassy [121] or active-particle suspension [122], or even the cytoplasm of a living cell [123]. It would certainly be of great interest to establish a self-contained coarse-grained description for the colloids in such situations. Yet, the usual equilibrium arguments invoked in the construction of a coarse-grained Langevin description, are not any more applicable. So the reduced stochastic description (assuming it still exists) must be found by other means, in the worst case by *explicitly* integrating out the dynamics of the nonequilibrium environment. It should go without saying that, for scientifically or technologically interesting systems, this is almost always an impossible task, since relying on the solution of the microscopic equations.

There is thus great interest in defining suitable conditions and finding general approximate methods [124, 125] that allow for reliable and useful predictions on the Brownian scale bypassing the integration of the microscopic dynamics, even if the degrees of freedom of the environment are driven far from equilibrium. A good candidate is suggested by the theory of Brownian Motion, itself. If the "fast" bath degrees of freedom of some Brownian system themselves admit a coarse-grained description by a mesoscopically driven Langevin theory routed in its own equilibrium bath, the resulting theory fulfils all of the above requirements. In other words, the presence of a nonequilibrium source requires the introduction of an intermediate level between the BPs (from now on called probes to avoid confusion) and the thermal environment as depicted in Fig. 3.1. More precisely, we do assume that the environment is made up of some sort of particles that evolve according to some driven Markovian stochastic dynamics enjoying local detail balance and coupled to an equilibrium reservoir providing for noise and friction. In contrast to standard Brownian dynamics, we thus do not require a direct buffering of the probe degrees of freedom by some equilibrium thermal reservoir but only an indirect one, mediated by the nonequilibrium environment. The effective dynamics for the probes, result of a further coarse-graining, derives from the elimination of the driven degrees of freedom. Technically, we employ nonequilibrium linear response theory [106, 112, 126–132] to derive a Langevin equation for the probe particles that we assume to be weakly coupled to the interacting many-body system acting as the environment. The response function is already a coarse-grained observable since average over certain degrees of freedom, as discussed
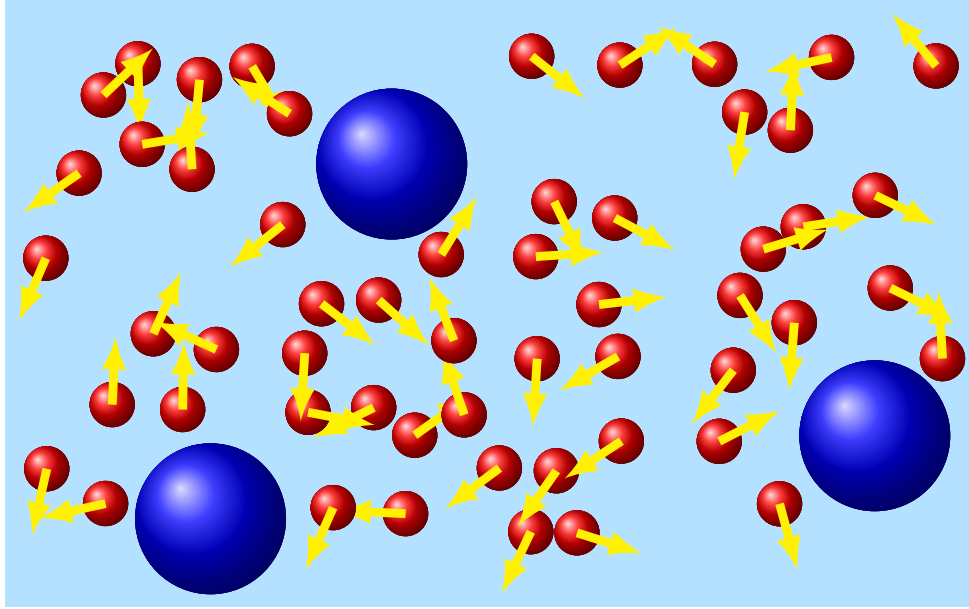
Figure 3.1: Schematic representation of the three-level scheme employed by our theory: the probes (blue) representing the system are embedded in a nonequilibrium environment, e.g. a fluid of smaller driven particles (red), which are in contact with an equilibrium thermal bath (light blue), providing for friction and noise.

in Sec. 2.6. Following [15, 133], we then go beyond a merely static description that would only account for systematic probe interactions induced by the nonequilibrium environment, such as nonequilibrium depletion forces [67, 134]. We explicitly look for the fluctuations of such induced forces around their average values. The discussion of the results in this Chapter follows the same structure of [16]. In Sec. 3.2 we obtain formal expressions for these fluctuating forces, the friction, and the noise statistics, emerging features of the coarse grained dynamics. When the driving is off, we retrieve the expected detailed balance condition connecting the noise correlation to the friction kernel. But we can also analyse how this relation changes when the environment is driven (far) out of equilibrium and quantify the violations of detailed-balance and the reciprocal relations in terms of both excess dynamical activity [135–138] and probability currents. The latter result in the lack of an action-reaction principle for the induced probe interactions [118, 119, 139, 140]. Section 3.3 exemplifies the theoretical scheme with the help of two paradigmatic examples that can explicitly be worked out. First, we treat analytically a single probe linearly coupled to a fluid of particles driven by a two-dimensional vortex. This toy model clearly displays the breakdown of detailed balance and allows us to touch on the scope of the notion of effective temperature. Secondly, we employ Brownian dynamics simulations to analyse the effective friction forces induced between two probes suspended in a driven fluid. The numerical evaluation of our general analytic expressions for the time-dependent friction matrix nicely reveals the expected violations of the action-reaction principle,

as well as the possible appearance of negative mobility.

3.2 General theory

We consider a d-dimensional system made up of N_p probe particles, with mass M_i and positions $\mathbf{X}_i$, which interact with an environment, composed of $N \gg 1$ degrees of freedom denoted $\mathbf{x}_k$. The environment is in contact with an equilibrium bath at inverse temperature β, respectively in blue, red and light blue in Fig. 3.1. The probes obey Newton's equation of motion

$$M_i\ddot{\mathbf{X}}_i = \mathbf{K}_i(\mathbf{X}_i) + \mathbf{g}_i(\{\mathbf{x}\}, \mathbf{X}_i), \tag{3.1}$$

where $\mathbf{g}_i \equiv -\lambda\partial_{\mathbf{X}_i}U_i(\{\mathbf{x}\}, \mathbf{X}_i)$ is the interaction force between the probe i and the environment, with λ a small dimensionless parameter. All the other forces are incorporated in $\mathbf{K}$, which are (optional) direct interactions between the probes and additional external ones. Their specific form is irrelevant in the following. They are only required to be sufficiently confining so as to allow for a unique stationary state. Throughout the text, we use the shorthand $\{\dots\}$ to denote the entire set of degrees of freedom, either the probes or the particles. We assume that the environment evolves according to a Markovian stochastic dynamics, enjoying local detail balance. Hence, with respect to standard approaches, we lift such condition from the dynamics of the system to that of the environment. For concreteness, we can think of the overdamped Langevin equations

$$\dot{\mathbf{x}}_k = \mu\mathbf{F}_k - \lambda\mu\sum_{i=1}^{N_p}\frac{\partial U_i}{\partial\mathbf{x}_k} + \sqrt{\frac{2\mu}{\beta}}\boldsymbol{\xi}_k. \tag{3.2}$$

Here $\mathbf{F}_k$ consists of inter-particle potential forces $-\partial_{\mathbf{x}_k}V(\{\mathbf{x}\})$, and external ones that may contain a non-potential driving $f(\{\mathbf{x}\})$ setting the environment out of equilibrium. The ξ's are centered Gaussian noises, white and uncorrelated. Let $\{\mathbf{Y}\}$ be the set of average positions around which the probes fluctuate as a consequence of the interactions with the environment. Here we are concerned with the fluctuations induced by the presence of the environment, for which we seek a reduced description. Namely, we aim at integrating out of (4.1) the environment coordinates by averaging the probe-environment coupling with the appropriate distribution for $\mathbf{x}_k$. We expect noise and friction to emerge in this process, together with indirect forces between the probes, mediated by the environment. To this end, we rewrite Eq. (4.1) as

$$M_i\ddot{\mathbf{X}}_i = \mathbf{K}_i + \langle\mathbf{g}_i\rangle + \boldsymbol{\eta}_i, \tag{3.3}$$

where we split the environment-probe coupling into a systematic part $\langle\mathbf{g}_i\rangle$ and a random contribution $\boldsymbol{\eta}_i \equiv \mathbf{g}_i - \langle\mathbf{g}_i\rangle$. The former is defined as the mean force exerted by the environment on probe i, and reads

$$\langle\mathbf{g}_i\rangle = \langle\mathbf{g}_i(\{\mathbf{x}\}, \mathbf{X}_i)\rangle \equiv \int d\{\mathbf{x}\}\mathbf{g}_i(\{\mathbf{x}\}, \mathbf{X}_i)\rho(\{\mathbf{x}\}|\{\mathbf{X}\}), \tag{3.4}$$

with $\rho(\{\mathbf{x}\}|\{\mathbf{X}\})$ the probability density of the environment conditioned by the probes being in positions $\{\mathbf{X}\}$ and thus, explicitly time-dependent. We work under the usual assumptions made in the derivation of Langevin equations, i.e. a small variation of the probe momentum after a single particle-probe interaction (large mass difference and big time scale separation), and a weak coupling between probes and environment. Under these conditions, the fluctuations of probe i around the preferred state $\mathbf{Y}_i$ are small, and its force on the whole environment can be expanded to linear order in the displacement from $\mathbf{Y}_i$:

$$\lambda \sum_{k=1}^{N} \frac{\partial U_i}{\partial \mathbf{x}_k} = \lambda \sum_{k=1}^{N} \frac{\partial U_i}{\partial \mathbf{x}_k}\bigg|_{\mathbf{X}_i=\mathbf{Y}_i} - (\mathbf{X}_i(t)-\mathbf{Y}_i) \cdot \sum_{k=1}^{N} \frac{\partial \mathbf{g}_i}{\partial \mathbf{x}_k}\bigg|_{\mathbf{X}_i=\mathbf{Y}_i} + \mathcal{O}(\mathbf{X}_i(t) - \mathbf{Y}_i)^2. \quad (3.5)$$

Here it is useful to regard $\mathbf{g}_i$ as an external potential perturbing the environment, modulated in time via the protocol $\mathbf{X}_i(t) - \mathbf{Y}_i$. If we neglect truncate the expansion to the linear order, (3.2) becomes

$$\dot{\mathbf{x}}_k = \mu \mathbf{F}_k - \lambda\mu \sum_{i=1}^{N_p} \frac{\partial U_i}{\partial \mathbf{x}_k}\bigg|_{\mathbf{X}_i=\mathbf{Y}_i} + \mu(\mathbf{X}_i(t) - \mathbf{Y}_i) \cdot \sum_{i=1}^{N_p} \frac{\partial \mathbf{g}_i}{\partial \mathbf{x}_k}\bigg|_{\mathbf{X}_i=\mathbf{Y}_i} + \sqrt{\frac{2\mu}{\beta}} \boldsymbol{\xi}_k. \quad (3.6)$$

In view of (3.5), it is then natural to express the conditional average (3.4) in in terms of unperturbed averages $\langle \ldots \rangle^0$, corresponding to all probes sitting in the mean positions $\{\mathbf{Y}\}$ that, if constant in time, entails for the unperturbed distribution the existence of a steady state. To do so we make use of the response theory for perturbations about non-equilibrium states (2.28). It can be applied verbatim for one probe [15]. Given N_p probes, the deviation of every average value from the unperturbed one should depend on all the probes fluctuations. At linear order we neglect correlations among those fluctuations and that allows to write the response as superposition of all the perturbations. Namely,

$$\langle \mathcal{A}(t) \rangle = \langle \mathcal{A}(t) \rangle^0 + \frac{\beta}{2} \sum_{j=1}^{N_p} \int_{t_0}^{t} ds\, h_j(s) \left(\frac{d}{ds} \langle \mathcal{B}_j(s); \mathcal{A}(t) \rangle^0 - \langle \mathcal{L}\mathcal{B}_j(s); \mathcal{A}(t) \rangle^0 \right) \quad (3.7)$$

where $\mathcal{A}$ is the observable of interest, $\mathcal{B}_j$ are the perturbation potentials switched on at time t_0 and modulated in time through the protocol $h_j(s)$. The operator $\mathcal{L}$ and the average $\langle \ldots ; \ldots \rangle^0$ stand for, respectively, the backward generator of the unperturbed dynamics and the connected average with respect to it. In (3.7) the first integrand is the usual correlation of the observable with the entropy production, as appearing in the Kubo formula (2.26). The second one is a frenetic contribution that contains the excess dynamical activity, $\mathcal{L}\mathcal{B}_j$, caused by the perturbation. In equilibrium, they make equal contributions [106]:

$$\frac{d}{ds} \langle \mathcal{B}_j(s); \mathcal{A}_i(t) \rangle^{\mathrm{eq}} = -\langle \mathcal{L}\mathcal{B}_j(s); \mathcal{A}_i(t) \rangle^{\mathrm{eq}}. \quad (3.8)$$

Here we are interested in the response of $\mathbf{g}_i(\{\mathbf{x}\}, \mathbf{X}_i)$ to the perturbations in (3.5). Hence, with the identifications $\mathcal{A} = \mathbf{g}_i$, $\mathcal{B}_j = \mathbf{g}_j$ and $\mathbf{h}_j = \mathbf{X}_j - \mathbf{Y}_j$, (3.7) becomes

$$\langle \mathbf{g}_i(t) \rangle = \langle \mathbf{g}_i \rangle^0 + \sum_{j=1}^{N_p} \frac{\beta}{2} \int_{t_0}^{t} \mathrm{d}s (\mathbf{X}_j(s) - \mathbf{Y}_j) \left[\frac{\mathrm{d}}{\mathrm{d}s} \langle \mathbf{g}_j(s); \mathbf{g}_i(t) \rangle^0 - \langle \mathcal{L} \mathbf{g}_j(s); \mathbf{g}_i(t) \rangle^0 \right] \tag{3.9}$$

where $\mathcal{L}$, the backward generator of the unperturbed dynamics of the environment, reads for (3.2):

$$\mathcal{L} = \mu \sum_{k=1}^{N} \left[\mathbf{F}_k \cdot \frac{\partial}{\partial \mathbf{x}_k} - \lambda \sum_{i=1}^{N_p} \frac{\partial U_i}{\partial \mathbf{x}_k} \bigg|_{\mathbf{X}_i = \mathbf{Y}_i} \cdot \frac{\partial}{\partial \mathbf{x}_k} + \frac{1}{\beta} \frac{\partial^2}{\partial \mathbf{x}_k^2} \right]. \tag{3.10}$$

The summands in (3.9) are the forces due to the linearised fluctuations of the probes around their preferred states. Assuming that the environment was put in contact with the probes at time $t_0 = -\infty$, so that no correlation with the initial conditions is retained, an integration by parts yields

$$\langle \mathbf{g}_i(t) \rangle = \langle \mathbf{g}_i \rangle^0 + \sum_{j=1}^{N_p} \left[\mathbf{G}_{ij}(t) - \int_{-\infty}^{t} \mathrm{d}s\, \zeta_{ij}(t-s) \dot{\mathbf{X}}_i(s) \right]. \tag{3.11}$$

Here we defined the memory kernel

$$\zeta_{ij}(t-s) \equiv \frac{\beta}{2} \left(\langle \mathbf{g}_j(s); \mathbf{g}_i(t) \rangle^0 - \int_{-\infty}^{s} \mathrm{d}\tau \langle \mathcal{L} \mathbf{g}_j(\tau); \mathbf{g}_i(t) \rangle^0 \right), \tag{3.12}$$

which enters both the friction, back-reaction of the fluid to the probe motion, and the statistical forces mediated by the environment [117, 141],

$$\mathbf{G}_{ij}(t) \equiv (\mathbf{X}_j(t) - \mathbf{Y}_j) \zeta_{ij}(0), \tag{3.13}$$

including the "self-interaction" ($i = j$) and the inter-probes forces ($i \neq j$). Equation (3.13) establishes the connection between the friction kernel and the fluctuating statistical force, namely,

$$\frac{\partial \mathbf{G}_{ij}}{\partial \mathbf{X}_j} = \zeta_{ij}(0). \tag{3.14}$$

For $i \neq j$, Eq. (3.14) relates environment-mediated interactions to cross-friction between probes, indicator of the propagation of the perturbation through the fluid. It was proposed by De Bacco *et al.* [142] for equilibrium systems arguing on the basis of Onsager's regression principle. Here we gave a formal proof of this relation that extends its validity to nonequilibrium states. In equilibrium, where averages are

denoted $\langle\ldots\rangle^{\mathrm{eq}}$, the frenetic term can be eliminated in favour of the entropic term, according to (3.8):

$$\langle \mathbf{g}_j(s); \mathbf{g}_i(t)\rangle^{\mathrm{eq}} = -\int_{-\infty}^{s} \mathrm{d}\tau \langle \mathcal{L}\mathbf{g}_j(\tau); \mathbf{g}_i(t)\rangle^{\mathrm{eq}}. \tag{3.15}$$

We thus retrieve that the friction kernel is a symmetric matrix

$$\zeta_{ij}(t-s) = \beta\langle \mathbf{g}_j(s); \mathbf{g}_i(t)\rangle^{\mathrm{eq}} = \zeta_{ji}(t-s), \tag{3.16}$$

since correlations are functions of $|t-s|$ only, thanks to time-reversal invariance. The symmetry (3.16) translates into the condition $\partial \mathbf{G}_{ij}/\partial \mathbf{X}_j = \partial \mathbf{G}_{ji}/\partial \mathbf{X}_i$, which suffices to make $\mathbf{g}_i$ derive from an effective (thermodynamic) potential $\mathcal{F}(\{\mathbf{X}\})$. That such potential is the Helmholtz free energy of the environment,

$$\mathcal{F} \equiv -\frac{1}{\beta} \ln \int \mathrm{d}\{\mathbf{x}\} e^{-\beta(\lambda \sum_{i=1}^{N} U_i + V)}, \tag{3.17}$$

is easily seen by introducing the Boltzmann factor in (3.4):

$$
\begin{aligned}
\langle \mathbf{g}_i \rangle^{\mathrm{eq}} &= -\int \mathrm{d}\{\mathbf{x}\} \lambda \frac{\partial}{\partial \mathbf{X}_i} U_i \, e^{-\beta(\sum_{i=1}^{N} U_i + V - \mathcal{F})} \\
&= \frac{1}{\beta} e^{\beta\mathcal{F}} \frac{\partial}{\partial \mathbf{X}_i} \int \mathrm{d}\{\mathbf{x}\} e^{-\beta(\lambda \sum_{i=1}^{N} U_i + V)} \\
&= \frac{1}{\beta} e^{\beta\mathcal{F}} \frac{\partial}{\partial \mathbf{X}_i} e^{-\beta\mathcal{F}} = -\frac{\partial}{\partial \mathbf{X}_i} \mathcal{F}.
\end{aligned} \tag{3.18}
$$

This ensues the action-reaction principle for the fluctuating forces among probes. Contrarily, when the environment is driven away from equilibrium, (3.15) is not applicable in general, as frenetic and entropic terms remain distinct. Hence the reciprocal relations are not satisfied, $\zeta_{ij} \neq \zeta_{ji}$, which implies that the action-reaction symmetry is broken. Now we turn to the random part of the interaction,

$$\boldsymbol{\eta}_i \equiv \mathbf{g}_i(\{\mathbf{x}\}, \mathbf{X}_i) - \langle \mathbf{g}_i(\{\mathbf{x}\}, \mathbf{X}_i)\rangle. \tag{3.19}$$

It has zero mean by definition, and its two-times correlation is obtained again by application of the response formula (3.7), with $\mathcal{A} = \mathbf{g}_i \mathbf{g}_j$,

$$\langle \boldsymbol{\eta}_i(t)\boldsymbol{\eta}_j(s)\rangle = \langle \mathbf{g}_i(\{\mathbf{x}(t)\}, \mathbf{X}_i(t)); \mathbf{g}_j(\{\mathbf{x}(s)\}, \mathbf{X}_j(s))\rangle \approx \langle \mathbf{g}_i(t); \mathbf{g}_j(s)\rangle^0. \tag{3.20}$$

The weak-coupling approximation allowed us to drop higher orders in λ, so that (3.20) simplifies to

$$\langle \boldsymbol{\eta}_i(t)\boldsymbol{\eta}_j(s)\rangle = \mathcal{C}_{ij}^0(t-s) = \frac{2}{\beta}\zeta_{ij}(t-s) + \int_{-\infty}^{s} \mathrm{d}\tau \langle \mathcal{L}\mathbf{g}_j(\tau); \mathbf{g}_i(t)\rangle^0. \tag{3.21}$$

Namely, in a first approximation, the noise depends on $\{\mathbf{Y}\}$ and not on the actual position of the probes and is therefore additive. In general, the noise correlation depends explicitly on the excess dynamical activity of the environment, $\mathcal{L}\mathbf{g}_i$. Yet, in equilibrium, exploiting again the equality of the frenetic and entropic term, (3.21) reduces to the FDT,

$$\langle \boldsymbol{\eta}_i(t)\boldsymbol{\eta}_j(s) \rangle^{\mathrm{eq}} = \mathcal{C}_{ij}^{\mathrm{eq}}(t-s) = \frac{1}{\beta}\zeta_{ij}(t-s). \tag{3.22}$$

Out of equilibrium (3.21) cannot be simplified further in general, and FDT (3.22) is evidently broken, resulting in asymmetric noise cross-correlations. Such violation of the FDT appears more transparent if (3.21) is written in terms of the state velocity of the environment, i.e. the vector

$$\mathbf{v}(\{\mathbf{x}\}, \{\mathbf{X}\}) \equiv \frac{\jmath(\{\mathbf{x}\}, \{\mathbf{X}\})}{\rho^0(\{\mathbf{x}\}|\{\mathbf{X}\})}, \tag{3.23}$$

with $\jmath$ the probability current of the environment, that vanishes identically in equilibrium. Even though it could be experimentally estimated [143–147], it has been analytically solved only in few simple situations where the stationary distribution is known [127, 148, 149]. From the identity $\mathcal{L} = \mathcal{L}^+ + 2\mathbf{v} \cdot \nabla$ [107, 127, 150], where ∇ is the vector of partial derivatives $\partial_{\mathbf{x}_k}$, and $\mathcal{L}^+$ is the adjoint of $\mathcal{L}$—the forward generator of the dynamics of the environment—one can easily prove:

$$\langle \mathcal{L}\mathbf{g}_i(\tau); \mathbf{g}_j(t) \rangle^0 = -\frac{\mathrm{d}}{\mathrm{d}\tau}\langle \mathbf{g}_j(\tau); \mathbf{g}_i(t) \rangle^0 + 2\langle \mathbf{v} \cdot \nabla \mathbf{g}_j(\tau); \mathbf{g}_i(t) \rangle^0. \tag{3.24}$$

Using Eqs. (3.12), (3.21) and (3.24) the broken FDT reads

$$\langle \boldsymbol{\eta}_i(t)\boldsymbol{\eta}_j(s) \rangle = \frac{1}{\beta}\zeta_{ij}(t-s) + \int_{-\infty}^{s} \mathrm{d}\tau \langle \mathbf{v} \cdot \nabla \mathbf{g}_j(\tau); \mathbf{g}_i(t) \rangle^0, \tag{3.25}$$

where the deviation from the equilibrium Kubo formula appears explicitly. In general, the noise (3.19) will not be Gaussian and thus the two-times correlation is not enough to fully characterize its statistics. Higher moments can be calculated with the same procedure, though, by successive application of the response formula (3.7) together with the weak-coupling assumption.

Noteworthy, the restriction of time-independent mean states $\{\mathbf{Y}\}$ can be easily lifted. If, instead, mean time-dependent trajectories $\{\mathbf{Y}(t)\}$ are taken, our approach still holds with the caveat that the perturbation potentials, $\mathbf{g}_i(\{\mathbf{x}\}, \mathbf{Y}_i(s))$, now carry an explicit time dependence via $\mathbf{Y}_i(t)$ (cf. Eq. (3.5)). An extension of the response formula (3.7) needs to be applied [15, 151], which features $\{\mathbf{Y}(t)\}$ as a quasi-static protocol, but the remaining procedure is very analogous. Consequently the unperturbed distribution is assumed to be quasi-stationary in agreement with the protocol for the probes mean positions. Therefore, the theory naturally extends to probes that are, e.g., acted upon by external time-dependent forces, or in direct contact with the

equilibrium bath, as well as with the environment. Plugging (3.11) into (3.3) we obtain the effective dynamics for the colloid.

$$M_i\ddot{\mathbf{X}}_i = \mathbf{K}_i + \langle \mathbf{g}_i \rangle^0 + \sum_{j=1}^{N_p} \left[\mathbf{G}_{ij}(t) - \int_{-\infty}^{t} \mathrm{d}s\, \zeta_{ij}(t-s)\dot{\mathbf{X}}_j(s) \right] + \boldsymbol{\eta}_i, \qquad (3.26)$$

which is typically called generalised Langevin equation, extension of the homonymous equation beyond the Markovian limit. The coarse-graining over the fluid degrees of freedom leads to new emergent behaviour, i.e. a coupling between the colloids mediated by the bath and the dissipation for the probes, previously characterised by a deterministic Newtonian dynamics and not directly coupled. Noteworthy, if the environment is out of equilibrium, the coupling between the colloids experiences violation of action-reaction principle, due to an explicit dependence of the friction on the features of the dynamics via the backward generator, consequence of the employ of response theory around nonequilibrium configurations. The dissipation for the probes is subjected to the violation of FDT, because the dissipation cannot be attributed to an external source, but it is intrinsic in the system, i.e. local detailed balance cannot be satisfied. In conclusion, whether certain symmetries of the underlying dynamics involving both the probes and the fluid, are inherited or not by the effective dynamics for the probes depends on the nature of the environment itself.

3.3 Examples

In this section we present two explicative examples. First, we consider a single probe linearly coupled to a fluid of noninteracting particles that are driven by an external vortex. Response and fluctuations in equations (3.12) and (3.21) are calculated analytically and used to show the breakdown of the FDT (3.22). Second, we show how to extract from Brownian simulations the friction memory kernel of two confined probes immersed in a stirred fluid. We prove numerically the breakdown of the reciprocal relations, that is the violation of the action-reaction principle for the fluid-mediated forces between the probes.

3.3.1 One probe in a vortex

We consider a two-dimensional system ($d = 2$) where a single probe ($N_p = 1$) under harmonic confinement, $\mathbf{K} = -K(\mathbf{X} - \mathbf{Y})$, interacts via a harmonic potential U (with constant stiffness denoted by k) with an environment of particles $\mathbf{x}_j = \mathbf{x}_j(t)$ driven by an external vortex,

$$\dot{\mathbf{x}}_j = A\,\mathbf{x}_j + \lambda k\mu\mathbf{X} + \sqrt{\frac{2\mu}{\beta}}\boldsymbol{\xi}_j, \qquad A = \begin{pmatrix} -\lambda k\mu & -h\mu \\ h\mu & -\lambda k\mu \end{pmatrix}. \qquad (3.27)$$

The probe dynamics $\mathbf{X} = \mathbf{X}(t)$ is given by

$$\ddot{\mathbf{X}} = -K\mathbf{X} - \lambda k \sum_{j=1}^{N} (\mathbf{X} - \mathbf{x}_j). \tag{3.28}$$

Since the potential U is harmonic, linear response theory around the minimum of the confining potential $\mathbf{Y}$ can be applied without any approximation by summing and subtracting $\lambda k \mu \mathbf{Y}$ in (3.27) to obtain an equation equivalent to (3.6). Following the general theory, the force on the probe,

$$\langle \mathbf{g}(t) \rangle \equiv \langle \mathbf{g} \rangle^0 + (\mathbf{X}(t) - \mathbf{Y})\zeta(0) - \int_{-\infty}^{t} ds\, \zeta(t-s)\dot{\mathbf{X}}(s) \tag{3.29}$$

is expressed through correlations of the unperturbed dynamics, which can exactly be solved by diagonalising the matrix A in (3.27) and introducing the variable, $z = ix + y$, $z^* = -ix + y$ leads to the explicit solution of $\mathbf{x}_j = (x_j, y_j)$. Accordingly we can calculate the systematic part of the interaction (3.11)

$$\langle \mathbf{g} \rangle^0 = -A_0 \mathbf{Y}, \qquad A_0 = \frac{N\lambda k h}{\lambda^2 k^2 + h^2} \begin{pmatrix} h & -\lambda k \\ \lambda k & h \end{pmatrix} \tag{3.30}$$

and the the stochastic one (3.19)

$$\boldsymbol{\eta} \equiv -\lambda k \sum_{j=1}^{N} (\langle \mathbf{x}_j \rangle - \mathbf{x}_j) = \lambda k \sum_{j=1}^{N} \int_{-\infty}^{t} ds\, e^{-\lambda k \mu(t-s)} \Gamma(t-s)\boldsymbol{\xi}_j(s) \tag{3.31}$$

where

$$\Gamma(\tau) = \sqrt{\frac{2\mu}{\beta}} \begin{pmatrix} \cos(h\mu\tau) & \sin(h\mu\tau) \\ \sin(h\mu\tau) & \cos(h\mu\tau) \end{pmatrix} \tag{3.32}$$

respectively. The noise is still Gaussian, but is no longer Markovian. The xx-component of friction kernel defined as in (3.12) for $\tau = t - s$,

$$\zeta_{xx}(\tau) = \frac{N\beta k^2 \lambda^2}{2} \sum_{j,k=1}^{N} \left\langle \left(x_j(0) + \mu \int_{-\infty}^{0} dr\, (\lambda k x_j(r) + h y_j(r)) \right) x_k(\tau) \right\rangle \tag{3.33}$$

contain simple correlation functions of the unperturbed process in the steady state. For the symmetry of the system $\zeta_{xx}(\tau) = \zeta_{yy}(\tau)$ and $\zeta_{xy}(\tau) = -\zeta_{yx}(\tau)$. From (3.12) we thus obtain the friction kernel components,

$$\zeta_{xx}(\tau) = \frac{N\lambda^2 k^2}{\lambda^2 k^2 + h^2} e^{-\lambda k \mu \tau} [\lambda k \cos(h\mu\tau) - h \sin(h\mu\tau)]$$

$$\zeta_{xy}(\tau) = -\frac{N\lambda^2 k^2}{k^2 + h^2} e^{-\mu\lambda k \tau} (h \cos(\mu h \tau) + \lambda k \sin(\mu h \tau)) \tag{3.34}$$

showing that dissipation happens on the characteristic timescale it takes the active particles to relax in the coupling potential U, up to the oscillation ruled by the vortex intensity h. Furthermore, the friction can turn negative as well, meaning that the colloid is accelerated by the fluid. Note that the friction does not depend on the probe position since the coupling is linear, regardless of the number of probes under survey. Namely, even if we would consider two probes, violation of action-reaction principle could not be observed unless a non-linear coupling is considered. The noise $\boldsymbol{\eta}$, expressed as correlation functions of the fluid dynamics, if interpreted as a Brownian Motion noise is responsible for the energy input into the system and it is calculable explicitly from (3.31), decays exponentially with the same characteristic time, but is subjected to different oscillations of frequency $h\mu$ due to the vorticity.

$$\beta \left\langle \eta_x \left(0\right) \eta_x \left(\tau\right)\right\rangle = \zeta_{xx}\left(\tau\right) + \frac{N\lambda kh}{\lambda^2 k^2 + h^2} e^{-\lambda k\mu\tau}\left(h\cos\left(h\mu\tau\right) + \lambda k\sin\left(h\mu\tau\right)\right)$$

$$\beta \left\langle \eta_x \left(0\right) \eta_y \left(\tau\right)\right\rangle = \zeta_{xy}\left(\tau\right) + \frac{N\lambda kh}{\lambda^2 k^2 + h^2} e^{-\lambda k\mu\tau}\left(\lambda k\cos\left(\mu h\tau\right) - h\sin\left(\mu h\tau\right)\right) \quad (3.35)$$

Interestingly, since the noise matrix is not diagonal the off-diagonal components of the noise are not independent. One may try to mend it by introducing a time-dependent effective temperature

$$\beta T_{\text{eff}}(\tau) = 1 + R\frac{R + \tan\left(\mu h\tau\right)}{1 - R\tan\left(h\mu\tau\right)} \quad (3.36)$$

where $R \equiv h/\lambda k$ compares the intensity of the vortex with respect to the coupling. Eq. (3.36) and following discussions are for the xx-correlation, but same conclusion can be drawn for the other components of the noise correlation matrix. Eq. (3.36) allows to formally restore the FDT for the noise correlation matrix. The price to pay is that the effective temperature can in general be negative and diverge. In particular, (3.36) periodically diverges when $R\tan(h\mu\tau) \to 1$, for which the friction diagonal components (3.34) are zero. The frequency of the divergence increases with h along with the tangent periodicity. It happens also in the weak-coupling regime $R \ll 1$, in which the interference of the probe on the fluid dynamics is small and therefore the probe should behave like a good thermometer. This strange behaviour is clearly revealed, by the simple model, as the consequence of an artefact, namely of selling a regular and periodic motion as heat. A meaningful definition of temperature for a many-body system requires a more random and chaotic behaviour as stated by statistical mechanics and kinetic theory [152, 153]. This condition is not satisfied by this system, due to the vortex which tends to make the dynamics very regular and predictable. In the next Chapter we will introduce the effective temperature for a colloid embedded in a fluid of active particles. Being this motion more random due to the rotational diffusion, it will be possible in a certain regime, to be discussed, to define a physically meaningful effective temperature. Effective temperatures definitions are delicate argument and the step from mathematical artefact to thermodynamics observable must be carefully faced. Diverging (3.36) does not have
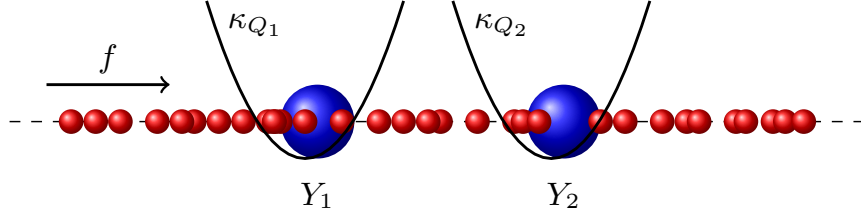
Figure 3.2: Schematic illustration of the simulated system, composed of $N + 2$ soft spheres in one spatial dimension with periodic boundary conditions. The probes (blue) have average positions $Y_i \sim Y_i^* + \jmath \int_0^\tau d\tau' \zeta_{ii}(\tau')/K_i$ resulting from the balance of the drag force due to the steady current $\jmath$ of fluid particles (red) and to the harmonic confinement with minimum in Y_i^* and stiffness K_i $(i = 1, 2)$.

to worry since it corresponds to zero friction, entailing a finite value for the noise correlation. Summing up, for the effective dynamics for the colloid embedded in the vortex (3.27) is given by the GLE for the probe,

$$\ddot{\mathbf{X}} = -(K - \zeta(0))(\mathbf{X} - \mathbf{Y}) - A_0 \mathbf{Y} - \int_{-\infty}^t ds\, \zeta(t - s)\, \dot{\mathbf{X}}(s) + \boldsymbol{\eta} \qquad (3.37)$$

where the friction memory kernel and the noise covariance are given by (3.34) and (3.31), respectively. Noteworthy, the components of the probe coordinates are no longer independent since neither A_0 in (3.30) nor

$$\zeta(0) = \frac{N}{\mu} \frac{\lambda^2 k^2}{\lambda^2 k^2 + h^2} \begin{pmatrix} \lambda k \mu & -h\mu \\ h\mu & \lambda k \mu \end{pmatrix} \qquad (3.38)$$

are diagonal. Noteworthy, $\zeta(0) = -N\lambda k \mu A^{-1}$, A^{-1} is the inverse of the matrix defined in (3.27). The effective dynamics is still a vortex with the same orientation, but some effective parameter. If $h = 0$, i.e. no vortex, $\zeta_{xx}(\tau) = N\lambda k e^{-\lambda k \mu \tau}$, $\zeta_{xy}(\tau) = 0$ and detailed balance is restored, with $T_{\text{eff}} = T$. Another example analytically solvable involves a fluid of active particles. We will treat it in Chapter 4.

3.3.2 Two probes in a stirred fluid

We consider a one-dimensional system $(d = 1)$ consisting of $N_p = 2$ probes under harmonic confinement and $N = 100$ fluid particles moving freely in a periodic domain $x_k \in [0, L]$, as sketched in Fig. 3.2. The fluid is driven out of equilibrium by an external constant force f that induces a net particle current $\jmath$ thanks to the periodic boundary conditions. The Langevin equation for the fluid particles,

$$\dot{x}_k = \mu f - \mu \frac{\partial}{\partial x_k} \left(V(\{x\}) + U_1(x_k, X_1) + U_2(x_k, X_2) \right) + \sqrt{\frac{2\mu}{\beta}} \xi_k \qquad (3.39)$$
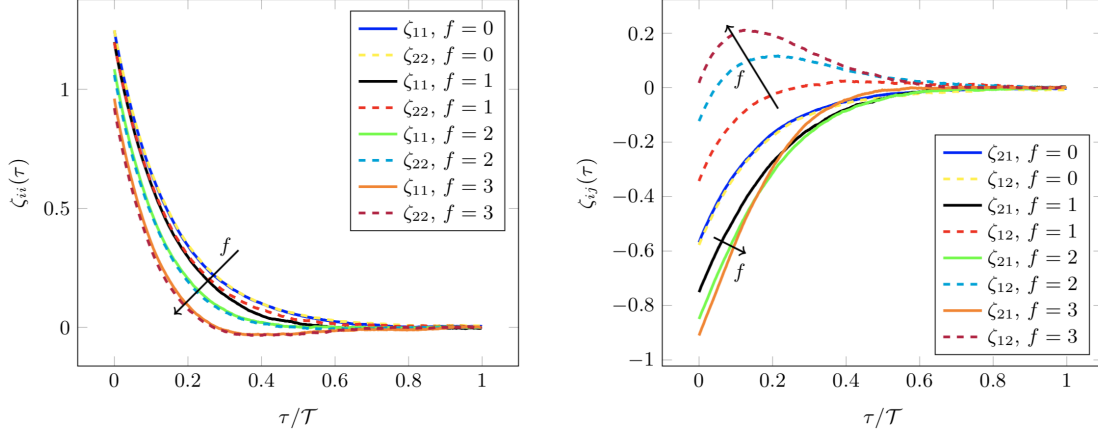
Figure 3.3: Diagonal (left panel) and off-diagonal (right panel) elements of the friction kernel $\zeta_{ij}(\tau)$ as function of time $\tau = t - s$, obtained by numerical evaluation of (3.12) in Brownian dynamics simulations, for various values of the nonequilibrium driving force f and $\beta = 1$, $\mu = 1$, $\sigma = 0.5$, $\sigma_p = 1$.

where, for $i = 1, 2$

$$V(\{x\}) = \sum_{k'=1}^{N} e^{-\frac{1}{2\sigma^2}(x_k - x_{k'})^2}, \quad U_i(x_k, X_i) = e^{-\frac{1}{2\sigma_p^2}(x_k - X_i)^2} \tag{3.40}$$

are respectively the particles mutual interaction and the coupling with the probes. They are both Gaussian soft repulsive potential with different characteristic length, namely σ and σ_p respectively, but we have checked numerically that anharmonic potentials lead to qualitatively similar results. While our investigation is only numerical, an analytical study of a similar system, provided that the particles mutual interaction is neglected, has been carried out in [154], aiming to estimate the probes steady state distribution. Differently, we focus on some dynamical properties of the probes. In particular, we have calculated the time-dependent entries of the friction kernel ζ_{ij} from formula (3.12) for various values of the external driving f. This was done by letting the fluid relax from an initial uniform density, fixing the probes in their preferred positions Y_i, and then performing the steady-state averages in (3.12) over 2×10^4 independent simulation runs of duration $\mathcal{T} = 10^3$. For $f \to 0$, equilibrium conditions are recovered. The diagonal elements ζ_{ii} of the friction kernel are positive and exhibit a monotonic time dependence. The two off-diagonal elements ζ_{12} and ζ_{21}, which quantify the mutual frictional forces between the probes, coincide. As expected, they are negative and decay to zero at late times according to a relaxation time stated by the dynamical features. Their negative sign can be understood on the basis of global momentum conservation. For example, consider the drag force

that probe 1 exerts on probe 2,

$$F_{1\to 2}^{\text{drag}} = -\int_{-\infty}^{t} \mathrm{d}s\, \zeta_{21}\left(t - s\right) \dot{X}_1\left(s\right). \tag{3.41}$$

It is easy to convince oneself that, given the configuration sketched in Fig. (3.2), a positive velocity $\dot{X}_1$ will on average cause a positive displacement of the fluid particles surrounding probe 1. Such perturbation spreads along the coordinate axis, from particle to particle, although dissipating part of the energy in the thermal environment, reaching probe 2, ultimately resulting in a positive momentum transfer $F_{1\to 2}^{\text{drag}} > 0$. This suggests that $\zeta_{21} \leqslant 0$ for all times, as well as for the propagation from probe 2 to probe 1, as depicted in the right panel of Fig. (3.3), blue solid and yellow dashed line for ζ_{21} and ζ_{12} respectively.

In contrast, with increasing nonequilibrium force $f > 0$, we observe a qualitative modification of the diagonal and non-diagonal elements of ζ_{ij}, as exemplified in Figs. (3.3). The diagonal elements ζ_{ii} develop a non-monotonic time dependence and eventually turn negative. Physically, this corresponds to a viscoelastic recoiling of the individual probe particles. A more dramatic, genuinely non-equilibrium effect is found for the off-diagonal elements $\zeta_{i\neq j}$. As revealed by the right panel of Fig. (3.3), the presence of a nonequilibrium flux in the bath breaks the symmetry of the friction matrix so that $\zeta_{ij} \neq \zeta_{ji}$, with $|\zeta_{21}|$ ($|\zeta_{12}|$) larger (smaller) with respect to equilibrium. Such an effect arises whenever a spatial asymmetry is imposed on top of broken detailed balance, analogously to a ratchet system [155]. Our periodic system is always spatially asymmetric unless $Y_1 - Y_2 = L/2$. Specifically, in the simulations, the probe reference positions are set to $Y_1 \approx L/3 < Y_2 \approx L/2$, and, for convenience, the trap stiffnesses K_i are chosen large enough to make the position Y_i almost coincide with the trap minimum Y_i^*. By increasing L, we checked that interactions with the periodic image particles are negligible. We conclude that global momentum conservation does not hold any more when the fluid dynamics becomes dissipative. This can be attributed to the asymmetric propagation (due to the current $\jmath$) of fluid perturbations. Namely, downstream propagation is progressively enhanced by increasing f, while upstream propagation is suppressed. As a result, the influence of probe 1 (2) on probe 2 (1) gets stronger (weaker) as we increase the driving. As for the diagonal elements, the sign of $\zeta_{12}(\tau)$ is transiently reversed. More remarkably, for sufficiently large values of f, the response coefficient of probe 2 to a uniform motion of probe 1, namely $\int_0^\infty \mathrm{d}\tau\, \zeta_{12}(\tau)$, turns positive. In contrast to the mentioned transient elastic recoil embodied in the diagonal terms ζ_{ii}, this kind of "absolute negative mobility" [156–159] is strictly forbidden in equilibrium, where dissipative transport coefficients depend only on the (positive) entropy production but not on the dynamical activity [105].

The dynamics of the system and the relaxation time of the friction kernel strongly depends on f. For the considered values the system exhibits a dissipation of the order of the thermal energy at the scale of the system size, i.e. $\beta f L \gg 1$ and thus called globally strong nonequilibrium regime [154], where the global refers to
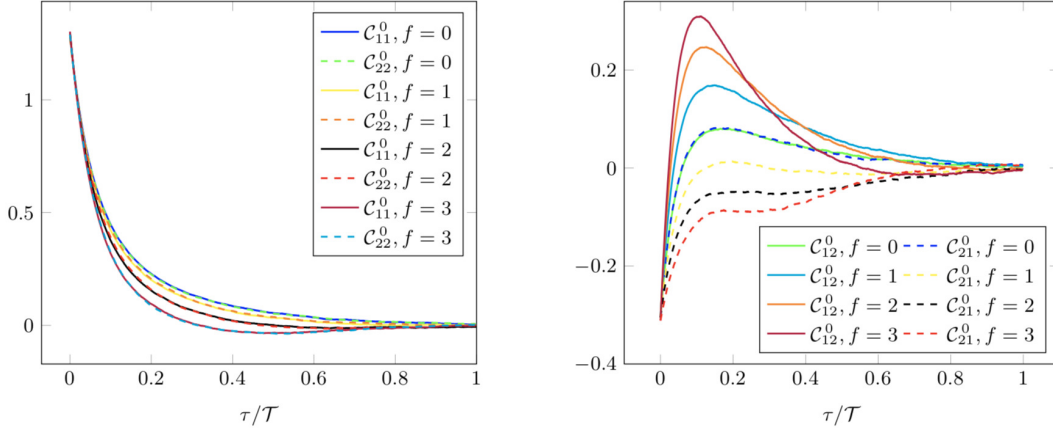
Figure 3.4: Diagonal (left panel) and off-diagonal (right panel) elements of the noise correlation as function of time $\tau = t - s$, obtained by numerical evaluation of (3.20) in Brownian dynamics simulations, for various values of the nonequilibrium driving force f and $\beta = 1$, $\mu = 1$, $\sigma = 0.5$, $\sigma_p = 1$.

the spatial scale. Higher value of f would drive the system to a so-called locally strong nonequilibrium regime, in which the same dissipation acts on a much shorter length scale, namely of the interaction range σ_p, i.e. $\beta f \sigma_p \gg 1$. Nonetheless, with increasing f, estimation of the friction assuming the probes fixed in the minimum is less and less reliable and the linear response theory for time-dependent perturbation must be employed [15]. For example, following the notation of the example, Y_i can be replaced by a deterministic trajectory $Y_i(t) = Y_i + vt$, where v is the linear velocity, $v = \mu f$, related to the fluid rotation frequency $\omega/2\pi = \mu f/L$.

Similarly we discuss the noise (3.19) felt by the two probes, whose correlations are given by (3.20). Their evolution as a function of time $\tau = t - s$ is depicted in Fig. 3.4. As we expected from the analysis of the friction kernel, the off-diagonal components of the noise matrix are not independent, namely the fluctuations of the probes are correlated due to the interaction mediated by the bath, even at equilibrium. The noise is not Markovian as the coupling g_i has a finite decorrelation time, nonetheless we have numerically proved that it still follows a Gaussian distribution for any value of f in Fig. (3.3). While at equilibrium the correlation $\mathcal{C}_{ij}$ completely defines the friction as stated by (3.22) and easily visible Fig. 3.4, with nonzero external driving substantial deviations emerge, implying the relevance of the frenetic contribution of the response function (2.28).

3.4 Markovian Limit

In Sec. 3.2 we have introduced a general theory to eliminate the fast degrees of freedom. While in Sec. 3.3 we have highlighted the features of the theory with two particular examples, in this Section we come back to the general theory. The GLE for the probes $\mathbf{X}_i = \mathbf{X}_i(t)$ is given by Eq. (3.26) and in general is neither Markovian nor Gaussian. A general solution of this equation is very complicate and probably not very enlightening. Therefore, relying on the already adopted approximations only, i.e. time-scale separation and weak-coupling limit, we pursue a simplified expression of (3.26). Intuitively and confirmed by the friction plots in Sec. 3.3, the memory kernel decays to zero with increasing time. The shorter is the decorrelation time, the faster the perturbation due to the probes fluctuations propagate through the fluid, which dissipates the extra energy into the heat bath and relaxes to a new nonequilibrium steady state labeled by the new probe configuration. Therefore an infinite time-scale separation that allows to treat the probes' dynamics as a quasi-static process relatively to the fluid dynamics is equivalent to taking the Markovian limit. This approximation is more reliable the shorter is the relaxation time of the memory kernel. The latter is directly affected by the dynamic parameters such as the fluid particles mobility, temperature, and the range of the mutual interaction σ and the coupling σ_p, respectively, introduced in (3.40). Namely, the bigger μ and β^{-1} the faster responds the fluid to the perturbation, which is quickly dissipated. On the other hand, the smaller σ (compared to the system size L), the longer is the relaxation time since the fluid particles interact on a shorter spatial scale and therefore share with more difficulty the excess energy coming from the perturbations. The same can be said for σ_p, provided that $\sigma_p > \sigma$ otherwise the colloids are effectively equal to the fluid particles and therefore it is no longer reliable to truncate the expansion around the minima of the probes confining potential to the linear order, necessary condition to employ the linear response theory [1]. From (3.41),

$$F_{j \to i}^{\mathrm{drag}} = -\dot{\mathbf{X}}_j \bar{\zeta}_{ij}, \quad \bar{\zeta}_{ij} = \int_{-\infty}^{t} ds \, \zeta_{ij}(t-s) \tag{3.42}$$

introducing a time-average friction $\bar{\zeta}_{ij}$, time-independent since the unperturbed dynamics is in the steady state. Therefore the Langevin equation becomes

$$M_i \ddot{\mathbf{X}}_i = \mathbf{K}_i + \langle \mathbf{g}_i \rangle^0 + \sum_{j=1}^{N_p} \left[\mathbf{G}_{ij} - \bar{\zeta}_{ij} \dot{\mathbf{X}}_j(t) \right] + \boldsymbol{\eta}_i \tag{3.43}$$

with noise correlation

$$\langle \boldsymbol{\eta}_i(t) \boldsymbol{\eta}_j(s) \rangle = \bar{\mathcal{C}}_{ij}^0 \delta(t-s), \quad \bar{\mathcal{C}}_{ij}^0 = \int_{-\infty}^{t} ds \, \langle \mathbf{g}_j(s); \mathbf{g}_i(t) \rangle^0. \tag{3.44}$$

---

[1] All those remarks are supported by numerical simulations checks.

entailing that for equilibrium systems FDT is still satisfied. Since the noise $\boldsymbol{\eta}$, in the weak-coupling limit is additive, we directly obtain the overdamped Langevin equation if we neglect the inertia term. The equations are still coupled,

$$\mathbf{K}_i + \langle \mathbf{g}_i \rangle^0 + \mathbf{G}_i - \sum_{j=1}^{N_p} \bar{\zeta}_{ij} \dot{\mathbf{X}}_j + \boldsymbol{\eta}_i = 0, \quad \mathbf{G}_i = \sum_{j=1}^{N_p} \mathbf{G}_{ij} \tag{3.45}$$

For the sake of simplicity we gather the drift terms $\mathbf{F}_i \left(\{ \mathbf{X} \} \right) = \mathbf{K}_i + \langle \mathbf{g}_i \rangle^0 + \mathbf{G}_i$ and we isolate the $\dot{\mathbf{X}}_i$ from the sum

$$\bar{\zeta}_{ii} \dot{\mathbf{X}}_i = \mathbf{F}_i \left(\{ \mathbf{X} \} \right) - \sum_{j \neq i}^{N_p} \bar{\zeta}_{ij} \dot{\mathbf{X}}_j + \boldsymbol{\eta}_i. \tag{3.46}$$

We decouple the equations for $N_p = 2$,

$$\bar{\zeta}_{11} \dot{\mathbf{X}}_1 = \mathbf{F}_1 \left(\{ \mathbf{X} \} \right) - \bar{\zeta}_{12} \dot{\mathbf{X}}_2 + \boldsymbol{\eta}_1$$
$$\bar{\zeta}_{22} \dot{\mathbf{X}}_2 = \mathbf{F}_2 \left(\{ \mathbf{X} \} \right) - \bar{\zeta}_{21} \dot{\mathbf{X}}_1 + \boldsymbol{\eta}_2 \tag{3.47}$$

If we assume linearity and isotropy for the potential interactions $\mathbf{K}_i = -K(\mathbf{X}_i - \mathbf{Y}_i)$,

$$\dot{\mathbf{X}}_1 = \frac{\bar{\zeta}_{22}}{|\bar{\zeta}|} \left[-K_{11} \left(\mathbf{X}_1 - \mathbf{Y}_1 \right) + K_{12} \left(\mathbf{X}_2 - \mathbf{Y}_2 \right) + \langle \mathbf{g}_1 \rangle^0 - \frac{\bar{\zeta}_{12}}{\bar{\zeta}_{22}} \langle \mathbf{g}_2 \rangle^0 + \tilde{\boldsymbol{\eta}}_1 \right]$$

$$\dot{\mathbf{X}}_2 = \frac{\bar{\zeta}_{11}}{|\bar{\zeta}|} \left[-K_{22} \left(\mathbf{X}_2 - \mathbf{Y}_2 \right) + K_{21} \left(\mathbf{X}_1 - \mathbf{Y}_1 \right) + \langle \mathbf{g}_2 \rangle^0 - \frac{\bar{\zeta}_{21}}{\bar{\zeta}_{11}} \langle \mathbf{g}_1 \rangle^0 + \tilde{\boldsymbol{\eta}}_2 \right] \tag{3.48}$$

where $|\bar{\zeta}| = \det \bar{\zeta} = \bar{\zeta}_{11} \bar{\zeta}_{22} - \bar{\zeta}_{12} \bar{\zeta}_{21}$,

$$K_{11} = \zeta_{21} \left(0 \right) \frac{\bar{\zeta}_{12}}{\bar{\zeta}_{22}} + \left(K - \zeta_{11} \left(0 \right) \right), \quad K_{12} = \zeta_{12} \left(0 \right) + \frac{\bar{\zeta}_{12}}{\bar{\zeta}_{22}} \left(K - \zeta_{22} \left(0 \right) \right) \tag{3.49}$$

$$K_{21} = \zeta_{21} \left(0 \right) + \frac{\bar{\zeta}_{21}}{\bar{\zeta}_{11}} \left(K - \zeta_{11} \left(0 \right) \right), \quad K_{22} = \left(K - \zeta_{22} \left(0 \right) \right) + \frac{\bar{\zeta}_{21}}{\bar{\zeta}_{11}} \zeta_{12} \left(0 \right) \tag{3.50}$$

$$\tilde{\boldsymbol{\eta}}_1 = \boldsymbol{\eta}_1 - \frac{\bar{\zeta}_{12}}{\bar{\zeta}_{22}} \boldsymbol{\eta}_2, \qquad \tilde{\boldsymbol{\eta}}_2 = \boldsymbol{\eta}_2 - \frac{\bar{\zeta}_{21}}{\bar{\zeta}_{11}} \boldsymbol{\eta}_1 \tag{3.51}$$

are the effective coupling coefficients and the noises respectively. The latter are linear combinations of the noises in (3.47) and therefore still white. Namely,

$$\langle \tilde{\boldsymbol{\eta}}_1 \left(0 \right) \tilde{\boldsymbol{\eta}}_1 \left(\tau \right) \rangle = \left[\bar{\mathcal{C}}_{11}^0 - \frac{2 \bar{\zeta}_{12}}{\bar{\zeta}_{22}} \bar{\mathcal{C}}_{12}^0 + \left(\frac{\bar{\zeta}_{12}}{\bar{\zeta}_{22}} \right)^2 \bar{\mathcal{C}}_{22}^0 \right] \delta \left(\tau \right)$$

$$\langle \tilde{\boldsymbol{\eta}}_2 \left(0 \right) \tilde{\boldsymbol{\eta}}_2 \left(\tau \right) \rangle = \left[\bar{\mathcal{C}}_{22}^0 - \frac{2 \bar{\zeta}_{21}}{\bar{\zeta}_{11}} \bar{\mathcal{C}}_{21}^0 + \left(\frac{\bar{\zeta}_{21}}{\bar{\zeta}_{11}} \right)^2 \bar{\mathcal{C}}_{11}^0 \right] \delta \left(\tau \right)$$

$$\langle \tilde{\boldsymbol{\eta}}_1 \left(0 \right) \tilde{\boldsymbol{\eta}}_2 \left(\tau \right) \rangle = \left[\left(1 + \frac{\bar{\zeta}_{12}}{\bar{\zeta}_{22}} \frac{\bar{\zeta}_{21}}{\bar{\zeta}_{11}} \right) \bar{\mathcal{C}}_{12}^0 - \frac{\bar{\zeta}_{21}}{\bar{\zeta}_{11}} \bar{\mathcal{C}}_{11}^0 - \frac{\bar{\zeta}_{12}}{\bar{\zeta}_{22}} \bar{\mathcal{C}}_{22}^0 \right] \delta \left(\tau \right)$$

$$\langle \tilde{\boldsymbol{\eta}}_2 \left(0 \right) \tilde{\boldsymbol{\eta}}_1 \left(\tau \right) \rangle = \left[\left(1 + \frac{\bar{\zeta}_{12}}{\bar{\zeta}_{22}} \frac{\bar{\zeta}_{21}}{\bar{\zeta}_{11}} \right) \bar{\mathcal{C}}_{21}^0 - \frac{\bar{\zeta}_{12}}{\bar{\zeta}_{22}} \bar{\mathcal{C}}_{22}^0 - \frac{\bar{\zeta}_{21}}{\bar{\zeta}_{11}} \bar{\mathcal{C}}_{11}^0 \right] \delta \left(\tau \right) \tag{3.52}$$

Note that all the effective coupling coefficient in (3.50) as well as the noise intensity in (3.52) depend on the one-time correlation of the unperturbed dynamics and are therefore a priori known. Eq. (3.48) is much easier than the initial GLE, being Markovian, due to the assumption of an infinitely fast fluid relaxation, and linearised by means of the introduction of effective coupling coefficients, and is suited for further investigation of the probes interaction mediated by the fluid.

3.5   Conclusion and Outlook

Employing nonequilibrium linear response theory we have derived GLEs for probe particles interacting with a driven environment. The latter was described by an explicit interacting many-body theory for overdamped colloidal particles. More generally, the colloids can be understood as a set of mesoscopic degrees of freedom. Also, the theoretical framework developed above can be easily adapted to cope with different sources of nonequilibrium (other than the nonconservative force f), such as a nonuniform bath temperature field $\beta(x_k)$. When only conservative forces are present, our theory correctly reproduces the expected equilibrium properties, i.e. it fulfils the FDT and conforms to Onsager's regression principle relating the fluctuations of statistical forces to the memory kernel. In general, it extends the Langevin approach into the nonequilibrium realm, predicting the violation of the FDT and the action-reaction law for the fluctuating effective forces. The breaking of these dynamical symmetries is traced back to the mismatch between the excess entropy and dynamical activity induced by probes fluctuations around their preferred states or, equivalently, to the existence of dissipative currents in the environment. We have shown that these phenomena appear already in simple systems, unless special symmetries are present. Namely, noise and friction felt by a single probe in a medium driven by a vortex do not obey the FDT, except if the relaxation timescales of system and fluid are properly tuned —in which case a constant effective temperature can be defined. Also, the cross-frictions between two confined probes in a stirred periodic fluid are dissimilar, and even change sign with respect to equilibrium, whenever the probe reference positions break the spatial symmetry. The theory allows to obtain quantitative information about the parameters of the environment from measuring average properties of the probes. For example, from (3.34) and (3.35) —which are accessible by measuring, e.g., the spectral density of the probe fluctuations in the trap and its response to a small external kick— the values of the relaxation times $k\mu$ and $h\mu$ can be inferred. Vice versa, one may even speculate that some mesoscopic parameters (e.g., $\zeta_{ij}(0)$) might be fixed at will by properly designing the non-conservative driving. It is in principle feasible since formal procedures are available [160] which determine an appropriate environment dynamics conditioned on prescribed mean values (e.g., those entering (3.12)).

Finally, a remark on the status of the approximation of weak coupling to the nonequilibrium environment seems in place. In a particle-based theory like the one we em-

ployed, this approximation is explicitly enforced by introducing a small coupling constant λ. Physically, the appropriate values λ may depend on the average number of bath particles the probes interact with. This should be clear from the example in Sec. 3.3.1, where the limit $N \to \infty$ produces an unphysical divergence of friction and noise strength if λ is not properly scaled. However, in practical applications, the weak coupling is often a dynamical, *emergent* property, resulting from the scale separation between the probe-particle system and the environment. For example, colloidal particles suspended in simple fluids are well described by a linear hydrodynamic theory, although the micro-dynamics of the fluid molecules is highly nonlinear. This feature is expected to be robust and to survive even far from equilibrium, as long as the driving energy input does not exceed the bath thermal energy [161]. Indeed, the peculiar feature of a time-dependent noise temperature, discovered within the weak-coupling approach, above, was already explicitly demonstrated (and its time-dependence analytically computed) in this setting [162]. Recently, new theoretical investigations [163, 164] have been spurred by a surge of experimental interest in systems with strongly coupled components, such as in active nonlinear micro-rheology [165], single-molecule (force spectroscopy) experiments [166], work extraction from active fluids [167]. Hence, it would be desirable to extend the above analysis to different dynamical descriptions of the environment, i.e. in terms (hydrodynamic) fields or discrete-state variables. This will possibly provide more versatile formal tools to account more reliably for the weak coupling and to address the strong coupling problem in a larger variety of stochastic systems.

Chapter 4

Passive colloid in an active bath

4.1 Introduction

Chapter 3 presented a general way to perform the coarse-graining of a many-body system, based on a time-scale separation of its own degrees of freedom, classified into fast and slow. The elimination of the fast ones strongly simplifies the initial system, now described by effective dynamics, characterised by emergent behaviour, absent before the coarse-graining. In equilibrium, the coarse-graining is helped by the existence of a thermodynamic free energy, whereas, from from equilibrium, it must be explicitly carried on and counterintuitive effects can arise. For example, surprising (with respect to the equilibrium case) experimental and numerical results have been found investigating the depletion forces of externally sheared bath [119, 134, 154, 168, 169] and of active particles [67, 170–173].

Active matter and, in particular, passive colloids embedded in an active particles fluid have recently attracted increasing interest. Due to the persistent dynamics, active particles experience non-Gaussian fluctuations and it has been experimentally observed [174, 175] that these fluctuations can be transmitted to the colloid, so that it behaves in a significantly different way from a passive Brownian particle in a thermal bath: e.g. it exhibits super-diffusion at short times, followed by normal diffusion at longer times and its distribution of the displacement shows non-Gaussian behaviour like exponential tails [176–178] or multiple peaks [77]. All these works, consistently with the experimental findings, consider as model for the effective dynamics for the colloid(s), the active Brownian particles model (ABPs) [61], that describes a single active particle in contact with a thermal environment. This choice is phenomenology-oriented and not based on on a coarse-graining from the microscopic dynamics. In this Chapter, we prove this choice to be legitimate and based on rigorous assumptions on the microscopic Langevin equation of the active particles environment. The discussion of the results in this Chapter follows the same structure of [17], still in preparation. Employing the theory introduced in Chapter 3 we are able to derive the effective equation for a colloid in an active particles fluid which, for a generic coupling will be equal to (3.26) for $N_p = 1$. Nonetheless, the active features are hid-

den in the correlations involving the coupling g (see (3.19) and (3.12)) and, thus, not very enlightening. For this purpose, we restrict our investigation to a toy model, i.e. a fluid of non-interacting active particles linearly coupled to the colloid. Although this model, introduced in Sec. 4.2, is very artificial compared to most practical realisation, is able to grasp many of the cited features. Interestingly, in the overdamped limit it boils down to the well known ABP model introduced in Sec. 2.4. Namely, under certain conditions stressed in Sec. 4.4 a passive colloid in an active bath behaves similarly to an active particles in a passive environment. A detailed discussion of its moments, presented in Sec. 4.5 accounts for the enhanced diffusion and the broadening of the position distribution, experimentally observed. In Sec. 4.5.1 and 4.5.2 we investigated the non-linear regime performing an analytical perturbative expansion and numerical simulations, respectively. We introduce a small non-linear force in the linear model and through perturbation theory expansion we estimate the first-order correction to the linear mean square displacement. Neglecting non-Gaussian correlations of the noise, this result is quite general for any force, but the correction can be analytically calculated only in few cases, e.g. a quartic potential, presented in Sec. 4.5.1. Next we simulate a fluid of active particles coupled to the colloid with a non-linear potential extracting the colloid position distribution aiming to confirm the analytical prediction. The variance obtained from the stationary position distribution, which in the considered regime is well-approximated by a Gaussian distribution, is compared with the variance provided by the toy model via a simple mapping. Namely, through the introduction of an effective parameter in the toy model one is able to replicate the position distribution observed for the complete model (probe + active particles) with a priori known error and to enrich the toy model predictability with non-linear corrections.

4.2 Model

We consider a 2D-deterministic colloid $\mathbf{X} = \mathbf{X}(t)$ under harmonic confinement, is linearly coupled to a bath of active Brownian particles $\{\mathbf{x}_j = \mathbf{x}_j(t)\}_{j=1}^N$ described by a set of Langevin equations. The active particles are not mutually interacting. The equations of motion are

$$M\ddot{\mathbf{X}} = -K\mathbf{X} - \frac{k}{N}\sum_{j=1}^N \left(\mathbf{X} - \mathbf{x}^j\right) \tag{4.1}$$

$$\dot{\mathbf{x}}^j = v_0\mathbf{n}^j + \frac{k\mu}{N}\left(\mathbf{X} - \mathbf{x}^j\right) + \sqrt{2\mu T}\boldsymbol{\xi}^j \tag{4.2}$$

for the colloid and for the fluid particles respectively. The configuration is equal to the one depicted in Fig. 3.1 with just one (blue) probe. Note that here the pre-factor N^{-1}, necessary to keep the energy extensive, takes the place of λ in Chapter 3, in agreement with the discussion in Sec. 3.5. The active particles are in contact with a thermal bath that provides for temperature T and mobility μ. Being internally

driven, they exhibit a drift velocity of constant magnitude v_0 pointing along the random particle orientation $\mathbf{n} = \mathbf{n}(\theta)$, characterised by the Wiener process $\dot{\theta}^j = \sqrt{2D_r}\xi_\theta^j$, with D_r the rotational diffusion coefficient. Here $\boldsymbol{\xi}^j$ and ξ_θ^j are standard Gaussian white noises with zero average and delta-correlation in time. K and k are the stiffness of the harmonic confinement potential of the colloid and the colloid-particle coupling coefficient, respectively. M is the colloid mass, while the active particles mass is set to 1. For such a toy model the elimination of the fast (active) degrees of freedom is exact and does not require any approximation. The GLE for the colloid after the-coarse-graining reads,

$$M\ddot{\mathbf{X}} = -K\mathbf{X} - \int_{-\infty}^{t} ds\, \dot{\mathbf{X}}(s)\,\gamma(t-s) + \boldsymbol{\Gamma} \tag{4.3}$$

where

$$\gamma(t-s) \equiv k e^{-\frac{k\mu}{N}(t-s)} \tag{4.4}$$

$$\boldsymbol{\Gamma} \equiv \int_{-\infty}^{t} ds\, \gamma(t-s)\,\boldsymbol{\eta}(s) \tag{4.5}$$

$$\boldsymbol{\eta} \equiv \frac{1}{N}\sum_{j=1}^{N}\left(v_0\mathbf{n}^j + \sqrt{2\mu T}\boldsymbol{\xi}^j\right) = \frac{1}{N}\sum_{j=1}^{N}\boldsymbol{\eta}^j \tag{4.6}$$

are respectively the colloid friction (memory) kernel, the colloid noise, and the stochastic contribution in (4.2) for the active particles. Interestingly, the coupling with the active particles is treated as a fluctuating noise (4.5), endowed with non-thermal features, due to the exponential tails already present in the active particles noise statistics and naturally propagated to the colloid one. Its stationary probability distribution, see Fig. 4.1, for non-zero active velocity, can exhibit two peaks (a ring in a 3D plot [179]), whose distance grows with increasing (decreasing) v_0 (D_r) or, more precisely, with increasing persistence length defined as $v_0 D_r^{-1}$. This effect, induced by the external confinement, is a manifestation of the phenomenon of wall accumulation [59, 60, 74], which is well-known for active particle. Noteworthy, the bimodality is not to be attributed to the well-known behaviour of the residence time for a harmonic oscillator at equilibrium. This is true in the overdamped regime, while in the underdamped, due to the presence of friction, the oscillations are quickly dissipated leading to a one-peak zero-centred distribution in the steady state. On the contrary, for active particles it is a genuine nonequilibrium effect valid in any regime of damping. Intuitively, the persistent motion restores the ballistic, and thus oscillatory, behaviour of the system, no longer dominated by the thermal diffusion. For $N > 1$ the phenomenon disappears since the independence of the active particles forces the noise distribution to obey the central limit theorem. For $N > 1$ the distribution becomes unimodal and broadens with increasing v_0. In Sec. 4.5 will discuss the dependence on activity of its lowest moments. In Sec. 4.3 and 4.4 we will analyse two extreme cases, namely, the low-friction underdamped motion and the
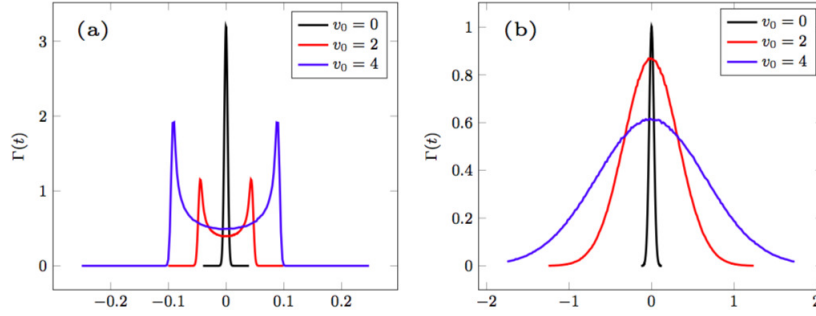
Figure 4.1: (a) Noise distribution for $N = 1$. (b) Noise distribution for $N = 100$. In both cases we consider $\mu = D_r = T = 1$, $k = 2$ and $v_0 = 0, 2, 4$.

overdamped regime, respectively. Since the environment is driven out of equilibrium, iff $v_0 \neq 0$, the friction (4.4) and the noise (4.5) emerging from the coarse-graining of the dynamics do not satisfy FDT, meant as balance between energy input and output. Namely for $\tau > 0$,

$$\langle \boldsymbol{\Gamma}(0)\,\boldsymbol{\Gamma}(\tau) \rangle = T\gamma(\tau) + \frac{v_0^2}{2\mu} \frac{k}{\frac{k^2\mu^2}{N^2} - D_r^2} \left(\frac{k\mu}{N} e^{-D_r\tau} - D_r e^{-\frac{k\mu}{N}\tau} \right). \qquad (4.7)$$

with $(k\mu/N)^{-1}$ the characteristic time-scale it takes the active particles to relax in the coupling potential and D_r^{-1} is the time needed to fully randomise the direction of the active velocity, respectively. Eq. (4.7) shows that the dissipation happens on the time scale $(k\mu/N)^{-1}$, while the energy input due to the noise is found to occur on multiple timescales, i.e. $(k\mu/N)^{-1}$ and D_r^{-1} respectively. The disparity of the time scales for noise and friction entails the breakdown of the FDT, as predicted by (3.21). One may try to mend it by introducing an effective temperature [180] via

$$\beta T_{\text{eff}} = 1 + \frac{\beta}{2\mu} \frac{v_0^2}{\left(\frac{k\mu}{N}\right)^2 - D_r^2} \left(\frac{k\mu}{N} e^{\left(\frac{k\mu}{N} - D_r\right)\tau} - D_r \right) \qquad (4.8)$$

Thereby, the FDT (3.22) is formally restored, albeit with the time-dependent function $T_{\text{eff}}(\tau)$ replacing the constant bath temperature $1/\beta$. In the weak coupling limit $k\mu/ND_r \ll 1$ we can expand (4.8) and obtain a more intuitive expression,

$$\beta T_{\text{eff}}(\tau) = 1 + \frac{\beta v_0^2}{2\mu D_r} \left(1 - R e^{-D_r\tau} \right) + \mathcal{O}(k^2/N^2) . \qquad (4.9)$$

The deviation from equilibrium is seen to be governed by the two dimensionless numbers $\beta v_0^2/2\mu D_r$ and $R \equiv k\mu/ND_r$. The former compares the active energy to the thermal one, while the latter compares the two characteristic times introduced in (4.7). For $R \to 0$, the temperature renormalisation becomes time-independent

and independent of the coupling coefficient k—it thus acquires the status of thermodynamic temperature. One can then justly say that the probe acts as an ideal measurement device for the constant effective temperature

$$T_{\text{eff}} = T + \frac{v_0^2}{2\mu D_{\text{r}}} \tag{4.10}$$

of the active fluid itself, which coincides with the known value for a suspension of free active particles [181, 182]. The $R \to 0$ limit leads to a regime characterised by a very short angular decorrelation time D_{r}^{-1} and thus a small persistence length, defined as $v_0 D_{\text{r}}^{-1}$, for the active particles dynamics which becomes equivalent to an equilibrium Brownian motion coupled to a hotter heat bath. Namely, the motion is enough random to define a physically meaningful effective temperature. The opposite limit, characterised by a high persistence length forces the dynamics to be quasi-ballistic and more predictable. In this regime the system is close to the example with the vortex we treated in Sec. 3.3.1. Similarly, the effective temperature in the quasi-ballistic regime diverges exponentially as clearly shown in (4.8).

The strength of the temperature renormalisation is controlled by the Peclét number $v_0(\mu D_{\text{r}}/\beta)^{-1/2}$ that weighs the relative importance of ballistic versus (translational and rotational) diffusive motion [68]. To first order in k/N, Eq. (4.10) exhibits a crossover from a short-time temperature to a long-time temperature. Moreover, T_{eff} can no longer be interpreted as a property of the particle bath alone, but characterises its interaction with the embedded probe. In fact, the ratio R can be interpreted as a measure for the interference of the coupling potential with the persistence of the active particles motion. The physical picture is that the apparent thermalisation at the constant effective temperature (4.10) takes some finite time to happen. In our toy model, this "equilibration time" is given by the rotational diffusion time of the active particles; i.e., the active motion of the bath particles can only be subsumed into an enhanced fluid temperature once it has lost its orientational persistence. This very plausible condition has been pointed out before (e.g. in [81]), albeit not for the time domain.

4.3   Fourier Analysis

Due to the memory kernel, (4.3) can be more easily solved considering a (time) Fourier Transform (FT) for $\mathbf{X}$, γ and $\mathbf{\Gamma}$. Namely,

$$\tilde{\mathbf{X}}(\omega) = \tilde{\mathbf{\Gamma}}(\omega)\,\mathcal{R}_{\tilde{\mathbf{X}}}(\omega), \quad \mathcal{R}_{\tilde{\mathbf{X}}}(\omega) = \frac{1}{K - M\omega^2 - i\omega\tilde{\gamma}^+(\omega)} \tag{4.11}$$

where $\tilde{\gamma}^+(\omega)$ is the FT of $\gamma^+(\tau) = \gamma(\tau)\theta(\tau)$, the retarded friction kernel, and $\mathcal{R}_{\tilde{\mathbf{X}}}$ is the response function to the position. Since the noise is zero-average and the harmonic confinement is centred in zero, $\langle\mathbf{X}\rangle = 0$. The colloid position correlation

can be obtained in terms of the colloid response function $\mathcal{R}_{\tilde{\mathbf{X}}}$,

$$S_{\tilde{\mathbf{X}}}(\omega) = \left\langle \tilde{\mathbf{X}}(\omega)\, \tilde{\mathbf{X}}^*(\omega) \right\rangle = |\mathcal{R}_{\tilde{\mathbf{X}}}(\omega)|^2\, S_{\tilde{\mathbf{\Gamma}}}(\omega), \tag{4.12}$$

with a noise correlation presenting thermal and active contributions:

$$S_{\tilde{\mathbf{\Gamma}}}(\omega) = \left\langle \tilde{\mathbf{\Gamma}}(\omega)\, \tilde{\mathbf{\Gamma}}^*(\omega) \right\rangle = S_{\tilde{\mathbf{\Gamma}}_{\mathrm{eq}}}(\omega) + S_{\tilde{\mathbf{\Gamma}}_{\mathrm{act}}}(\omega) \tag{4.13}$$

The correlation of the thermal (equilibrium) noise is given by the fluctuation-dissipation relation (FDR) $S_{\tilde{\mathbf{\Gamma}}_{\mathrm{eq}}}(\omega) = 2T\mathrm{Re}\tilde{\gamma}^+(\omega)$, while the active correction in (4.13) reads

$$S_{\tilde{\mathbf{\Gamma}}_{\mathrm{act}}}(\omega) = \int_{-\infty}^{\infty} d\tau\, \langle \mathbf{\Gamma}_{\mathrm{act}}(\tau)\, \mathbf{\Gamma}_{\mathrm{act}}(0) \rangle\, e^{i\omega\tau}. \tag{4.14}$$

Using the known two-times noise correlation [16], from (4.14) we obtain

$$S_{\tilde{\mathbf{\Gamma}}_{\mathrm{act}}}(\omega) = \frac{1}{N} \frac{k^2 v_0^2 D_{\mathrm{r}}}{(\omega^2 + k^2\mu^2/N^2)(\omega^2 + D_{\mathrm{r}}^2)}. \tag{4.15}$$

Therefore the position correlation becomes,

$$S_{\tilde{\mathbf{X}}}(\omega) = 2\, |\mathcal{R}_{\tilde{\mathbf{X}}}(\omega)|^2\, \mathrm{Re}\tilde{\gamma}^+(\omega)\, \mathcal{T}_{\mathrm{eff}}(\omega) = \frac{2}{\omega}\, \mathrm{Im}\mathcal{R}_{\tilde{\mathbf{X}}}(\omega)\, \mathcal{T}_{\mathrm{eff}}(\omega), \tag{4.16}$$

where we have introduced the real part of the memory kernel and the frequency-dependent effective temperature

$$\mathrm{Re}\tilde{\gamma}^+(\omega) = \frac{1}{N} \frac{k^2\mu}{k^2\mu^2/N^2 + \omega^2}, \quad \mathcal{T}_{\mathrm{eff}}(\omega) = T + \frac{v_0^2}{2\mu D_{\mathrm{r}}} \frac{D_{\mathrm{r}}^2}{\omega^2 + D_{\mathrm{r}}^2}. \tag{4.17}$$

respectively. The latter is depicted in Fig. 4.2: activity strongly enhances its value, but not the position of its maximum, coinciding with the characteristic frequency, which is always zero. This is in contrast to what has been found for the frequency-dependent temperature of a colloid coupled to a constantly driven particle [183], whose maximum depends on the external forcing. The position correlation in the time domain is given by the anti-transform of (4.16),

$$S_{\mathbf{X}}(\tau) = \frac{1}{2\pi} \int_{-\infty}^{+\infty} d\omega S_{\tilde{\mathbf{X}}}(\omega)\, e^{-i\omega\tau} \tag{4.18}$$

while the value of the second moment of the position, $\langle \mathbf{X}^2 \rangle = S_{\mathbf{X}}(\tau = 0)$ is given by,

$$\langle \mathbf{X}^2 \rangle = \frac{1}{2\pi} \int_{-\infty}^{+\infty} d\omega S_{\tilde{\mathbf{X}}}(\omega) \tag{4.19}$$

Due to the complexity of the response function such integral is calculable only numerically. An analytical result is obtainable in the important limit of small friction.
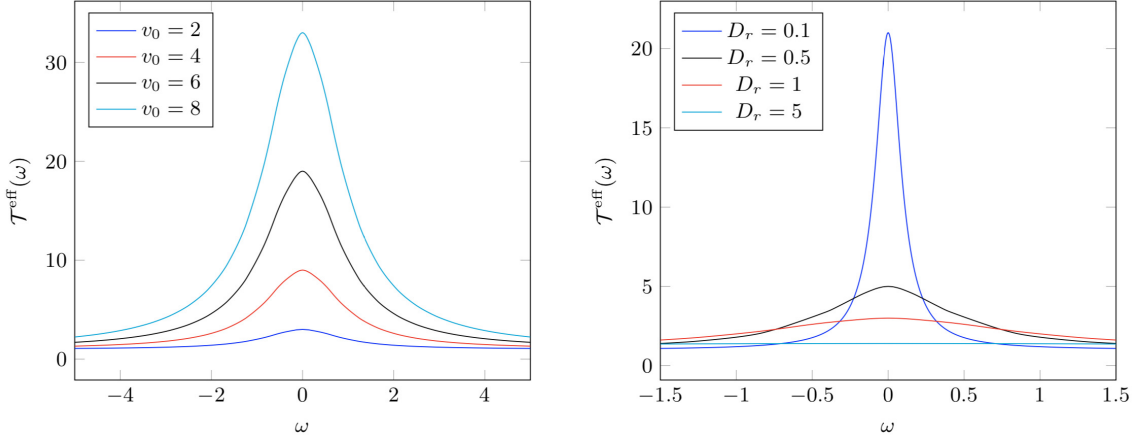
Figure 4.2: Effective temperature (4.17) as a function of the frequency ω for different values of v_0 and D_r left and right panel respectively.

In this case, the system oscillates at the characteristic frequencies, $\omega_0 = \pm\sqrt{K/M}$, imposed by the harmonic confinement, so that only those frequencies are excited in the spectrum of $\mathcal{T}_{\text{eff}}(\omega)$. Formally, if $\tilde{\gamma} \ll 1$, equivalent to $k\mu/N \gg 1$, then $\text{Re}\tilde{\gamma}^+ \gg \text{Im}\tilde{\gamma}^+$ and (4.19) simplifies to

$$\langle \mathbf{X}^2 \rangle \approx \int_{-\infty}^{+\infty} \frac{d\omega}{2\pi} \frac{S_{\tilde{\mathbf{\Gamma}}}(\omega)}{(K - M\omega^2)^2 + \omega^2 \left(\text{Re}\tilde{\gamma}^+(\omega)\right)^2}. \tag{4.20}$$

Following [184] we approximate the response with a delta function centred in its poles, valid if $\text{Re}\tilde{\gamma}^+ \ll 1$, and we obtain

$$\langle \mathbf{X}^2 \rangle \approx \frac{1}{K} \left(T + \frac{v_0^2}{2\mu D_{\text{r}}} \frac{D_r^2}{\frac{K}{M} + D_{\text{r}}^2} \right) \tag{4.21}$$

In the small-friction regime, as anticipated, the poles of the response function, $\pm\omega_0$, are proportional to the stiffness of the confining potential. This has relevant implications if the colloid is employed as a heat engine. Namely, a time-dependent potential whose stiffness changes periodically between two values $K_+ > K_-$, can induce a cyclic motion on the colloid, so that heat and work will be exchanged with the active bath, at a certain efficiency–the latter quantities being defined according to Stochastic Thermodynamics [6,185]. Active particles engines are treated in details in Chapter 5, here we highlight that the independence from D_{r} or v_0 of the maximum of the effective temperature $\mathcal{T}_{\text{eff}}(\omega)$ has strong consequences on the performance of such heat engine. For example, consider the Otto cycle discussed in [183] (albeit the same conclusions can be drawn for a Stirling cycle as well). The latter is established changing instantaneously the stiffness from K_- to K_+ followed by a thermalisation

at a hotter temperature with constant stiffness. Then, the stiffness is reduced to the initial value K_- followed by a relaxation which brings the system to the initial configuration. The mean square position (4.21), changes during the cycle and it is used to define (average) work and heat

$$\langle W \rangle \equiv \frac{1}{2} \int_i^f dK \left\langle X^2 \right\rangle, \qquad \langle Q \rangle \equiv \frac{1}{2} \left[K \left\langle X^2 \right\rangle \right]_i^f - \langle W \rangle \qquad (4.22)$$

from an initial state i to a final state f. The bigger the change in effective temperature during the cycle for a fixed variation of the stiffness, the more efficient the engine. If the maximum of $\mathcal{T}_{\text{eff}}(\omega)$ could be shifted away from zero (e.g. increasing the distance from equilibrium of the working fluid, as in [183]), increasing the stiffness (or equivalently ω_0), would increase the particle variance $\langle \mathbf{X}^2 \rangle = \mathcal{T}_{\text{eff}}(\omega_0)/K$. This is necessary to build the cycle described above and to make it run as a heat engine, extracting positive work. This is the case, for example, when the nonequilibrium is due to a constant external driving as discussed in [183]. On the contrary, eq. (4.17) clearly shows that the effective temperature can be increased only reducing the stiffness, i.e. by expanding the volume where the colloid is confined. Namely, a cycle which employs an active particle bath behaves as a heat engine only if the expansion is performed at the cooler temperature, otherwise it behaves like a heat pump. We will come back to this counterintuitive effect, due to the nature of this effective temperature, in Sec. 5.6.1.2.

4.4 Overdamped Limit

Since for typical micro-sized colloidal particles velocity fluctuations decorrelate on a much faster time scale compared to positions/orientation, we are interested in the overdamped limit of (4.3). If we neglect inertia in (4.3),

$$k \int_{-\infty}^t ds\, \dot{\mathbf{X}}(s)\, e^{-\frac{k\mu}{N}(t-s)} = -K\mathbf{X} + \mathbf{\Gamma} \qquad (4.23)$$

If the fluid particles equilibrate quickly ($k\mu/N \gg 1$), we approximate the exponential in with a δ-function taking the limit $k\mu/N \to \infty$, [186]. Proceeding similarly with the noise (4.5), we arrive at

$$\dot{\mathbf{X}} = -\frac{K\mu}{N}\mathbf{X} + \boldsymbol{\eta} \qquad (4.24)$$

with noise properties,

$$\langle \boldsymbol{\eta} \rangle = 0, \quad \langle \boldsymbol{\eta}(0)\,\boldsymbol{\eta}(\tau) \rangle = \frac{2\mu T}{N}\delta(\tau) + \frac{v_0^2}{2N}e^{-D_\mathrm{r}|\tau|} \qquad (4.25)$$

since thermal and active noises are assumed to be independent. Eq. (4.24) is one of the main results of this Chapter. Starting from a microscopic description of the probe

in an active bath, we are able to conclude that the effective overdamped equation for the confined colloid is equivalent to a ABP process with the active contribution included into a noise term, which is non-Markov and non-Gaussian. Deviations from Gaussianity are not visible from (4.25), but will be treated in Sec. 4.5. Namely, the colloid can be thought of as coupled to two environments, one active and one thermal, characterised by different properties and, thus, affecting in different way the dynamics of the colloid. Noteworthy, (4.24) is mathematically equivalent to the ABP equation introduced in Sec. 2.4 to describe an active particle coupled to a thermal environment, entailing that a passive particle in an active environment behaves like an active particle in a passive environment. Such double interpretation plays an important role in Chapter 5.

Eq. (4.24) has been used in several works [177, 187, 188]. Here, we have derived it from a mean-field model for the linearly coupled dynamics of probe and active particles. Note that the analogy with previous approaches is complete once we identify $\mu/N \overset{N\to\infty}{\Longrightarrow}$ constant as the dressed mobility of the colloid. One last remark concerns the rotational diffusion of the colloid. Looking at (4.25) the intensity of the active noise is reduced by N, but the decorrelation time is the same as for fluid particles, i.e. D_{r}. Intuitively this is not realistic, since, upon including hydrodynamic interaction, the effective rotational diffusion of the colloid should be the result of a collective effect of the fluid particles, which cannot be explained with our toy model.

4.5   Moments

In this section we study the average dynamics of the colloid displacement in the steady state. From (4.25), $\langle \mathbf{X} \rangle = 0$ evidently, while for $\tau > 0$,

$$\langle \mathbf{X}(\tau)\,\mathbf{X}(0) \rangle = \frac{T}{K} e^{-\frac{K\mu}{N}\tau} + \frac{v_0^2}{2K\mu D_{\mathrm{r}}} \frac{1}{R^2 - 1} \left[R e^{-D_{\mathrm{r}}\tau} - e^{-\frac{K\mu}{N}\tau} \right] \tag{4.26}$$

where $R \equiv K\mu/N D_{\mathrm{r}}$ has been introduced in Sec. 4.2. For $\tau = 0$ (4.26) boils down to

$$\langle \mathbf{X}^2 \rangle = \frac{1}{K} \left(T + \frac{v_0^2}{2\mu D_{\mathrm{r}}} \frac{1}{R + 1} \right) \tag{4.27}$$

If $R \ll 1$, $\langle \mathbf{X}^2 \rangle \approx T_{\mathrm{eff}}/K$, the dynamics is an equilibrium-like Brownian motion at an increased temperature [181, 182, 189], given by (4.10), so that the colloid behaves like an equilibrium Brownian particle in contact with a hotter reservoir. If $R \gg 1$, $\langle \mathbf{X}^2 \rangle \approx (T + v_0^2/(2\mu D_{\mathrm{r}} R))/K$. The potential then strongly confines the quasi-ballistic active dynamics, entailing a smaller effective temperature compared to (4.10).

Due to the noise symmetries, it is straightforward to show that $\langle \mathbf{X}^3 \rangle = 0$, i.e. zero skewness for the position distribution [77]. The fourth moment $\langle \mathbf{X}^4 \rangle$, which gives

information about deviations from Gaussianity, is derived in Appendix A.1,

$$\langle \mathbf{X}^4 \rangle = \frac{3T}{K^2} \left(T + \frac{v_0^2}{\mu D_r} \frac{1}{R+1} \right) + \frac{3}{2} \left(\frac{v_0^2}{2\mu D_r} \right)^2 \frac{1}{NK^2} \frac{3R+4}{(R+1)(R+2)(3R+1)} \quad (4.28)$$

From (4.27) and (4.28) we calculate the kurtosis, i.e. $\kappa = \langle \mathbf{X}^4 \rangle / \langle \mathbf{X}^2 \rangle^2 - 3$,

$$\kappa = \frac{3}{2} \frac{\left(\frac{v_0^2}{2\mu D_r} \right)^2}{\left(T + \frac{v_0^2}{2\mu D_r} \frac{1}{R+1} \right)^2} \frac{\frac{1}{N} \frac{(3R+4)(R+1)}{(R+2)(3R+1)} - 2}{(R+1)^2} \quad (4.29)$$

which becomes

$$\kappa \underset{R \ll 1}{\approx} -3 \frac{N-1}{N} \left(1 - \frac{T}{T_{\text{eff}}} \right)^2 < 0, \qquad \kappa \underset{R \gg 1}{\approx} -\frac{3}{2} \frac{2N-1}{N} \left(\frac{1}{\frac{TR}{T_{\text{eff}} - T} + 1} \right)^2 < 0 \quad (4.30)$$

in the close-to-equilibrium regime ($R \ll 1$) and in the high-persistency regime ($R \gg 1$), respectively. Typical values for a $1\,\mu$m-radius particle are: $v_0 \sim 10^{-5}\text{m s}^{-1}$, $k_B T \sim 3 \cdot 10^{-21}\text{kg m}^2\,\text{s}^{-2}$, $D_r \sim 10^{-1}\,\text{s}^{-1}$ and $\mu \sim 10^8\,\text{kg}^{-1}\text{s}$, so that $T_{\text{eff}} \gg T$. In both regimes the kurtosis is negative, converges to zero from below [188] as $T_{\text{eff}} \to T$ and strongly depends on the effective temperature and may converge to the saturation value $\kappa \approx -3$ for some choices of the parameters able to strongly enhance the effective temperature. The negative kurtosis, associated to a broadening of the position distribution and to lighter tails (with respect to a Gaussian distribution which has by definition zero kurtosis), is a consequence of the fact that, as we already pointed out in this regime the dynamics is quasi-ballistic and very persistent. Namely, with respect to the low persistency regime and even more to an equilibrium Ornstein-Uhlenbeck process, the colloid spends less time around the minimum since forced to oscillate in the potential. Nevertheless, the strong confinement prevents the colloid from exploring regions further distant from the minimum and thus very rare and unlikely to reach, similarly indeed to a deterministic harmonic oscillator. Fig. 4.3 a) we compare the analytical formula (4.29) with a numerical simulation of (4.24). As obvious from (4.29), the kurtosis depends on many parameters, but as shown in Fig. 4.3 b)-c)-d), such effect reaches a saturation for large (or small) values of the parameters.

4.5.1   Beyond linear coupling: analytics

In Sec. 4.2 we have introduced an effective description for a many-body system. Assuming linear colloid-active particles coupling and non-interacting active particles, no approximation is required to eliminate the fast degrees of freedom and to shown that, in the overdamped limit, the colloid behaves like an ABP in contact with a thermal environment. The result remains correct, though less eye-catching, even relaxing these strong assumptions [16]. Treating the colloid as a perturbation to the
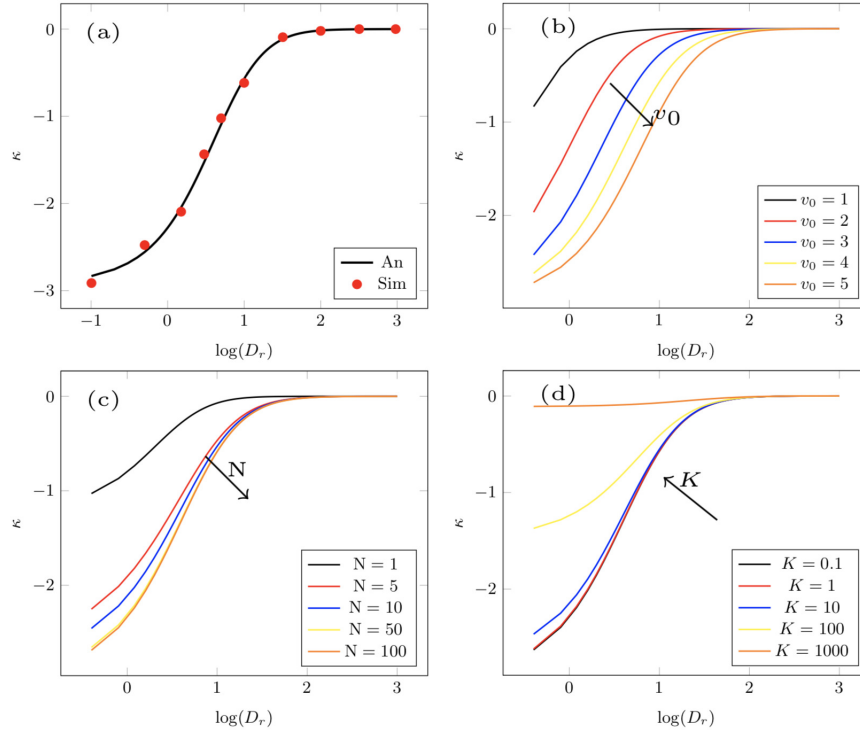
Figure 4.3: On panel (a) we compare the numerical results (dots) of colloid molecular dynamics with analytical result as a function of the 10-logarithm of D_r. The parameter are $T = K = \mu = 1$, $v_0 = 4$, $N = 30$. On panel (b)-(c)-(d) analytical curves of (4.29) for different value of v_0, N and K as a function of the 10-logarithm of D_r. The other parameters are the same.

fluid, the effective dynamics is expressed through the response function, averaged over the active particles fluid, see Chapter 3. Precisely in those averages the activity of the underlying environment implicitly survives, and therefore is not very informative. In this Section we perform a first step towards including a nonlinear force between probe and active particles, whose leading effect on the probe variance will be computed perturbatively.

We include in (4.2) the (potential) perturbation $\mathbf{f}(\mathbf{X}(t) - \mathbf{x}^j(t)) \equiv \mathbf{f}^j(t) = -\partial_{\mathbf{x}^j} U(\mathbf{X} - \mathbf{x}^j)$ $\forall j = 1, \ldots, N$ where U is a generic pair potential. Note that the perturbation is a function of the relative position between the colloid and the j-th particle. For the ease of notation we denote it as $\mathbf{r}^j(t) \equiv \mathbf{X}(t) - \mathbf{x}^j(t)$. The same perturbation influences the colloid dynamics (4.1). Consistently, we expand the process in powers of ε, namely, $\mathbf{x}^j = \mathbf{x}_0^j + \varepsilon \mathbf{x}_1^j + \mathcal{O}(\varepsilon^2)$ and $\mathbf{X} = \mathbf{X}_0 + \varepsilon \mathbf{X}_1 + \mathcal{O}(\varepsilon^2)$. We plug the expansion into (4.1) and (4.2) and we compare them order by order. Of course, the order ε^0 gives back the unperturbed dynamics. At the order ε, we find for the fluid

particles and the colloid, respectively,

$$\dot{\mathbf{x}}_1^j = -\frac{k\mu}{N}\mathbf{x}_1^j + \frac{k\mu}{N}\mathbf{X}_1 + \varepsilon\frac{\mu}{N}\mathbf{f}_0^j, \quad \forall j \tag{4.31}$$

$$M\ddot{\mathbf{X}}_1 = -(K+k)\mathbf{X}_1 + \frac{1}{N}\sum_{j=1}^{N}\left(k\mathbf{x}_1^j + \varepsilon\mathbf{F}_0^j\right), \tag{4.32}$$

where $\mathbf{f}_0^j \equiv \mathbf{f}(\mathbf{r}_0^j)$ is the zero order of a Taylor expansion of $\mathbf{f}$ in its argument and $\mathbf{F}_0^j = -\partial_{\mathbf{X}_0}U(\mathbf{r}_0^j) = -\mathbf{f}_0^j$, due to action-reaction principle satisfied at the level of the microscopic dynamics. Note that (4.31) is equivalent to (4.2) with $\mathbf{f}_0^j$ thought as a fluctuating noise for $\mathbf{x}_1^j$. Plug (4.31) into (4.32) and using the action-reaction principle $\mathbf{F} = -\mathbf{f}$, gives an equation for $\mathbf{X}_1$ similar to (4.3) with $\mathbf{f}_0^j$ being the noise,

$$M\ddot{\mathbf{X}}_1 = -K\mathbf{X}_1 - \frac{1}{N}\sum_{j=1}^{N}\int_{-\infty}^{t}ds\, k\,\dot{\mathbf{X}}_1(s)\,e^{-\frac{k\mu}{N}(t-s)} - \frac{1}{N}\sum_{j=1}^{N}\int_{-\infty}^{t}ds\,\dot{\mathbf{f}}_0^j(s)\,e^{-\frac{k\mu}{N}(t-s)}, \tag{4.33}$$

whose solution (obtained as we did for (4.4) after neglecting the inertia) in the overdamped regime, employing the limit $k\mu/N \to \infty$ in (4.33), is

$$\mathbf{X}_1 = \frac{1}{Nk}\sum_{j=1}^{N}\left[\mathbf{F}_0^j - \frac{K\mu}{N}\int_{-\infty}^{t}ds\,e^{-\frac{K\mu}{N}(t-s)}\,\mathbf{F}_0^j(s)\right]. \tag{4.34}$$

The first correction to the second moment relies on the solution of (4.24) and (4.34):

$$\langle\mathbf{X}^2\rangle \approx \langle(\mathbf{X}_0 + \varepsilon\mathbf{X}_1)^2\rangle \approx \langle\mathbf{X}_0^2\rangle + 2\varepsilon\langle\mathbf{X}_0\mathbf{X}_1\rangle \tag{4.35}$$

The first term in (4.35) is (4.27). The second is obtained in App. A.2 and it depends on the ratio K/k. Namely,

$$\langle\mathbf{X}_0\mathbf{X}_1\rangle \underset{K\gg k}{=} -\frac{1}{2NK^2}\left(T + \frac{v_0^2}{2\mu}\frac{1}{\frac{k\mu}{N}+D_r}\right)\left\langle\sum_{j=1}^{N}\frac{\partial\mathbf{F}_0^j}{\partial\mathbf{r}_0^j}\right\rangle, \tag{4.36}$$

$$\langle\mathbf{X}_0\mathbf{X}_1\rangle \underset{K\ll k}{=} -\frac{1}{2Nk^2}\left(T + \frac{v_0^2}{2\mu}\frac{1}{\frac{k\mu}{N}+D_r}\right)\left\langle\sum_{j=1}^{N}\frac{\partial\mathbf{F}_0^j}{\partial\mathbf{r}_0^j}\right\rangle. \tag{4.37}$$

We explicitly calculate the correction (4.36) for a quartic potential, i.e. the leading non-zero term in a Taylor expansion of the interaction potential U function of $\mathbf{r}_0^j$ and thus centred in the active particles position $\mathbf{x}_0^j$. The force on the colloid becomes $\mathbf{F}^j = \alpha(\mathbf{r}_0^j)^3$ and

$$\left\langle\sum_{j=1}^{N}\frac{\partial\mathbf{F}_0^j}{\partial\mathbf{r}_0^j}\right\rangle = 3\alpha\left\langle\sum_{j=1}^{N}(\mathbf{r}_0^j)^2\right\rangle = 3\alpha\frac{N}{k}\left(T + \frac{v_0^2}{2\mu}\frac{1}{\frac{k\mu}{N}+D_r}\right). \tag{4.38}$$

Noteworthy, the correction $\langle \mathbf{X}_0 \mathbf{X}_1 \rangle$ is negative in both the regimes of the ratio K/k. Namely, due to the quartic potential, the colloid is more strongly confined, as expected. We consider the close-to-equilibrium regime, $k\mu, K\mu \ll N D_\mathrm{r}$ in which

$$\left\langle \sum_{j=1}^N \frac{\partial \mathbf{F}_0^j}{\partial \mathbf{r}_0^j} \right\rangle \approx 3\alpha \frac{N}{k} \left(T + \frac{v_0^2}{2\mu D_\mathrm{r}} \right) = 3\alpha \frac{N T_\mathrm{eff}}{k}. \tag{4.39}$$

Next, we discuss the two possible regimes of the ratio K/k[1]:

$K \gg k$ In this regime the non-linear correction is given by (4.36) and the mean square position becomes

$$\left\langle \mathbf{X}^2 \right\rangle \underset{K \gg k}{\approx} \frac{T_\mathrm{eff}}{K} \left(1 - 3\varepsilon \frac{\alpha T_\mathrm{eff}}{k^2} \right) \underset{\varepsilon \ll 1}{\approx} \frac{T_\mathrm{eff}}{K} \frac{1}{1 + 3\varepsilon \frac{\alpha T_\mathrm{eff}}{k^2}} \tag{4.40}$$

where we used $(1 + \varepsilon)^{-1} \approx 1 - \varepsilon$ to include the first order non-linear correction into the denominator. In this regime the fluid is weakly coupled to the colloid which on the other hand is strongly trapped. The equilibration time of the colloid in the potential is short compared to the relaxation to a steady state of the active particles carried out by the linear coupling k. This means that, on the time scale $K\mu/N$, the active bath acts as a quenched disorder background potential renormalising the stiffness K. The colloid results effectively more confined and this entails a reduction of the colloid fluctuations, clearly visible by a reduction of the mean square position relative to $\langle \mathbf{X}_0^2 \rangle$ obtained in absence of non-linearities. The ratio $\alpha T_\mathrm{eff}/k^2$ rules the relevance of the non-linear coupling compared to the linear one. If $\alpha T_\mathrm{eff}/k^2 \gg 1$ the colloid is perfectly confined by the anharmonic potential and it does not feel at all the linear one. Namely, the probability to find the colloid beyond the region marked by the quartic potential is practically zero. On the contrary, if $\alpha T_\mathrm{eff}/k^2 \ll 1$ (e.g. the quartic potential is very flat), the colloid is confined by the linear potential and the non-linear correction in (4.40) is indeed negligible.

$K \ll k$ In this regime the non-linear correction is given by (4.37) and the mean square position becomes

$$\left\langle \mathbf{X}^2 \right\rangle \underset{K \ll k}{\approx} \frac{T_\mathrm{eff}}{K} \left(1 - 3\varepsilon \frac{\alpha T_\mathrm{eff}}{k^2} \frac{K}{k} \right) \approx \frac{T_\mathrm{eff}}{K}. \tag{4.41}$$

The coupling colloid-active particles is very strong, in other words the active particles are effectively confined by the same potential as the colloid and relax to a steady state with the same characteristic time. The colloid effectively gains mass and friction but this does not lead to a sizeable reduction of

---

[1] More remarks about the two different regimes can be found in the App. A.2

the mean square position with respect to $\langle\mathbf{X}_0^2\rangle$, as the non-linear correction with respect to the linear contribution is further reduced by $k/K \gg 1$ so that it is practically negligible under the necessary perturbative assumption $\alpha T_{\text{eff}}/k^2 \ll 1$.

Noteworthy, this interpretation is valid also without activity up to replacing the effective temperature (4.10) with the heat bath temperature.

4.5.2 Beyond linear coupling: numerics

If we divide (4.40) by T_{eff}/K, we note that the first non-linear correction to the second moment can be related to the linear estimation, obtained from (4.24), via an algebraic relation. Namely,

$$\frac{\langle\mathbf{X}^2\rangle}{\langle\mathbf{X}_0^2\rangle} = \frac{1}{1 + 3\varepsilon\frac{\alpha T_{\text{eff}}}{k^2}} \tag{4.42}$$

Now, we employ Brownian Dynamics simulations aiming to a quantitative confirmation of these effect of non-linearities resulting in (4.40) on the active particle dynamics. We consider a non-linear extension of Eqs. (4.1), (4.2). We simulate a two-dimensional system consisting of one colloid under harmonic confinement and a set of $N = 1000$ active particles, both moving in a square domain with linear size $L = 2$ and with periodic boundary conditions. The active particles interact (mutually and with the colloid) through a soft repulsive potential assumed, in the following, to be Gaussian.

$$M\ddot{\mathbf{X}} = -K\mathbf{X} - \sum_{j=1}^{N}\partial_{\mathbf{X}}V_1\left(\mathbf{X}, \mathbf{x}_j\right) \tag{4.43}$$

$$\dot{\mathbf{x}}^j = v_0\mathbf{n}^j + \partial_{\mathbf{x}^j}\left(V_1(\mathbf{X}, \mathbf{x}_j) + V_2\left(\mathbf{x}_j, \mathbf{x}_{j'}\right)\right) + \sqrt{2\mu T}\boldsymbol{\xi}^j \tag{4.44}$$

where

$$V_1(\mathbf{x}^j, \mathbf{X}) = V_0 e^{-\frac{1}{2\sigma_c^2}\left(\mathbf{x}^j - \mathbf{X}\right)^2}, \qquad V_2(\mathbf{x}^j, \mathbf{x}^{j'}) = V e^{-\frac{1}{2\sigma_p^2}\left(\mathbf{x}^j - \mathbf{x}^{j'}\right)^2}, \tag{4.45}$$

are the potential for the particle-particle and particle-colloid interaction respectively. We let the system relax to a steady state over which we take average values of the colloid dynamics. The averages have been done over 10^5 independent simulation runs of duration $\mathcal{T} = 1.5 \times 10^3$.

We have calculated in the many-body model (from now on denoted as model A) the colloid position distribution and, in particular, its second and fourth moments for several values of v_0 in the steady state, see Fig. 4.4 a)-b)-c) respectively. As expected, the colloid is seen to behave qualitatively like an active Brownian particle embedded in a thermal environment, modelled by the coarse-grained model (4.24), for the colloid alone (from now on denoted as model B). Noteworthy, at equilibrium

models A and B should lead to the same results provided that the environment made by passive particles in model A behaves like a perfect thermal bath and thus can be effectively replaced by a Gaussian white noise. This is true in the limit $N \to \infty$, therefore any deviation in the two models is then to be attributed to a finite size effect, given that N is finite. Increasing v_0 leads to a broadening of the position distribution as seen by the growth of the second and the fourth moment. The observed dependence on v_0 differs between the two models. As evident from (4.27) and (4.28), in the model B the second and the fourth moment grow with v_0^2 and v_0^4 respectively. In the model A, they both grow linearly, see Fig 4.5 a) for the MSD, due to the short-range potential that prevents the colloid from interacting with all the active particles. Furthermore, for bigger v_0 we expect a saturation effect, already visible in Fig 4.4 a) for the position distribution. When $v_0 D_\mathrm{r}^{-1} \sim L$, the system size (here $L = 2$), the particles interact briefly and rarely with the colloid, leading to a reduction of its effective active behaviour. Similar conclusion can be deduced by the position-position correlation in Fig. 4.4 d).

In Fig 4.5 b) we compare the ratio between the variance of the position distribution in the model A denoted by σ and in the model B denoted by σ_0 and given by eq. (4.27). Namely, $\sigma = \mathcal{K}\sigma_0$. At equilibrium they are almost equal, $\mathcal{K} = 0.973 \simeq 1$, meaning that in a good approximation the environment behaves like a perfect thermal bath. Since we are not interested in keeping in our model finite size effect which produces a systematic error in all the data we decided to rescale the variances for each value of v_0 by the finite size effect value (so to obtain $\mathcal{K} = 1$ at equilibrium). With increasing v_0 the variance of the model B becomes much bigger ($\mathcal{K} < 1$), due to the replacement of colloid-active particles short-range interactions with a noise, whose statistics is equal for all the active particles. Encouraged by the analytical result (4.40), we have fitted $\mathcal{K}$ using

$$\sigma = \frac{\sigma_0}{1 + \mathrm{a}v_0^2}, \tag{4.46}$$

with $\mathrm{a} = 0.069 \pm 0.002$, the error given by the fit. We can then proceed to map σ obtained by the dynamics of model A onto the model B with an effective parameter. We define the respective variance as $\tilde{\sigma}_0$, that we impose to be equal to σ. Namely, $\sigma = \sigma_0 \mathcal{K} = \tilde{\sigma}_0$. Due to the big number of active particles needed to create an acceptable bath for the colloid, (4.27) must be considered in the regime $R \ll 1$ (from the simulations: $N = 1000$, $K = 6$, $D_\mathrm{r} = 4$ and $\mu = 1$ entails $R = 1.5 \cdot 10^{-3}$),

$$\frac{1}{K}\left(T + \frac{v_0^2}{2\mu D_\mathrm{r}}\right)\frac{1}{1 + \mathrm{a}v_0^2} = \frac{1}{\tilde{K}}\left(T + \frac{v_0^2}{2\tilde{\mu}\tilde{D}_\mathrm{r}}\right) \tag{4.47}$$

For sake of simplicity we suppose $\mu = \tilde{\mu}$ and $\tilde{D}_\mathrm{r} = D_\mathrm{r}$ obtaining for the external confinement the relation

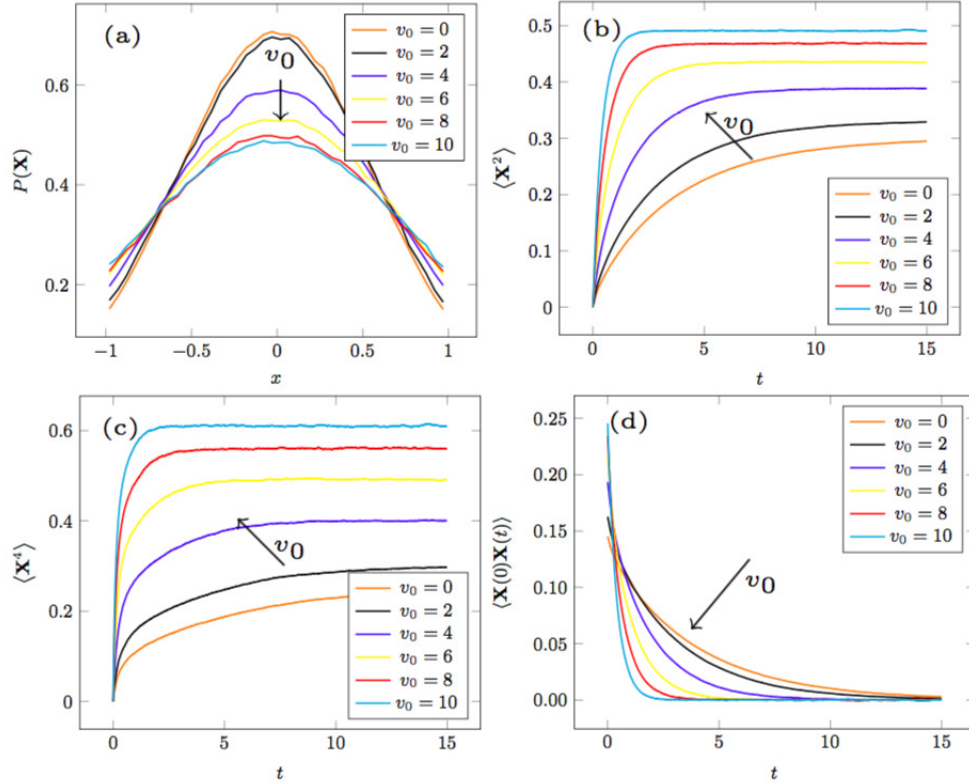$$\frac{\tilde{K}}{K} = 1 + \mathrm{a}v_0^2 \tag{4.48}$$

Figure 4.4: Dynamics of the colloid in the model A. The stationary distribution of the colloid position (a), the mean square displacement (b), the fourth moment (c) and the position time-decorrelation (d) for several values of v_0. The parameters are $T = \mu = 1$, $M = 10$, $D_{\mathrm{r}} = 4$, $\sigma_p = 0.1$, $\sigma_c = 0.15$, $V = 3$, $V_0 = 2$.

With increasing v_0, $\tilde{K} > K$ entails an effective increase of the confinement caused by the collision with the active particles and thus a reduction of the variance for model B. Having identified the renormalised parameter, we perform other simulations of the model B using the effective stiffness and we obtain a new set of position distributions for the different values of v_0. Fig. 4.6 shows how little those distributions deviate from the distributions of model A, demonstrating that the mapping (4.48) established for the variance extends to the entire particle distribution.

In conclusion, we have numerically established a simple mapping between the models A and B. Namely, in a first (mean-field) approximation, the non-linear features of the original model can be reproduced with the introduction of an effective confinement potential. The entire analysis has been carried out on the variance alone, because, due to the high number of particle involved (necessary for the relaxation of the colloid in the model A), the coarse-grained system is in the close-to-equilibrium regime $R \ll 1$ and, therefore the equivalent condition (4.48) for the quartic moment
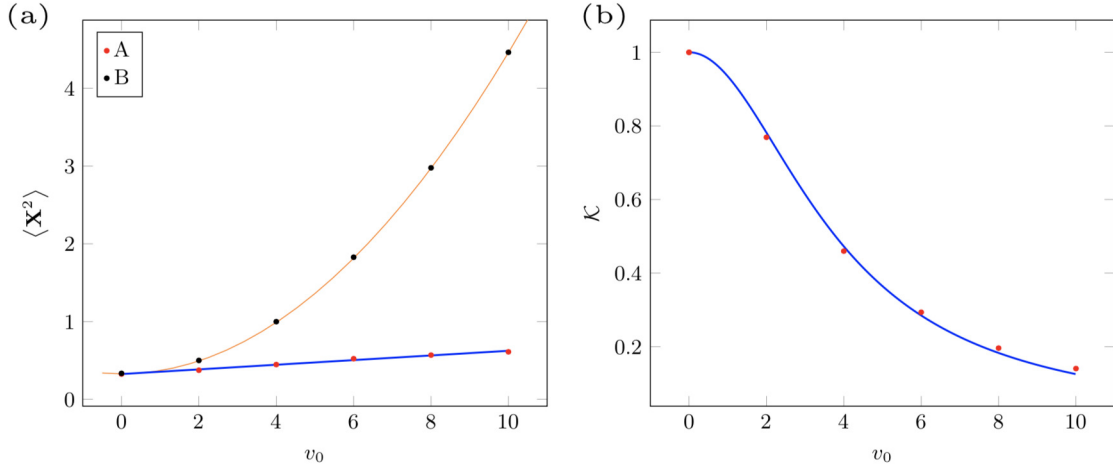
Figure 4.5: Fit of the numerical results. The colloid MSD (a) for the model A (blue line the fit and red points the data from simulations) compared with the model B (orange line the fit and black points the value from (4.27)), the ratio of variance (b) for the model A over the variance for the model B for different values of v_0. The parameters are the same used in Fig. 4.4.

is not giving further constraints. As a last remark we note that the variance of the colloid position distribution does not coincide with the MSD shown in Fig. 4.4 b) even at equilibrium, i.e. $(\sigma^2 - \langle \mathbf{X}^2 \rangle)/ \langle \mathbf{X}^2 \rangle \simeq 7\%$, because the fluid is not behaving like a perfect (canonical) heat bath for the colloid, providing to it just the temperature.

4.6   Conclusion and Outlook

In this Chapter we discussed the dynamic and static properties of a colloid embedded in an active particles environment. Performing a coarse-graining over the active particles degrees of freedom, assumed fast variables compared to the colloid, we derived a generalised Langevin equation for the colloid alone. Although the general theory presented in Chapter 3 is valid for any many-body system describable via Langevin equations, we decided to restrict the discussion to a toy model, characterised by linear probe-active particles coupling and no mutual interaction of the active particles themselves. Such model is analytically solvable and thus is suitable for a more complete understanding of the underlying physics. Remarkably, activity appears in the effective dynamics only through the noise term, given that the friction is independent of activity. Intuitively, the colloid is coupled to two baths, one active and one thermal which interact and can exchange energy with the colloid in different ways, although the dissipation is related to the thermal bath alone. Consequently, we observe a violation of the fluctuation-dissipation relation between noise and fric-
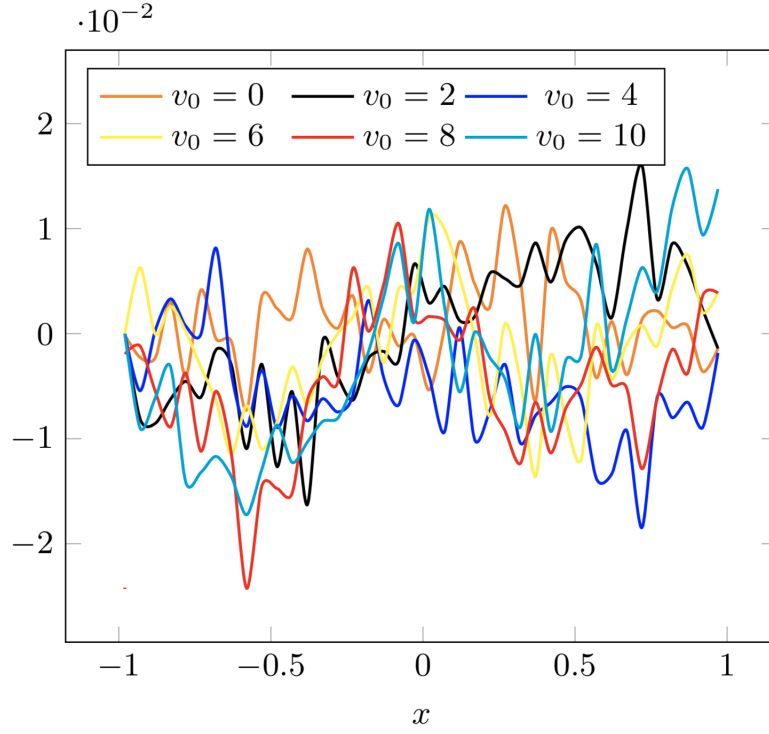
Figure 4.6: Deviations of the position distribution for the model B with the effective rotational diffusion coefficient according to (4.48) from the position distribution of the model A for $v_0 = 0, 2, 4, 6, 8, 10$. The parameters are the same used in Fig. 4.4.

tion. Such a violation is due to the presence of an extra term in the noise two-times correlation (4.7), which depends explicitly on the active particles parameters, as v_0 and D_r. Remarkably, FDT can be formally restored introducing a time-dependent effective temperature. The latter does have a clear physical interpretation only in certain regime of the parameters, namely $k\mu/ND_r \ll 1$. It corresponds to a fast rotational diffusion regime in which the active particles exhibit a short persistency and behave like Brownian particles in contact with a hotter heat bath. Noteworthy in the opposite regime, in which the active particles are very persistent and move quasi-ballistically the effective temperature can even diverge in time losing its thermodynamic interpretation.

Being linear, the generalised Langevin equation can be solved both in the under- and overdamped limit. In the underdamped regime we perform a Fourier analysis obtaining an extension to active particles systems of the Kubo relation for the response function in the frequency spaces [36], with the introduction of a frequency-dependent effective temperature $\mathcal{T}(\omega)$, reported in eq. (4.17). It is important to stress that this effective temperature $\mathcal{T}(\omega)$ is not the Fourier Transform of (4.8), but rather of (4.10). Part of the effective temperature (4.8), indeed responsible for the diverging

behaviour, has been absorbed in $\text{Re}\tilde{\gamma}^+(\omega)$. This is confirmed by the fact that (4.13) is the Fourier Transform of the noise-correlation (4.7).

The overdamped limit coincides, for our system, to a Markovian limit, based on a short relaxation time to the steady state of the active particles, i.e. $k\mu/N \gg 1$. In this regime the effective dynamics is formally equivalent to the well-known ABP model we used for active particles themselves, entailing that in this regime a passive colloid embedded in an active bath behaves like an active particle in a passive bath. Eq. (4.24) differs only for the introduction of a reduced (by N) mobility and intensity of the active noise. Afterwards, we investigated the moments of (4.24), in particular we discussed the kurtosis, observed to be negative, confirmation of a non gaussian behaviour in the stationary position distribution of the colloid.

Later on, we investigated a non-linear coupling between the colloid and the active particles as a small perturbation to the linear dynamics and we perform a perturbative expansion of the mean square position obtaining a first-order correction proportional to the mean square position of the active particles themselves. In a first approximation we proved that the non-linear mean square position decays algebraically with respect to the linear one, $\sim (1 + \mathrm{a}v_0^2)^{-1}$. This result should be corrected if the active particles are mutually interacting, in view of the caging effects typical in a real active bath. Active particles provided with a short-range interaction and kept at high density experience a reduced effective velocity due to the tendency of creating clusters. Nevertheless, performing Brownian dynamics simulations for the system colloid and active particles with focus on the position distribution and the moments, we obtain a good agreement with the theoretical prediction (4.46), although derived from non-interacting active particles. We expect that the introduction of a reduced velocity would further increase the accuracy of the fit. Then, we investigated the position distribution introducing a mapping between the many-body and the coarse-grained system variances. This mapping allows, via the introduction of an effective rotational diffusion coefficient, to replicate the same position distribution obtained with the many-body model, using the toy model alone. The mapping is able to funnel the non-linear features into the introduction of an effective confining potential. Noteworthy, the simulations have been performed in a regime in which non-Gaussian behaviour is negligible since $N \gg 1$, necessary for the active particles to be a good bath for the colloid. We measured the kurtosis from the simulation, which is not zero at equilibrium as it should be. Namely, the passive particles (for $v_0 = 0$) do not behave as a perfect bath and a bigger number should be considered to improve the precision of our estimation. On the other hand, it would be interesting to perform further simulations involving less active particles but more strongly coupled to the colloid, enhancing non-Gaussian behaviour.

Chapter 5

Active Brownian Stirling Engine

5.1 Introduction

In Chapter 4 we have derived the effective equation for a colloid embedded in an active particles bath and we have shown that if, the active particles are subjected to linear coupling with the colloid and no mutual interaction, such equation is formally equivalent to the ABP for an active particle in a passive bath. In this Chapter we apply our achievements to Brownian thermodynamical machines with the purpose to establish whether activity enhances their efficiency. The discussion of the results in this Chapter follows the same structure of [18], still in preparation.

The study of efficiency is a topic as old as the industrialisation of the world itself. Its practical importance, together with the theoretical interest, has pushed many physicists and engineers to perform numerous experiments that contributed to establish Thermodynamics. The industries-oriented aspect is particularly visible concerning the thermodynamic cycles, e.g. Stirling, Carnot etc, based on a clear principle: to use the easily accessible "disordered" energy called as heat to perform work, that can be viewed as an "ordered" or "directed" form of energy. During the last few decades, the advances in technology allow and require [190–193] building machines so small that thermal fluctuations of the surrounding environment render their operation stochastic. The need for a theoretical description of such machines has led to the set up of Stochastic Thermodynamics [6, 10, 32, 194], a theory combining classical thermodynamics and stochastic processes. In this theory, basic thermodynamic notions such as heat, work, and entropy are defined at the level of the individual stochastic trajectories of the system in question. While the resulting average thermodynamic properties of the system obey the principles of thermodynamics, fluctuations are allowed to go beyond these limitations. The probability of such rare events is described by so-called fluctuation theorems that generalise the second law of thermodynamics [6]. Many recent studies have been devoted to the understanding of microscopic versions of thermodynamics cycles (see for example Refs. [195–200] for experimental studies and Refs. [201–210] for theoretical ones). Between these studies, a paradigmatic role is played by Brownian heat engines [198–200, 209, 210] based on a colloidal

particle diffusing in an equilibrium bath and driven by a time-dependent potential – realisable in practice by optical tweezers – which plays the role of a volume-regulating piston [198, 199, 211]. During the last few years, increasing interest has been devoted to the thermodynamics of systems involving active particles [188, 212, 213] that convert energy provided by some internal degrees of freedom into a persistent motion. Dynamics of these systems involve non-Gaussian heavy-tailed fluctuations. Accordingly, many questions naturally arise. To name few of them, can the persistent motion be harvested and lead to an increase of the extracted work? Can such fluctuations consistently enhance the efficiency of a machine and go beyond the limit imposed by equilibrium thermodynamics? Furthermore, as we discussed in Chapter 4.5, the characteristic energy associated to an active particle, deduced by the effective temperature, e.g. (4.10) can produce, just by tuning parameters like the active velocity v_0 and the rotational diffusion coefficient D_r, very big temperature differences, not easily reachable with a thermal environment, and thus entail higher efficiency according to standard definitions from Thermodynamics.

In this Chapter we aim to give a contribution in this direction, discussing a Stirling heat engine for an active particle embedded in a thermal environment providing for friction and noise, i.e. active Brownian particle (ABPs) [61], able to capture the main properties of active particles system although its simplicity. Remarkably, ABPs model with harmonic confining potential has recently been used to describe a much more complex system, namely, a passive Brownian colloid embedded in an active particles environment [67, 170, 173], encouraged by experimental evidence [174, 214]. Namely, the bath affects the colloid dynamics only through an extra noise, sharing the same statistics with the noise felt by each individual active particle. In the previous Chapters we have stressed that such an assumption cannot be true in full glory but relies on certain approximations, e.g. weak-coupling between colloid and active particles, mean field approach and Markovian limit concerning the memory effects in the friction kernel. Due to these approximations, collective effects, typical for active systems like clustering or accumulation around obstacles, are lost during the derivation. Nevertheless, it is an open question whether these effects are important for the considered system. To our knowledge, ABP model has been used to describe a passive colloid in an active environment only in [188] with the aim to reproduce the surprising experimental results [212] for a Stirling engine based on a colloidal particle diffusing in a bacterial bath. The authors of the [212] have found that their Stirling engine can operate with efficiencies surpassing the thermodynamic bound on the efficiency of an equilibrium Stirling cycle. Unfortunately, the analysis given in [188] failed to explain this observation. However, even the simple ABP in an equilibrium bath, a throughout study of both dynamics and thermodynamics is lacking: the engine in [188] was investigated in the quasi-static limit only, mainly focusing on the possibility of surpassing the classical efficiency. Thus we present a detailed study of dynamics and thermodynamics of the active heat engine of [188, 212], which is based on an active Brownian particle immersed in an equilibrium bath and driven by the parabolic potential with time-dependent stiffness $k(t)$, but this model can de-

scribe a passive particle in an active environment, provided that the approximations introduced in Chapter 4 are satisfied.

The most remarkable result of this Chapter, shown in Secs. 5.2.4 and 5.3, is that the average energetics of this model can be mapped on that of a passive heat engine in contact with an equilibrium bath at an effective temperature. This mapping allows us to adopt many known results for passive Brownian heat engines to the active engine. It includes not only the quasi-static results such as the second law upper bounds on the efficiency of individual thermodynamic cycles (as pointed out in [188] for Stirling cycle), but also the finite-time results such as the efficiency at maximum power [209], maximum efficiency at arbitrary power [215] and approachability of equilibrium (Carnot's) efficiency at a nonzero power [216].

Although the results for standard heat engines can be mapped on those for the active ones, the effective temperature on which the correspondence is built, is a dynamical quantity determined by the external driving, as expressed by the differential equation (5.12)–(5.13). Therefore, it is not trivial to realise standard thermodynamic cycles, such as the Stirling cycle or Carnot cycle, using this temperature. For example, fixing the bath activity and the bath temperature does not imply that the active temperature is constant, see Fig. 5.1 e). This behaviour may lead to unexpected directions of heat flows through the system thus affecting the correct definition of the engine efficiency. We discuss this and other peculiarities in detail both in the quasi-static regime, which allows for simple analytical description, and also for driving at arbitrary speeds (Secs. 5.3 and 5.6).

The mapping cannot be extended beyond the mean energetics. Indeed, the active and passive heat engines differ in variables which depend on higher moments of position than the second one, e.g. the full position distribution, system entropy production (EP) and fluctuations of work, heat and entropy. One thus cannot take for granted the results obtained for equilibrium baths such as fluctuation theorems, e.g. the Jarzinski equality [8], Crooks fluctuation theorem [7], Hatano-Sasa equality [217], and various inequalities containing higher moments of work, heat and entropy (examples are thermodynamic uncertainty relations [218,219] and the trade-off between power, efficiency and constancy [220]). The non-Gaussianity enhances the output work and power, but it also affects the heat flowing into the system (see Secs. 5.5 and 5.6). As a result, the efficiency is always bounded by the 2nd law containing effective EP corresponding to the effective temperature. Therein, we also propose two possible EP formulas for the active heat engine. They are derived using path-integral formalism [221] depending on the chosen parity of activity under time reversal – even (odd) if it is regarded as a force (velocity).

5.2   Active heat engine

5.2.1   Dynamics

For sake of simplicity we limit our investigation to the two-dimensional case, where the particle state is described by its position $\mathbf{x}$ and its orientation angle θ. We employ the same Langevin equation introduced in 2.4 with time-independent parameters, for an active particle confined by a harmonic potential with time-dependent stiffness $k(t)$ and embedded in a thermal environment,

$$\dot{\mathbf{x}} = -k(t)\mu\mathbf{x} + v(t)\mathbf{n}(\theta) + \sqrt{2D(t)}\boldsymbol{\xi}, \quad \dot{\theta} = \sqrt{2D_{\mathrm{r}}(t)}\xi_\theta. \tag{5.1}$$

Here $\boldsymbol{\xi}$ and ξ_θ are independent standard Gaussian white noises with zero average and delta-correlation in time, μ is the mobility constant, $D(t) = \mu T(t)$ and $D_{\mathrm{r}}(t)$ stand for the translational and rotational diffusion coefficient respectively (T is the heat bath temperature). The active velocity has time-dependent magnitude $v(t)$. Lumping the noises together as $\boldsymbol{\eta} = \sqrt{2D(t)}\boldsymbol{\xi} + v(t)\mathbf{n}(\theta)$, (5.1) becomes

$$\dot{\mathbf{x}} = -k(t)\mu\mathbf{x} + \boldsymbol{\eta}, \tag{5.2}$$

equivalent to (4.24). Here, the active velocity is treated as a non-Gaussian coloured noise which is still zero averaged, but it possesses exponentially decaying correlations,

$$\langle\boldsymbol{\eta}(t)\boldsymbol{\eta}(t')\rangle = 2\sqrt{D(t)D(t')}\delta(t - t') + \frac{1}{2}v(t)v(t')\exp\left(-\int_{\min(t,t')}^{\max(t,t')} dt''\, D_{\mathrm{r}}\left(t''\right)\right). \tag{5.3}$$

Higher order correlation functions [77] are not needed hereafter. This formula is suitable for assessing the thermodynamics of the system. Noise terms in Langevin equations are standardly identified as results of coupling the system to surrounding baths. The two contributions in the noise $\boldsymbol{\eta}$ may be thought as pertaining to two different baths, one at equilibrium (the solvent) and one active (the suspended self-propelled particles). They influence the exchange of heat with the system in a different way, as we will show explicitly in Sec. 5.6.1.

Note that the system described by (5.1) and thus also (5.2) involves in its most general variant three ingredients which can bring it far from equilibrium:

(i) If the stiffness $k(t)$ changes on time-scales shorter than the system relaxation time, the system is not fast enough to relax to equilibrium.

(ii) If the rotational diffusion coefficient D_{r} is not given by the Einstein relation, the rotational degree of freedom can be considered as a second bath at a temperature different than T. In general, connecting a system to reservoirs at different temperatures can bring it out of equilibrium.

(iii) The velocity term in the Langevin system can be formally considered as a non-conservative force. Presence of such a force causes currents in the system, bringing it out of equilibrium.
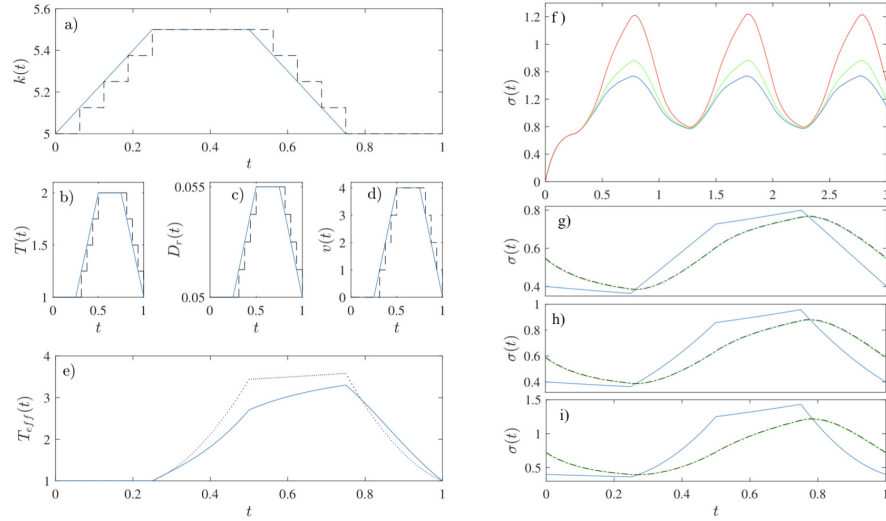
Figure 5.1: The trap stiffness (a), bath temperature (b), rotational diffusion coefficient (c) and active velocity (d) as functions of time during the cycle. Full blue lines show actual time dependences, while dashed black lines depict approximate step-wise constant driving used for the numerical calculation. The effective temperature (e), full blue line for for driving (a)–(d) (5.16), dotted for a quasi-static process (5.17). Parameters used: $t_p = 1$, $k_- = 5$, $k_+ = 5.5$, $T_+ = 2$, $T_- = 1$, $D_{\mathrm{r}}^+ = 0.055$, $D_{\mathrm{r}}^- = 0.05$, $v_+ = 4$ and $v_- = 0$. Variance of the particle position as function of time. (f) Relaxation to limit cycle for $v_+ = 0, 2, 4$, from the lower curve to the upper one (BD simulations). In panels (g) – (i) the variance behaviour during the limit cycle for activity $v_+ = 0, 2, 4$. The broken blue lines stand for the variances corresponding to infinitely slow driving (5.15). Full green (BD simulations), dot-dashed black (numerics), and dotted red (analytical formula (5.13)) curves show the variance corresponding to the driving depicted in Fig. 5.1. The perfect overlap of the curves implies that the individual methods are equivalent.

5.2.2   Driving

We periodically modulate with a linear protocol the stiffness k, the reservoir temperature T, the rotational diffusion coefficient D_{r} and the active velocity v in the manner that resembles the Stirling cycle considered in [212] (see Fig. 5.1). The driving consists of four branches of equal duration:

A→B "isothermal" compression, with k increased from k_- to k_+ at $(T_-, D_{\mathrm{r}}^-, v_-)$

B→C isochoric (iso-stiffness) heating $(T_-, D_{\mathrm{r}}^-, v_-)$ to $(T_+, D_{\mathrm{r}}^+, v_+)$ at $k = k_+$

C→D "isothermal" expansion, with k decreased from k_+ to k_- at $(T_+, D_{\mathrm{r}}^+, v_+)$

D→A isochoric (iso-stiffness) cooling $(T_+, D_{\mathrm{r}}^+, v_+)$ to $(T_-, D_{\mathrm{r}}^-, v_-)$ at $k = k_-$

We denote t_p the duration of the whole cycle. The "isothermal" branches are characterised by constant heat bath temperature and activity, but, in general, a varying effective temperature, see Fig. 5.1e), thus quoted. It boils down to a constant in special limiting regimes only, as discussed in Secs. 5.6.1.2 and 5.4. Only there the considered "isothermal" branches are really isothermal and the considered cycle is a real Stirling cycle. The engine consumes (performs) work during the "isothermal" branch A $\rightarrow$ B (C $\rightarrow$ D). Since the isochoric branches are characterised by constant stiffness, there the system only exchanges heat with reservoirs as explained in the next section.

5.2.3 Energetics

Given the microscopic nature of the system, thermodynamics quantities such as work and heat are represented by certain functionals over the individual trajectories of the underlying stochastic process $\{\mathbf{x}(t), \theta(t)\}$ and thus become also stochastic, for systems in contact with equilibrium bath [6, 32] in contact with an active bath [222]. In this work, we are interested in average values of these functionals which can be calculated from the definition of the internal energy,

$$U(t) = \frac{1}{2}k(t)\sigma(t), \tag{5.4}$$

where $\sigma(t) = \langle \mathbf{x}^2(t) \rangle$, for each component of position. Combining (5.4) with the first law of thermodynamics $\Delta U(t_i, t_f) = \int_{t_i}^{t_f} dt\, \dot{U}(t) = W(t_i, t_f) + Q(t_i, t_f)$, we identify:

- the work done on the particle during the time window (t_i, t_f),

$$W(t_i, t_f) = \frac{1}{2}\int_{t_i}^{t_f} dt\, \dot{k}(t)\sigma(t) = \frac{1}{2}\int_{k_i}^{k_f} dk\, \sigma(t), \tag{5.5}$$

as the energy flowing into the system from an external source controlling the potential,

- the heat,

$$Q(t_i, t_f) = \frac{1}{2}\int_{t_i}^{t_f} dt\, k(t)\dot{\sigma}(t) = \frac{1}{2}\int_{\sigma_i}^{\sigma_f} d\sigma\, k(t), \tag{5.6}$$

as the energy flowing into the system from the reservoir.

With the definitions (5.5)–(5.6), we can describe performance of the engine in terms of output power P and efficiency η:

$$P \equiv \frac{W_{\text{out}}}{t_p} \qquad\qquad \eta \equiv \frac{W_{\text{out}}}{Q_{\text{in}}}. \tag{5.7}$$

Here, $W_{\text{out}} = -W(0, t_p)$ is the work done by the engine per cycle and

$$Q_{\text{in}} = \int_0^{t_p} dt \, \dot{Q}(0,t) \Theta[\dot{Q}(0,t)] = \frac{1}{2} \int_0^{t_p} dt \, k \, \dot{\sigma}(t) \Theta[\dot{\sigma}(t)] \tag{5.8}$$

$$Q_{\text{out}} = \int_0^{t_p} dt \, \dot{Q}(0,t) \Theta[-\dot{Q}(0,t)] = \frac{1}{2} \int_0^{t_p} dt \, k \, \dot{\sigma}(t) \Theta[-\dot{\sigma}(t)] \tag{5.9}$$

is the heat coming into the system from the environment and from the system to the environment respectively ($\Theta(x)$ denotes the unit step function). While the definition of the output power bares no controversy, it must be stressed that in the definition of the efficiency we have neglected the energy which drives the active velocity v (i.e the housekeeping heat). Noteworthy, all these thermodynamic quantities are determined solely by the variance σ. In the next section, we show how to calculate this function for an arbitrary protocol.

5.2.4 Variance

Due to the periodic driving, the average state of the system eventually, after a transient period, attains a periodic steady state. Due to the symmetry of the potential, the average particle displacement during this cycle will be zero. The long-time solution for the variance σ arbitrary v fulfils the system of two coupled differential equations (see Appendix B.1 for the derivation)

$$\dot{H} = -(\mu k + D_{\text{r}})H + v, \tag{5.10}$$

$$\dot{\sigma} = -2\mu k \sigma + 4D + 2vH. \tag{5.11}$$

where vH is thought as an active contribution to (translational) diffusivity. This system has the time-periodic solution

$$H(t) = H_0 e^{-K(t,0)-F(t,0)} + \int_0^t v(s) \, e^{-K(t,s)-F(t,s)}, \tag{5.12}$$

$$\sigma(t) = \sigma_0 e^{-2K(t,0)} + 4 \int_0^t dt' \, D_{\text{eff}}(t') e^{-2K(t,t')}. \tag{5.13}$$

with functions $K(t,t_0) = \mu \int_{t_0}^t dt' k(t')$ and $F(t,t_0) = \int_{t_0}^t dt' D_{\text{r}}(t')$ and $D_{\text{eff}}(t) = D(t) + v(t)H(t)/2$. The constants H_0 and σ_0 in Eqs. (5.12) and (5.13) secures time-periodicity of the solution. They are given by

$$H_0 = \frac{\int_0^{t_p} dt' \, v(t') \, e^{-K(t_p,t')-F(t_p,t')}}{1 - e^{-K(t_p,0)-F(t_p,0)}}, \quad \sigma_0 = 4 \frac{\int_0^{t_p} dt' \, D_{\text{eff}}(t') e^{-2K(t_p,t')}}{1 - e^{-2K(t_p,0)}}. \tag{5.14}$$

Given the formal complexity of (5.13), it is useful to consider limiting situations where the variance attains a more transparent form. Along a quasi-static process with the driving much slower than relaxation times of the system, $(\mu k + D_{\text{r}})^{-1}$ and

$(2\mu k)^{-1}$ for H and σ respectively, the functions H and σ are always relaxed and the variance can be obtained from the condition $\dot{H} = \dot{\sigma} = 0$:

$$\sigma = \sigma_\infty \equiv \frac{2}{k}\left(T + \frac{v^2}{2\mu}\frac{1}{k\mu + D_r}\right). \tag{5.15}$$

The first correction in the velocity of the driving to the above formula is derived in Appendix B.2. For a driving much faster than the system relaxation times, the system is too slow to react to any change so that the variance is given by (5.17) with time-averaged values of the parameters k, T, v and D_r. In all other intermediate regimes we use the full expression (5.13). To be sure that we calculate the nested integral correctly, we cross-check the obtained results with other two independents methods, the BD simulations and the numerical method [223]. The finite-time variances follow the quasi-static ones, similarly to donkey chasing a carrot, c.f. Fig. 5.1 (g)-(i). The distance between the quasi-static and the finite-time curves is larger for faster variation of parameters and thus, in the present case, the distance is proportional to v_+. As can be expected intuitively and also observing the role of v in (5.11), larger active velocities lead to larger variances.

5.3 Mapping to passive cycle

The formula (5.11) for the variance has the same form valid for equilibrium baths (see, e.g., [209]) up to the term $2vH$, which can be, however, absorbed in the diffusion coefficient so to obtain an effective diffusion coefficient $D_{\text{eff}} = D + vH/2$ corresponding to the effective temperature

$$T_{\text{eff}}(t) = \frac{D_{\text{eff}}(t)}{\mu} = T(t) + \frac{v(t)H(t)}{2\mu}, \tag{5.16}$$

always larger than T and determined jointly by the bath temperature and the activity. The latter enters indirect through the dynamical equation for H (5.10) that makes the effective temperature acquire the relaxation time, $(k\mu + D_r)^{-1}$. While for a general cycle it is a t_p-periodic function described by Eq. 5.12, for a quasi-static process, it boils down to the simple expression

$$T_{\text{eff}}^\infty \equiv T + \frac{v^2}{2\mu}\frac{1}{k\mu + D_r}. \tag{5.17}$$

Let us stress that the effective temperature (5.16), defined from the variance, is well defined in the limit cycle only and not during the initial relaxation. Then, it allows for a consistent thermodynamic description of the engine performance including definition of effective EP, which is an increasing function of time and sets standard second law bounds on engines power and efficiency (see Sec. 5.4.2). During any transient relaxation to the periodic steady state, the effective temperature would have to be defined from the right-hand side of Eq. B.2, which contains a memory term.

In this case, it is in general not possible to define a thermodynamically consistent entropy associated with the transient effective temperature. In what follows, we will consider the time-periodic effective temperature only. The effective temperature possesses several nonintuitive features. First, it is t_p-periodic even for a constant bath temperature in case of periodically modulated activity or trap stiffness. Moreover, due to its dynamical nature, the effective temperature can change with time even during those parts of the cycle where the model parameters are held constant. Thus to realize an isothermal process for the effective temperature one should carefully control the model parameters in order to make the expression (5.16) or, in the quasi-static limit (5.17), constant. We demonstrate this behaviour in Fig. 5.1 (e), where we plot the effective temperature (5.16) (full blue line) and also the quasi-static effective temperature (5.17) which would be obtained if the used driving were sufficiently slow (black dotted line). The quasi-static effective temperature runs approximately along a Stirling cycle, in accord with the bath temperature and activity. Conversely, the finite-time effective temperature exhibits completely different behaviour. The hereby identified mapping implies that the dynamics of the variance in the active model is exactly the same as the dynamics of the variance in a model with equilibrium bath at the temperature T_{eff}. The variance determines the behaviour of average thermodynamic variables such as work, heat, and efficiency and thus these variables for the active heat engine must obey the standard results obtained for heat engines with equilibrium baths. Namely, the following findings on the optimal performance of classical heat engines are still valid in our case:

- The upper bound on the efficiency of our engine is given by the Carnot's efficiency

$$\eta \le \eta_C = 1 - \frac{\min(T_{\text{eff}})}{\max(T_{\text{eff}})} \,, \tag{5.18}$$

  which can be reached only if the effective temperature and the stiffness are varied along a Carnot cycle composed of two isotherms and two adiabatics. Thus, reaching η_C in our heat engine requires fine tuning of the parameters (T, v, D_{r} and k) such that the effective temperature (5.16) is constant during the isotherms.

- To reach the upper bound on efficiency η_C, the engine must work at quasi-static conditions and thus the corresponding power vanishes rendering such machine uninteresting for practical purposes [216]. That is why other measures of engine performance have been proposed. A prominent role among them plays the maximum power condition. For overdamped Brownian heat engines, the regime of maximum power has been investigated in [209]. Employing their result, we find that the efficiency at maximum power for our heat engine is given by

$$\eta_{\text{MP}} = 1 - \sqrt{\frac{\min(T_{\text{eff}})}{\max(T_{\text{eff}})}}. \tag{5.19}$$

  This result holds for Carnot like cycles using a special protocol for the trap stiffness k which minimises the work dissipated during the isothermal branches.

In the next section, after defining the EP for the effective passive model (Sec. 5.4.2) we show how the mapping fails in predicting the correct EP of the active heat engine (Sec. 5.4.1). To show that the correspondence with the passive model should not be overstretched, we also display the deviations of the probability distribution of the active particle position (Appendix B.3) from that predicted by the passive model.

5.4   Entropy production

The total entropy production due to the operation of the engine comprises of the entropy change of the bath and entropy change of the position distribution of the particle. The change of the bath entropy is given by the energy delivered into the bath divided by the bath temperature. This energy influx comprises of three contributions:

(i) the energy influx due to changes in the particle potential energy as the particle moves in the external potential,

(ii) the energy of the active motion of the particle dissipated due to the friction,

(iii) the energy transferred into the system via the mechanism sustaining activity of the particle.

In our discussion of the entropy production, we consider only the contributions (i) and (ii), while we neglect the contribution (iii), which is nevertheless in practice the largest one. The *real* change in the entropy of the bath resulting from the contributions (i) and (ii) depends on the physical realisation of the active velocity of the particle – whether the active velocity of the particle is a result of dragging the particle through the fluid by an external force (see Fig. 5.2 b)), or it is rather a real swimming when the particle "pushes away" from the surrounding liquid (see Fig. 5.2 c). Besides the real change in the bath entropy, one should also define the *effective* change in the bath entropy corresponding to the above-introduced mapping to the passive system in contact with a bath at the effective temperature (see Fig. 5.2 a)). In the following section, we discussed these quantities in detail.

5.4.1   Actual entropy production

The actual entropy produced during the cycle can be identified by comparing probabilities of forward and time-reversed trajectories of the stochastic process $(\mathbf{x}(t), \theta(t))$ using a path integral formulation [221] starting from (5.1). In this calculation, one has to choose whether the active component v is even or odd with respect to the time-reversal [224, 225]. Even active velocity corresponds to the situation where the active particles are dragged by an active force, which dissipates energy against the friction in a thermal environment at temperature T. An intuitive sketch of this scenario is given by Fig. 5.2) b). This is well visible from the resulting expression for
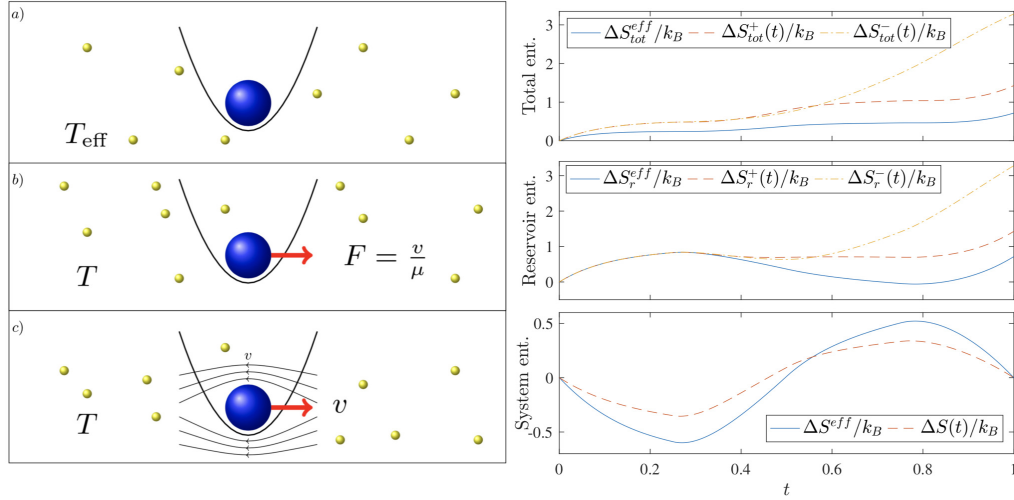
Figure 5.2: Left Panel. Sketch for the effective entropy production (a)), the entropy S^+ (b)) and the entropy S^- (c)). Right Panel. The total EP (upper panel), the entropy flowing in the reservoirs (middle panel) and the change in the system entropy (lower panel) as functions of time during the cycle depicted in Fig. 5.1 with $v_+ = 4$. The individual entropies are defined in Eqs. (5.20)–(5.23) and (5.25)–(5.28).

the amount of entropy flowed in the bath during the time interval $[0, t]$,

$$S_\mathrm{R}^+(t) = \int_0^t dt' \, \frac{1}{T(t')} \left\langle (v\mathbf{n} - \mu\nabla V) \cdot \frac{\dot{\mathbf{x}}}{\mu} \right\rangle = -\int_0^t dt' \, \frac{1}{T(t')} \left(\dot{Q} + kvH - \frac{v^2}{\mu} \right)(t'), \quad (5.20)$$

where $v\mathbf{n} - k\mu\mathbf{x}$ is the velocity caused by the external forcing and $\dot{\mathbf{x}}/\mu$ is the friction force. The last equality follows after using the formula $k\langle \mathbf{x} \cdot \dot{\mathbf{x}} \rangle = \dot{Q}(0, t) = \dot{Q}$ in the second term and substituting (5.1) in the first, given that $\langle v\mathbf{n} \cdot \mathbf{x} \rangle = vH$.

If v is regarded as a proper momentum (per unit mass) it is odd under time reversal. Hence, the active velocity acts as a negative friction. That could be seen as resulting, e.g. from a convecting background flow, as depicted in Fig. 5.2) c). In this case, we obtain for the amount of entropy flowed in the bath during the time interval $(0, t)$,

$$S_\mathrm{R}^-(t) = -\int_0^t dt' \, \frac{1}{T(t')} \langle (\dot{\mathbf{x}} - v\mathbf{n}) \cdot (-k\mathbf{x}) \rangle = -\int_0^t dt' \, \frac{1}{T(t')} \left(\dot{Q} - kvH \right)(t'), \quad (5.21)$$

where the second equality is obtained in a similar way as in the even case. In Eq. (5.21), the term $\dot{\mathbf{x}} - v\mathbf{n}$ stands for the relative particle velocity with respect to the drift velocity of the solution $v\mathbf{n}$. This relative velocity is nonzero due to the force applied by the external potential $-k\mathbf{x}$, which dissipates energy into the solution. Having defined the EP in the reservoir, the total entropy produced by the machine in the time-window $(0, t)$ reads

$$\Delta S_\mathrm{tot}^\pm(t) = \Delta S_\mathrm{R}^\pm(t) + \Delta S(t), \quad (5.22)$$

where $\Delta S(t) = S(t) - S(0)$ is the change in the system entropy

$$S(t) = -\int_{-\infty}^{\infty} dx \int_{-\infty}^{\infty} dy \int_{0}^{2\pi} d\theta \, p \log p. \tag{5.23}$$

Here, the probability distribution $p = p(\mathbf{x}, \theta, t)$, solution of the FPE associated to (5.1),

$$\frac{\partial p}{\partial t} = \left(k\mu \nabla_{\mathbf{x}} \cdot \mathbf{x} - v\mathbf{n} \cdot \nabla_{\mathbf{x}} + D\nabla_{\mathbf{x}}^2 + D_{\mathrm{r}} \frac{\partial^2}{\partial \theta^2} \right) p, \tag{5.24}$$

describing the full state of the particle at time t. Noteworthy, (5.24) is the only object in the present thermodynamic analysis which can not be determined using σ. Instead, we evaluate it either numerically from Eq. (B.15) or using BD simulations of (5.1) The main difference between the EPs $S_{\mathrm{R}}^+(t)$ and $S_{\mathrm{R}}^-(t)$ is that the former is always positive due to the ever-present dissipation caused by forcing the active particles, while the later vanishes for $k\mathbf{x} = 0$. Moreover, in the limit $D_{\mathrm{r}} \to \infty$ where the active velocity rotates so fast that it has no persistence, we have $kvH = k\langle v\mathbf{n} \cdot \mathbf{x} \rangle = 0$ and the EP (5.21) is just given by the standard formula $\Delta S_{\mathrm{R}}^-(t) = \int_0^t dt' \dot{Q}/T$ valid for equilibrium bath. In this limit, we also have $T_{\mathrm{eff}} = T$ and thus (5.21) is further equivalent to the effective EP (5.25).

5.4.2 Effective entropy production

Pursuing further the analogy of our heat engine with the effective model connected to the equilibrium bath, c.f. Fig. 5.2 a), one can define an effective EP which gives standard upper bound on efficiency of the effective model. This is done just by substituting the active temperature T_{eff} for the temperature T in classical stochastic thermodynamic definitions [209]. This way we obtain the relation

$$\Delta S_{\mathrm{R}}^{\mathrm{eff}}(t) = -\int_0^t dt' \frac{\dot{Q}}{T_{\mathrm{eff}}}, \tag{5.25}$$

for the change in the bath entropy during the time interval $[0, t]$. Similarly, the effective system entropy is (up to a constant) the Shannon entropy

$$S^{\mathrm{eff}}(t) = -\int_{-\infty}^{\infty} dx \int_{-\infty}^{\infty} dy \int_{0}^{2\pi} d\theta \, p^{\mathrm{eff}} \log p^{\mathrm{eff}} = 2\log\sigma(t) + 2\log\pi + 1, \tag{5.26}$$

with $p^{\mathrm{eff}} = p^{\mathrm{eff}}(\mathbf{x}) = \exp\left[-(x^2 + y^2)/\sigma\right]/\pi\sigma$, effective distribution solution of the FPE

$$\frac{\partial p^{\mathrm{eff}}}{\partial t} = \nabla_{\mathbf{x}} \cdot (k\mu\mathbf{x} + D_{\mathrm{eff}} \nabla_{\mathbf{x}}) \, p^{\mathrm{eff}}, \tag{5.27}$$

Obtained, in the spirit of the mapping to equilibrium introduced in the previous section, by putting $v = 0$ and replacing D with the effective diffusion coefficient

defined in (5.16) in the (5.24). Namely p^{eff}, result of an equilibrium Brownian Motion with a higher diffusion coefficient, has the same variance as the solution of Eq. (5.24), but with Gaussian fluctuations only. Since the system entropy (5.26) is a state function, it does not contribute to EP over a full cycle, see Fig. 5.2. Using these definitions, the total amount of EP during the time interval $(0, t)$ in the effective model reads

$$\Delta S_{\text{tot}}^{\text{eff}}(t) = \Delta S_{\text{R}}^{\text{eff}}(t) + \Delta S^{\text{eff}}(t), \tag{5.28}$$

where $\Delta S^{\text{eff}}(t) = S^{\text{eff}}(t) - S^{\text{eff}}(0)$. Using the dynamical equation for the variance (5.13) and the definition of heat (5.6), one can show that the effective EP (5.28) is consistent with the second law of thermodynamics, i.e. it is a nondecreasing function of time:

$$\dot{S}_{\text{tot}}^{\text{eff}}(t) = \mu T_{\text{eff}} \sigma \left(\frac{2}{\sigma} - \frac{k}{T_{\text{eff}}} \right)^2 \geq 0. \tag{5.29}$$

This property of $\Delta S_{\text{tot}}^{\text{eff}}(t)$ can be used for showing that the limitations on performance of the active engine are the same as those of the passive one with $T_{\text{eff}} \geq T$. For example, the quasi-static cycle where the parameters k, v and D_{r} vary very slowly and thus the variance is given by (5.15) is described by zero total EP (5.29). The corresponding efficiency then represents the upper bound for any finite-time cycle where the control parameters vary in the same way as for the quasi-static driving. Note that such EP is expected to be a lower bound, rather than a good proxy, for the actual EP. This is because a degree of freedom, θ, which falls out of equilibrium due to the action of the nonconservative active force on the coupled variables $\mathbf{x}$, is basically coarse-grained and treated as a bath. In general, the coarse-graining of nonequilibrium degrees of freedom is known to lower the EP [226]. Nevertheless, useful insights can be gained. For example, the quasi-static cycle where the parameters k, v and D_{r} vary very slowly and thus the variance is given by Eq. (5.15) is described by zero total EP (5.29). The corresponding efficiency then represents the upper bound for any finite-time cycle where the control parameters varies in the same way as for the quasi-static one.

5.4.3 Comparison of the entropies

Interestingly, the change in the bath entropy $\dot{S}_{\text{R}}^{-} = \dot{S}_{\text{R}}^{-}(t)$ due to the swimming is always larger than its effective counterpart $\dot{S}_{\text{R}}^{\text{eff}} = \dot{S}_{\text{R}}^{\text{eff}}(t)$ as follows from Eqs. (5.21) and (5.25):

$$\dot{S}_{\text{R}}^{-} - \dot{S}_{\text{R}}^{\text{eff}} = k^2 \mu \sigma \frac{T^{\text{eff}} - T}{T T^{\text{eff}}} > 0. \tag{5.30}$$

To draw such a general conclusion for the change in the bath entropy $\dot{S}_{\text{R}}^{-} = \dot{S}_{\text{R}}^{-}(t)$ $\dot{S}_{\text{R}}^{+} = \dot{S}_{\text{R}}^{+}(t)$ due to the dragging is not so straightforward since it is not easy to prove

that the difference

$$\dot{S}_{\mathrm{R}}^{+} - \dot{S}_{\mathrm{R}}^{\mathrm{eff}} = \frac{v^2}{\mu T} + \dot{S}_{\mathrm{R}}^{-} - \dot{S}_{\mathrm{R}}^{\mathrm{eff}} - \frac{4k\mu}{T}\left(T^{\mathrm{eff}} - T\right) \tag{5.31}$$

has a definite sign. We were able to prove the inequality $\dot{S}_{\mathrm{R}}^{+} - \dot{S}_{\mathrm{R}}^{\mathrm{eff}} > 0$ analytically only in the quasi-static limit, where the variance is given by the solution of (5.10) and (5.11) with $\dot{\sigma} = \dot{H} = 0$. Then the differences (5.30) and (5.31) boil down to

$$\dot{S}_{\mathrm{R}}^{-} - \dot{S}_{\mathrm{R}}^{\mathrm{eff}} = \frac{k^2\mu\sigma}{T}\frac{1}{D_{\mathrm{r}} + k\mu} > 0, \qquad \dot{S}_{\mathrm{R}}^{+} - \dot{S}_{\mathrm{R}}^{\mathrm{eff}} = \frac{D_{\mathrm{r}}}{k\mu}(\dot{S}_{\mathrm{R}}^{-} - \dot{S}^{\mathrm{eff}}) > 0, \tag{5.32}$$

and we get $\dot{S}_{\mathrm{R}}^{+} - \dot{S}_{\mathrm{R}}^{\mathrm{eff}} > 0$ as a consequence of $\dot{S}_{\mathrm{R}}^{-} - \dot{S}_{\mathrm{R}}^{\mathrm{eff}} > 0$. For finite cycle durations, we tested validity of the inequality $\dot{S}_{\mathrm{R}}^{+} - \dot{S}_{\mathrm{R}}^{\mathrm{eff}} > 0$ numerically. In Fig. 5.2 (a) we show the total EPs (5.28) and (5.22) as functions of time during the cycle. All these functions monotonously increase with time and thus they represent valid entropies with respect to the second law of thermodynamics. Notice that the actual EPs $\Delta S_{\mathrm{R}}^{\pm}$ are always larger then the effective EP $\Delta S_{\mathrm{tot}}^{\mathrm{eff}}$, as anticipated in the previous section. The changes in the reservoir entropy during the cycle according to the definitions (5.25), (5.20) and (5.21), of the entropy of the system, (5.23) and (5.26), and of the total EPs are depicted in Fig. 5.2 (right panel).

We are finally prepared to investigate the performance of the engine connected to the active bath. First, in the next section, we study the performance of finite time cycles, which can deliver non-zero output power. Using the specific protocol introduced in Sec. 5.2.2, this can be to great extend done only by numerical evaluation of the formulas derived in the preceding sections. In Sec. 5.6, we investigate performance of the engine analytically in the limit of infinitely slow driving.

5.5 Finite time performance

In this section, we consider a cycle that follows the most general protocol described in Sec. 5.2.2 and we calculate the efficiency, the output power and the output work according to the definitions of Sec. 5.2.3, and the total EPs according to the previous section. In the calculation, we use both the analytical results for the variance given in Sec. 5.2.4 and the results obtained using the numerical method described in App. B.2. The obtained curves always perfectly overlap. In Fig. 5.3 (a), the efficiency monotonically increases with increasing t_p and eventually it reaches the quasi-static limit (the red line). Notably, whether the efficiency is increased or decreased by the bath activity depends on the cycle duration (dashed and dot-dashed lines are sometime above and sometime below the full line). Together with enhancing W_{out} (b) and power (c), the activity thus also leads to increased heat flow into the system. As expected, the output power vanishes for large cycle durations and exhibits a maximum for a certain value of t_p. On the contrary, W_{out} is, for large cycle times, an increasing function which converges to the maximum quasi-static value.
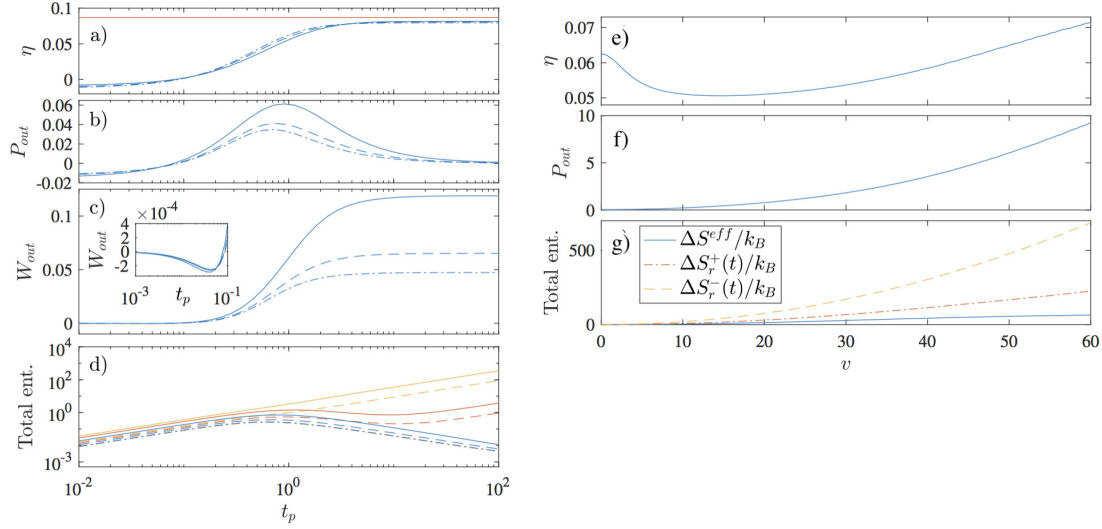
Figure 5.3: Efficiency (a), output power (b), output work (c) and total EP (d) for $v_+ = 0$ (dot-dashed lines), $v_+ = 2$ (dashed lines) and $v_+ = 4$ (full lines) as functions of cycle duration, in the limit cycle. In panel (d), yellow lines stand for ΔS_{tot}^-, red lines for ΔS_{tot}^+ and blue lines for $\Delta S_{\text{tot}}^{\text{eff}}$. Other parameters are the same as in Fig. 5.1. Efficiency (e), power (f) and total EP (g) of the engine as functions of the maximum active velocity v_+ for the protocol shown in Fig. 5.1.

Interestingly, for $10^{-2} \lesssim t_p \lesssim 10^{-1}$, W_{out} exhibits a negative minimum as shown in the inset. This implies that there is a certain lower bound on the cycle duration below which the system does not operate as a heat engine any more, but as a heat pump. As can be observed in Fig. 5.3 (d), for small and large cycle durations the behaviour of the total EPs $\Delta S_{\text{tot}}^{\text{eff}}$ and $\Delta S_{\text{tot}}^{\pm}$ can be described by a power law. For small times, Taylor expansion in t_p of Eqs. (5.29) and (5.22) gives $\Delta S_{\text{tot}}^{\pm} \propto \Delta S_{\text{tot}}^{\text{eff}} \propto t_p$. For large times and $v \neq 0$, $\Delta S_{\text{tot}}^{\pm} \propto t_p$, because then the integrands in Eqs. 5.20 and 5.21 become positive functions of the form $f(t/t_p)$ determined by the quasi-static forms of σ (Eq. (5.15)) and $H = H_\infty = v/(\mu k + D_r)$. For large times regardless of v, $\Delta S_{\text{tot}}^{\text{eff}} \propto 1/t_p$ as can be seen as follows. The effective total EP (5.29) can be written as (cf [9, 209])

$$\Delta S_{\text{tot}}^{\text{eff}} = \frac{1}{4\mu} \int_0^{t_p} dt \, \frac{1}{T_{\text{eff}}} \frac{\dot{\sigma}^2}{\sigma} = \frac{1}{4 t_p \mu} \int_0^1 d\tau \, \frac{1}{\tilde{T}_{\text{eff}}} \frac{\dot{\tilde{\sigma}}^2}{\tilde{\sigma}}, \tag{5.33}$$

where $\tilde{\sigma}(\tau) = \sigma(t/t_p)$, $\dot{\tilde{\sigma}} = d\tilde{\sigma}(\tau)/d\tau$ and $\tilde{T}_{\text{eff}}(\tau) = T_{\text{eff}}(t/t_p)$. For large t_p, the functions $\tilde{\sigma}$ and $\tilde{T}_{\text{eff}}$ are in the leading order in $1/t_p$ determined by Eq. (5.15) and Eq. (5.17), respectively, which proves the above scaling. For $v = 0$, all three definitions of EP are equivalent since $T = T_{\text{eff}}$. In Fig. 5.3 e)-g), we fix $t_p \equiv 1$ and vary the maximum active velocity v_+. For small values of v_+ the efficiency is decreased

by the activity, while, it is increased for large values of v_+, where it eventually attains a constant maximum value. This behaviour can be understood as follows. The efficiency of the heat engine quite generally increases with the largest difference in the effective temperature $\max(T_{\text{eff}}) - \min(T_{\text{eff}})$, similarly as in the Carnot formula. Even out of the quasi-static regime one can expect that the effective temperature is qualitatively described by (5.17). For small values of v_+, Eq. (5.17) implies that the difference can be decreased by variations of the rotational diffusion coefficient depicted in Fig. 5.1 (c), while for large values of v_+ it becomes an increasing function of v_+. More intuitive behaviour is observed for the power Fig. 5.3 f) and the EPs $\Delta S_{\text{tot}}^{\text{eff}}$ and $\Delta S_{\text{tot}}^{\pm}$ (g) that monotonically grows with v_+, extending the behaviour already seen in Fig. 5.3 a)-d). Let us now turn to the quasi-static situation, where we will investigate performance of the engine in several analytically treatable regimes and bring further inside into the behaviour of the engine communicating with the non-equilibrium bath [188, 213].

5.6 Quasi-static performance

In the quasi-static regime where the parameters k, T, v and D_{r} are varied very slowly, the engine dynamics is described by the simple formulas (5.15) and (5.17), i.e. $\sigma = \sigma_\infty = 2T_{\text{eff}}/k$ and $T_{\text{eff}} = T + v^2/[(2\mu D_{\text{r}})(1+R)]$. Here, the ratio $R \equiv k\mu/D_{\text{r}}$ compares the inverse timescale $k\mu$ needed to relax in the potential to the inverse timescale D_{r} need to fully randomise the direction of the active velocity. For $k\mu \gg D_{\text{r}}$ ($R \gg 1$), the dynamics is persistent and the particle moves quasi-ballistically in the potential. On the other hand, for $k\mu \ll D_{\text{r}}$ ($R \ll 1$) the dynamics is an equilibrium-like Brownian motion at an increased temperature $T_{\text{eff}} > T$.

5.6.1 Iso-activity Stirling cycle

We first investigate a proper quasi-static cycle where $\sigma = \sigma_\infty$ during the whole cycle and thus the effective EP (5.28) vanishes. The resulting efficiency is hence given by the equilibrium efficiency of a heat engine connected to an equilibrium bath at temperature T_{eff} which depends on the protocol along which the parameters k and T_{eff} are varied. Here we demonstrate that in order to define the efficiency of an active heat engine correctly, one should pay special attention to the actual type of thermodynamic cycle formed by T_{eff}. Specifically, we use the protocol depicted in Fig. 5.1 with $v_- = v_+$ and thus we consider the case of constant active velocity. We consider the rotational diffusion as a thermal effect described by the Einstein relation, i.e. we take $D_{\text{r}}^{\pm} \propto T_{\pm}$.

In order to evaluate the engine efficiency, we need to identify W_{out} and the heat flowing into the system from the reservoirs given by Eq. (5.8). In general, the heat flows into the system whenever the variance σ increases and vice-versa, see (5.8) and
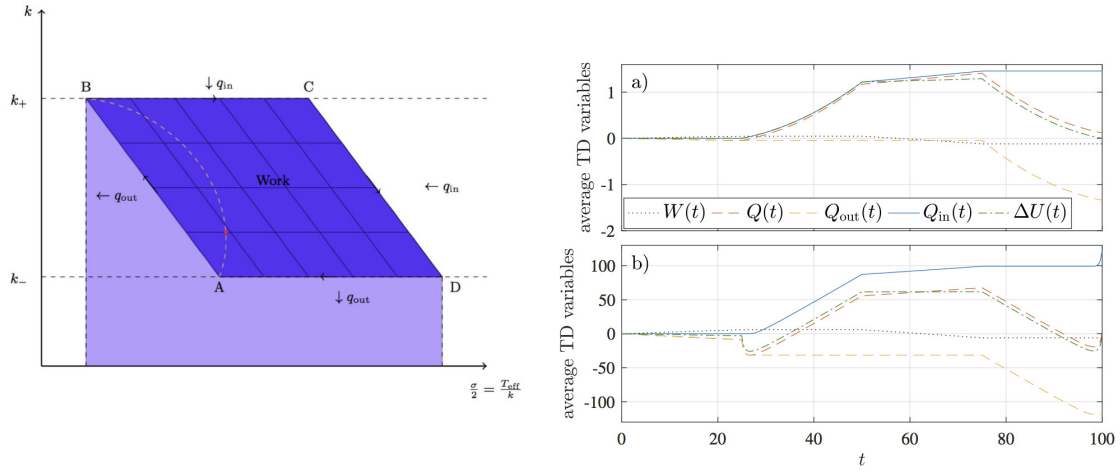
Figure 5.4: Left panel. The thermodynamic diagram of the active heat engine. The oriented area below the individual parts of the cycle give the heat flowing into the system during these branches. The blue area enclosed by the cycle determines the work done by the engine on its environment per cycle, $W_{\text{out}} = Q_{\text{in}} - Q_{\text{out}}$. The sum of purple and blue areas below the line ABD gives the input heat (5.8) and the purple area alone is given by the output heat (5.9).
Right panel. Energetic variables $W, Q, Q_{\text{out}}, Q_{\text{in}}$ and ΔU as functions of time during one cycle. In panel a) we take $v_+ = 4$ and $t_p = 100$. In panel b) we have $v_+ = 500$, $v_- = 50$, $D_{\text{r}}^+ = 500$ and $D_{\text{r}}^- = 5$. Other parameters are the same as in Fig. 5.1.

(5.9). Plugging (5.15) into (5.5) gives the expression

$$W_{\text{out}} = (T_+ - T_-)\log\frac{k_+}{k_-} - \frac{v^2}{2\mu}\left[\frac{1}{D_{\text{r}}^-}\log\left(\frac{k_+}{k_-}\frac{k_-\mu+D_{\text{r}}^-}{k_+\mu+D_{\text{r}}^-}\right) - \frac{1}{D_{\text{r}}^+}\log\left(\frac{k_+}{k_-}\frac{k_-\mu+D_{\text{r}}^+}{k_+\mu+D_{\text{r}}^+}\right)\right] \quad (5.34)$$

for the work done by the engine controlled by the protocol considered in this section. The sign of W_{out} is controlled by the values of the parameter R during the individual branches. Similarly, the sign of the heat Q_{BC},

$$Q_{\text{BC}} = T_+ - T_- - \frac{v^2}{2\mu}\frac{D_{\text{r}}^+ - D_{\text{r}}^-}{(k_+\mu + D_{\text{r}}^+)(k_+\mu + D_{\text{r}}^-)}, \quad (5.35)$$

is also controlled by the behaviour of the parameter R during the cycle. The system is in contact with two reservoirs (active and passive) which do not necessarily absorb and release heat at the same time. As a result, the effective temperature (5.17) may behave in a nonintuitive way. For example, it may decrease when the bath temperature T and the rotational diffusion coefficient D_{r} increase at the same time. The issue with the definition of the input heat becomes even more pronounced after considering relatively large values of the parameters as shown in Fig. 5.4 (b). Here,

the processes BC and DA are composed of two parts with respect to the direction of heat flow. During one of them heat is released into the system (red dashed curve increases) and vice versa during the other one. In the left panel of Fig. 5.4 such a behaviour would for example correspond to the dashed yellow curve, along which heat is released into the system from the point A up to the red point and vice versa during the rest of the branch. To conclude, Fig. 5.4 highlight the importance of a correct definition of absorbed heat, that in general is given only by Eq. (5.8). Let us now investigate the performance of the engine in the two limiting situations of large and small R, where the input heat can be easily identified.

5.6.1.1 $k\mu \gg D_{\rm r}$: high-persistency regime

If $k\mu \gg D_{\rm r}$, the output work becomes, to first order in R^{-1},

$$W_{\rm out} = (T_+ - T_-)\log\frac{k_+}{k_-} - {\rm a}v^2, \quad {\rm a} \equiv \frac{1}{4\mu D_{\rm r}^+}\frac{1}{R^2}\frac{D_{\rm r}^+ - D_{\rm r}^-}{D_{\rm r}^+}\frac{k_+^2 - k_-^2}{k_-^2} > 0. \quad (5.36)$$

a is small but positive and thus it decreases the work with respect to the situation with an equilibrium bath solely, i.e. $0 < W_{\rm out} < W_{\rm out}^{\rm eq} = (T_+ - T_-)\log(k_+/k_-)$. Similarly, the heat

$$Q_{\rm BC} = T_+ - T_- - \frac{v^2}{2\mu D_{\rm r}^+}\frac{1}{R^2}\frac{D_{\rm r}^+ - D_{\rm r}^-}{D_{\rm r}^+} \quad (5.37)$$

is positive for typical values[1]: radius active particles $\sim 1\mu$m, $v \sim 10^{-5}$m s^{-1}, $D_{\rm r} \sim 10^{-1}$ s^{-1}, $k \sim 10^{-6}$Nm^{-1} and $\mu \sim 10^8$kg^{-1}s. Heat is absorbed during the expansion and the isochoric heating, i.e. $Q_{\rm in} = Q_{\rm BC} + Q_{\rm CD}$, as for the equilibrium bath. The average efficiency reads

$$\eta = \frac{(T_+ - T_-)\log\frac{k_+}{k_-} - {\rm a}v^2}{T_+ - T_- + T_+\log\frac{k_+}{k_-} + {\rm b}v^2}, \quad {\rm b} \simeq \frac{1}{2\mu D_{\rm r}^+}\frac{1}{R}\left(\frac{k_+ - k_-}{k_+} - \frac{1}{R}\right) > 0. \quad (5.38)$$

Any correction to the heat flow coming from activity is always positive and proportional to R^{-1} (during the isochoric branch the absorbed heat is reduced by activity, while it is increased during the iso-active expansion). In the limit of large persistence, active heat engines are thus less efficient than the passive ones with a=b=0. Intuitively, persistence is useful during the expansion, but is counter-productive during the compression. In the absence of aligning constraints, the net effect is averaged out and it even leads to the slight decrease in efficiency. To conclude, we remark that the effective temperature to first order in R^{-1}, $T_{\rm eff} \approx T + v_0^2/2k\mu^2$, depends on k and thus it is not constant during the isotherms as shown in Fig. 5.1 (e). The cycle in this regime is thus not a real Stirling cycle. The specific choice of the driving can magnify or reduce this effect.

---

[1]The chosen parameters are comparable with the experiment in [212]

5.6.1.2 $\ k\mu \ll D_{\mathrm{r}}$**: equilibrium-like regime**

If $k\mu \ll D_{\mathrm{r}}$, the output work becomes $W_{\mathrm{out}} = \left(T_{\mathrm{eff}}^+ - T_{\mathrm{eff}}^-\right)\log(k_+/k_-)$ with the standard k-independent effective temperature, $T_{\mathrm{eff}}^{\pm} = T_{\pm} + v^2/2\mu D_{\mathrm{r}}^{\pm}$, given by the limit $R \to 0$ in (5.17). In this regime, the cycle is indeed a Stirling cycle with true isothermal branches with respect to T_{eff}. Note that $T_+ > T_-$ does not imply $T_{\mathrm{eff}}^+ > T_{\mathrm{eff}}^-$ since the active correction is decreasing with the (heat bath) temperature via D_{r}. For typical parameters we have $\left(T_{\mathrm{eff}} - T\right)/T \gg 1$ and thus the usual definition of W_{out} yields a negative value: the environment performs work on the system as we introduced in Sec. 4.3. Similar considerations may be done for the absorbed heat that turns out to be $Q_{\mathrm{in}} = Q_{\mathrm{DA}} + Q_{\mathrm{CD}}$. In this regime, where the active term in the active temperature dominates, T_{eff}^+ is no longer the hot temperature and the cycle must be inverted. Namely, the compression occurs at T_{eff}^+, while the expansion at T_{eff}^-. The inverted active cycle provides output work larger than the corresponding passive one, i.e. $0 < W_{\mathrm{out}}^{\mathrm{eq}} < W_{\mathrm{out}}$. Furthermore, the isochoric heat $Q_{\mathrm{BC}} = T_{\mathrm{eff}}^- - T_{\mathrm{eff}}^+$ is now positive such that the input heat is given by $Q_{\mathrm{in}} = Q_{\mathrm{BC}} + Q_{\mathrm{CD}}$. The resulting efficiency reads

$$\eta = \frac{\left(T_{\mathrm{eff}}^- - T_{\mathrm{eff}}^+\right)\log \frac{k_+}{k_-}}{T_{\mathrm{eff}}^- - T_{\mathrm{eff}}^+ + T_{\mathrm{eff}}^- \log \frac{k_+}{k_-} + \frac{v^2}{2\mu D_{\mathrm{r}}^+}\frac{(k_+ - k_-)\mu}{D_{\mathrm{r}}^+}} \tag{5.39}$$

and $R \ll 1$ implies that the last term in the denominator can be neglected. If we divide the numerator and the denominator in (5.39) by $T_{\mathrm{eff}}^- - T_{\mathrm{eff}}^+$, the efficiency becomes

$$\eta = \frac{\log \frac{k_+}{k_-}}{1 + \frac{1}{\eta_C^{\mathrm{eff}}}\log \frac{k_+}{k_-}}, \quad \eta_C^{\mathrm{eff}} = 1 - \frac{T_{\mathrm{eff}}^+}{T_{\mathrm{eff}}^-} \tag{5.40}$$

which resembles the efficiency of a passive Stirling heat engine η^{eq}, which is given by Eq. (5.40) up to the replacement $\eta_C^{\mathrm{eff}} \leftrightarrow \eta_C = 1 - T_-/T_+$. For a constant ratio k_+/k_-, $\eta > \eta^{\mathrm{eq}}$ (5.40) whenever $\eta_C^{\mathrm{eff}} > \eta_C$, i.e. if the difference in the effective temperatures is larger than the difference in temperatures. We suppose that $T_+ = \alpha T_- = \alpha T$, $D_{\mathrm{r}}^+ = \beta D_{\mathrm{r}}^- = \beta D_{\mathrm{r}}$ and $k_+ = \gamma k_- = \gamma k$ and we look for constraints on (α, β, γ) such that $\eta_C^{\mathrm{eff}} > \eta_C$. Solving a simple inequality, we obtain

$$\beta > \frac{v^2\alpha}{v^2 - 2\mu T D_{\mathrm{r}}\left(\alpha^2 - 1\right)}, \quad D_{\mathrm{r}} < \frac{v^2}{2\mu T}\frac{1}{\alpha^2 - 1}. \tag{5.41}$$

Interestingly, we obtain an upper bound for the rotational diffusion coefficient, in addition to the lower bound given by $R \ll 1$, i.e. $k\mu \ll D_{\mathrm{r}} < \frac{v^2}{2\mu T}\frac{1}{\alpha^2 - 1}$. For typical values, $R \ll 1$ is not easily reached and it requires a weak confinement, if compared to values used in [212]. Although efficiency can be enhanced with respect to equilibrium if $\beta > \alpha$ (for our parameters choice $\beta \approx 2.2$, see Fig. 5.5 a)), it cannot go beyond
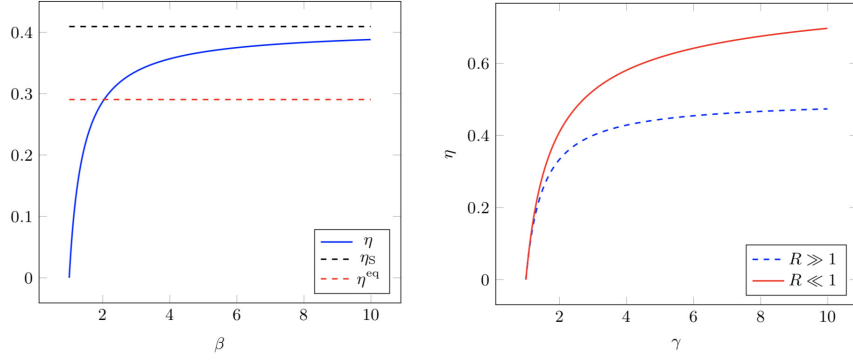
Figure 5.5: Panel (a), the efficiency (5.40) (blue), equilibrium Stirling efficiency (red) and equilibrium saturation Stirling efficiency (black). The parameters are: $\alpha = 2$, $\gamma = 2$, $T = 1$, $\mu = 1$, $D_{\mathrm{r}} = 1$, $v = 10$. Panel (b), sketch of the behaviour of the efficiency in the high persistence regime (blue) and the equilibrium-like regime (red) with respect to the scaling of the stiffness k. For $\gamma = 1$, $\eta = 0$.

the ultimate equilibrium upper bound of efficiency for a Stirling cycle,

$$\eta_S \equiv \lim_{\frac{T_-}{T_+} \to 0} \eta^{\mathrm{eq}} = \frac{\log \frac{k_+}{k_-}}{1 + \log \frac{k_+}{k_-}}. \tag{5.42}$$

Efficiency (5.40) reaches η_S in the limit $\beta \to \infty$, without violating the conditions (5.41). In this section, we considered two extremal regimes of cycle operation and we have found that the efficiency is enhanced by the activity only if $D_{\mathrm{r}}^- > D_{\mathrm{r}}^+$. In particular, η cannot exceed η^{eq} when D_{r} is proportional to the temperature as demanded by the Einstein relation. Yet, such relation need not be satisfied when rotational diffusion itself is influenced by some active process, e.g., if it seen as a long time result of run-and-tumbling [65].

5.6.2 Isothermal Stirling Cycle

Let us now consider another special case of the protocol depicted in Fig. 5.1. We keep the temperature and the rotational diffusion constant during the whole cycle. Furthermore, we set the active velocity v to a positive constant during the branches BC (iso-choric heating) and CD (isothermal expansion) and to zero otherwise. We assume that the changes of the active velocity from 0 to v and vice-versa at the ends of the branches AB and CD are instantaneous, such that no heat is exchanged and no work is done. The cycle is now quasi-static in the sense that after changing v, we let the system relax before we continue changing the other parameters. The important difference between the present setting and the true quasi-static cycle of the previous section is that now the effective EP (5.28) is in general positive which

leads to a lower bound on efficiency compared to the quasi-static situation.

In order to quantify the efficiency we introduce a new state $\tilde{B}$, such that during the abrupt transition $B \to \tilde{B}$ where v is activated no heat is exchanged while it does during the following relaxation $\tilde{B} \to C$. Equivalently for the de-activation $D \to A$ we introduce a state $\tilde{D}$. As a result, the mean square displacements during the branches AB and CD can be written as $\sigma_{AB} = 2T/k$ and $\sigma_{CD} = 2T_{\text{eff}}^{\infty}/k$ with T_{eff}^{∞} given by (5.17). Plugging the variance into Eqs. (5.5) and (5.6) we obtain the output work

$$W_{\text{out}} = \frac{v^2}{2\mu D_{\text{r}}} \log\left(\frac{k_+}{k_-} \frac{k_- \mu + D_{\text{r}}}{k_+ \mu + D_{\text{r}}} \right) \tag{5.43}$$

and the heats

$$Q_{AB} = -T\log\frac{k_+}{k_-}, \ \ Q_{B\tilde{B}} = Q_{D\tilde{D}} = 0, \ \ Q_{\tilde{B}C} = \frac{v^2}{2\mu}\frac{1}{k_+\mu + D_{\text{r}}}, \ \ Q_{\tilde{D}A} = -\frac{v^2}{2\mu}\frac{1}{k_-\mu + D_{\text{r}}}, \tag{5.44}$$

$$Q_{CD} = \frac{v^2}{2}\frac{k_+ - k_-}{(k_+\mu + D_{\text{r}})(k_-\mu + D_{\text{r}})} + T\log\frac{k_+}{k_-} + \frac{v^2}{2\mu D_{\text{r}}}\log\left(\frac{k_+}{k_-}\frac{k_-\mu + D_{\text{r}}}{k_+\mu + D_{\text{r}}}\right). \tag{5.45}$$

The work is positive for every R. Similarly, the input heat is given by the standard formula $Q_{\text{in}} = Q_{\tilde{B}C} + Q_{CD}$. Note that for $v = 0$ the part of heat $T\log\frac{k_+}{k_-}$ in Q_{CD} should not be considered as input heat, because we have only one bath and the heat just leaves the bath and then returns, so the internal energy of the bath after one cycle remains unchanged. For sake of consistency, we do not consider this part of the heat even for $v \neq 0$. The resulting efficiency reads

$$\eta = \frac{\log\left(\frac{k_+}{k_-} \frac{k_-\mu + D_{\text{r}}}{k_+\mu + D_{\text{r}}} \right)}{\frac{D_{\text{r}}}{k_+\mu + D_{\text{r}}}\left(1 + \frac{(k_+ - k_-)\mu}{k_-\mu + D_{\text{r}}}\right) + \log\left(\frac{k_+}{k_-} \frac{k_-\mu + D_{\text{r}}}{k_+\mu + D_{\text{r}}} \right)}. \tag{5.46}$$

Noteworthy, as long as we do not count the contribution $T\log\frac{k_+}{k_-}$ into the absorbed heat, the efficiency does not depend on the magnitude of the active velocity,

$$\eta \underset{R \gg 1}{=} \frac{1 - \frac{k_-}{k_+}}{2 - \frac{k_-}{k_+}} \qquad \eta \underset{R \ll 1}{=} \frac{\log\frac{k_+}{k_-}}{1 + \log\frac{k_+}{k_-}}. \tag{5.47}$$

In Fig. 5.5 b) we plot the efficiency in the two regimes using $k_+ = \gamma k_- = \gamma k$. Noteworthy, the efficiency in the high-persistence regime is smaller than the efficiency in the equilibrium-like regime for each γ. Note that the efficiency in both regime does not depend on v_0. We have confirm it with numerical simulation of the dynamics (5.1). In the simulation we defined as absorbed heat $\langle Q_{\text{in}} \rangle = \langle Q_{CD} \rangle + \langle Q_{\tilde{B}C} \rangle$, therefore $T\log(k_1/k_2)$ is included, for small active velocity it is influencing the efficiency while it is negligible for bigger value of v_0. The efficiency for $R \ll 1$ formally coincides with standard two-heat-baths Stirling efficiency η_S in the limit $T_-/T_+ \to 0$. This is because, we are not counting the equilibrium contribution (equivalent to $T \to 0$) and

we are treating activity as an effective, higher, temperature. The latter result is surprising, because the effective EP (5.29) for the cycle is not zero in general due to the infinitely fast switching during the branches $B \rightarrow \tilde{B}$ and $D \rightarrow \tilde{D}$. Using Eq. (5.29), the total effective EP during the relaxation process $B \rightarrow \tilde{B}$ reads

$$\Delta S_{\text{tot}}^{\text{eff}}(\tilde{B} \rightarrow C) = \mu \int_{\tilde{B}}^{C} T_{\text{eff}}\, \sigma \left(\frac{2}{\sigma} - \frac{k}{T_{\text{eff}}} \right)^2 \geq 0 \tag{5.48}$$

and similarly for $D \rightarrow \tilde{D}$. EP (5.48), is always non-negative and it is zero if and only if $\sigma_C \sim \sigma \sim \sigma_{\tilde{B}}$. Interestingly, this condition is met for $R \rightarrow 0$, which is equivalent to $D_r \rightarrow \infty$. In this limit, the effective temperature T_{eff} boils down to T and thus i) the abrupt changes of the activity does not bring the system out of equilibrium and ii) the engine delivers vanishing amount of work. In conclusion, we have found that at least in the situations investigated in this section, the upper bound on efficiency of the active heat engine with the driving introduced in Sec. 5.2.2 is the ultimate equilibrium Stirling efficiency (5.42).

5.7 Conclusion and Outlook

In this Chapter we discussed the properties of a Stirling engine based on an active particle embedded in a thermal environment. The particle is confined by a harmonic potential whose stiffness is periodically changed inducing a cyclic dynamics. This system is studied in the framework of Stochastic Thermodynamics and, given that the confinement is linear, the energetics (heat, work and internal energy) is completely ruled by the variance of the particle alone. Active systems, compared to passive ones, are characterised by non-Gaussian fluctuations which, among other things, enhance the variance, so that it comes naturally to ask if this is able to improve the performance of the cycle and lead to higher efficiencies, with respect to the same cycle run in contact with a thermal environment. From the variance an effective temperature can be defined, key element for a mapping to equilibrium, which allows us to adopt many known results for passive Brownian heat engines to the active engine. We studied the system both in quasi-static regime, analytically and in the finite-cycle-time regime, numerically. In the latter the power can be defined and remarkably, it increases with activity, together with the work, although the efficiency is just slightly affected. Namely, active particles environment are probably more suited to enhance the power of an engine rather than the efficiency. Similar conclusions for the efficiency have been drawn in the quasi-static limit as well.

Those results are valid for a passive particle embedded in an active particles fluid too, provided that the assumptions introduced in Sec. 4 are satisfied, in particular linear coupling between the colloid and the active particles and no mutual interaction between the active particles themselves, so that the system can be analytically solved and traced back to the ABP model. To our knowledge, the latter has been

used to describe a passive colloid in an active environment only in [188] yet, aiming to reproduce the surprising experimental results presented in [212] for a Stirling engine based on a colloidal particle diffusing in a bacterial bath. Namely, in [212] it has discussed a consistent increase of the efficiency, beyond the upper limit for a classical Stirling cycle, realised with the same system coupled to an equilibrium thermal bath. On the other hand, with the set of parameters of [212] (we stress that the value of the rotational diffusion coefficient is not provided in the paper, therefore we have used typical value for bacteria, c.f. [68]), simple ABP model cannot provide such an increase of efficiency, unless the model is modified to include a dependence on the stiffness of the active velocity is assumed.

Interestingly, an even greater increase could be related to rare fluctuations described by large deviation theory [227] and associated, for example, to alignment configurations for the particles, supporting the hypothesis that collective effects should be taken more into consideration to build a more efficient active-particles Stirling cycle. Intuitively, if during the compression the active particles are in average pointing towards the minimum of the potential and in the opposite direction during the expansion, the efficiency would go beyond Carnot and even beyond one, since we are not counting into the definition of efficiency the housekeeping heat, necessary to keep the particles active. In our model the persistence of the active particles cannot be harvested and, when not negligible, does not bring any benefit, c.f. 5.6.1.1. On the other hand, for big rotational diffusion for which the system is relegated to an equilibrium-like regime, activity effect is confined to an increase of temperature, which indeed can trigger a gain in efficiency, with a fine-tuning of the parameters. In this Chapter we have investigated in details this linear model and we have discussed its limit. Further theoretical investigation into this field should be based on more refined model, able to take into account alignment interaction between active particles and as a response to external stimuli.

Chapter 6

The pressure of active particles

6.1 Introduction

The surging field of active matter aims for a microscopic understanding and control of the material properties of assemblies of interacting active elements. A main strategy is to revisit the paradigms of established many-body theories for inanimate matter, and to elucidate the new physics arising from the nonequilibrium energy consumption and possibly unusual interactions of its "atoms". If successful, this might help to classify such seemingly diverse systems as artificial self-propelled colloidal particles [228], motile bacteria [229], or even flocking birds [230], as examples of a unified new state of matter, and to inform potential biological or medical applications [193, 231]. A versatile model for systematic theoretical investigations is provided by an active-particle suspension. Despite its simplicity, it captures the most crucial property of active matter, that is its intrinsic nonequilibrium. Namely, the latter is not brought about by the application of external forces to a quiescent system, but rather by the continuous *local* energy input that fuels the autonomous particle motion, itself. For experimental realisations, one can draw on a large arsenal of technologies for tuning the particle-interactions and propulsion. This promises good control over the various mechanisms by which the local breaking of detailed balance can manifest itself on the material level [16, 67, 83, 170]. For example, if spatial symmetries are broken (e.g. by funnel barriers or asymmetric obstacles), this allows the microscopic activity to be concerted. Thereby, persistent macroscopic currents can be induced [65] and gears can be set in perpetual motion [167, 232], so that macroscopic work can be extracted from the microscopic activity [233]. As a consequence, the status of basic thermodynamic notions, such as temperature and pressure, on which any coarse-grained description of equilibrium many-body systems relies, has become a matter of debate even for the simplest of such model systems [182, 234]. Only in the limit of weakly persistent particle motion and weak interactions, the associated conceptual and practical problems were unambiguously resolved. An effective Hamiltonian can then be assigned to the equations of motion, with the activity subsumed into an appropriate nonequilibrium noise term. This gives rise to an effective Maxwell-

Boltzmann steady state, weighted by an effective temperature, from which also the pressure can be derived [23, 83, 235]. But this somewhat trivial limit essentially amounts to neglecting the most genuine nonequilibrium features, and it is clearly of interest to venture beyond it and systematically address the more spectacular effects alluded to above. For equilibrium systems, pressure can be defined in three ways:

(a) the derivative of a free energy,

(b) the mechanical force per unit area on confining walls

(c) the trace of the hydrodynamic stress tensor, which represents the momentum flux in the system.

Definitions (b) and (c) apply even out of equilibrium, where a unique concept of free energy is still lacking, as they are based on purely kinematic (mechanical) arguments. Indeed, they have already been employed within different theoretical approaches: overdamped Fokker-Planck equations (FPE) [21], the virial theorem for Langevin equations [76, 116], empirical continuum models supported by numerical simulations [235], and density functional theories for overdamped systems [173][1]. All these derivations consider as their starting point the ABP model [21, 68], in which overdamped particles are allowed to perform translational and rotational Brownian motion, and the activity is ascribed to a propulsion force of constant magnitude along the instantaneous particle orientation. Despite its analytical and numerical simplicity, this model allows to include many features of active particles, but it neglects their hydrodynamic interactions via the solvent flow they excite. Using the nomenclature introduced in [79], ABP is a model of "dry" active matter, in contrast with "wet" models, in which the momentum exchanged among the active particles and their solvent is taken more seriously. Two main facts are so far agreed upon. First, pressure is, in general, not a state function, as it depends on the system's microscopic features and hence cannot be expressed only in terms of thermodynamic variables. Secondly, the pressure of an interacting ABP suspension exhibits a non-monotonic density dependence that manifests itself in a self-caging or clustering of the particles and a tendency to accumulate at (curved) walls [236–238]. A model-independent, "thermodynamic" notion of pressure has so far only been established for particular cases, such as the mentioned limit of small persistence of the active motion, assuming non-interacting particles, or at least torque-free pairwise inter-particle forces, with torque-free wall interactions. Such special conditions can only (approximately) be realised for dilute and weakly confined suspensions of spherical self-propelled particles [21, 236]. The pressure is then surmised to depend only on bulk properties, which are usually assumed to be homogeneous and isotropic, and the wall-force is neglected as a subdominant surface term. For example, Yang et al. calculate the pressure via the Irving-Kirkwood formula [239] for the stress tensor, but

---

[1]Personal Communication by Raphael Wittkowski from Westfälische Wilhelms-Universität Münster

consider a spatial average, while Winkler et al. [76] obtain the pressure from the virial theorem, but assume it to be uniform. As a consequence, possible inhomogeneities necessarily remain hidden, in all cases. The microscopic derivation of hydrodynamic equations of motion arguably represents a natural framework to shed light on these issues and to venture beyond the limitations of current theories. The recent literature provides a wealth of hydrodynamic theories derived phenomenologically, i.e., based on the macroscopic space-time symmetries [240–242]. A potential difficulty with such approaches to active matter may be seen in the anticipated breaking of microscopic symmetries at a mesoscopic level [16], which could potentially jeopardise the derivation and judicious application of the phenomenological hydrodynamic equations. Yet, attempts to derive them directly from the underlying microscopic equations of motion are rare. A notable exception is the work by Bertin et al. [243], which is however only valid for an infinitely dilute gas of active particles with certain specific alignment interactions. Though exceptionally valuable for the understanding of the emergence of collective behaviour, such approaches tell us little about an increasing number of interesting experimental systems characterised by high densities, potentially complex mutual interactions of the particles, and often narrowly confining geometries. Therefore, our aim is to derive the hydrodynamic equations for an active fluid by a systematic coarse-graining of the (underdamped) microscopic equations of motion of a potentially strongly interacting and dense active particle suspension. The discussion of the results in this Chapter follows the same structure of [20]. In the present contribution, we exemplify the procedure for a swimmer model that neglects the hydrodynamics of the solvent and reduces to the ABP model in the limit of large friction. We thus only deal with "dry swimmers", here, and defer the discussion of a more realistic microscopic model to a future contribution. In particular, we derive the balance equation for the local momentum, which allows us to uniquely identify the pressure from definition (c). The obtained hydrodynamic equations keep track of the local inhomogeneities of the fluid through local averages, performed over the many-body microscopic probability function. Section 6.2 introduces the microscopic model and, on a formal level, the hydrodynamic equations for the relevant macroscopic fields, namely, particle density, momentum and polarisation. In sections 6.3.1 we develop a multiple-scale theory that helps us to close this set of conservation equations based on a systematic coarse-graining of the underlying microscopic model. In sections 6.3.2-6.3.4 we apply it to the momentum equation to access the high-friction limit and obtain a closed expression for the stress tensor. In section 6.3.3 we investigate the slowest dynamics in the system, as captured by the equation of motion for the particle density, neglecting momentum dynamics, in order to make contact with previous work on the ABP model. Finally, in section 6.3.5, we perform a weakly-inhomogeneous-density approximation and in section 6.3.6 a low-density approximation of the pressure, in order to derive some explicit results for the stationary pressure of an ABP suspension interacting by a short-range repulsion.

6.2 Derivation of the hydrodynamic equations

Consider the equations for N underdamped ABPs in d$=2$ with coordinates $(x_i, v_i, \theta_i) \in \mathbb{R}^{2d+1}$ immersed in a fluid providing friction and noise (unitary masses):

$$\dot{x}_i = v_i, \qquad \dot{v}_i = -\gamma v_i + F_i^{\text{int}} + F^{\text{A}} n_i + F_i^{\text{ext}} + \sqrt{2\gamma T} \xi_i, \qquad \dot{\theta}_i = \sqrt{2D_{\text{r}}} \chi_i \quad (6.1)$$

where $F_i^{\text{int}} = \sum_{j \neq i}^{N} F_{ij}^{\text{int}}$, and F_{ij}^{int} is the interaction force exerted by particle j on particle i. Possible external forces (e.g. confining walls, gravity) are included in F_i^{ext}. Internal and external forces may depend on both positional and angular coordinates. The noises ξ_i and χ_i are standard Gaussian ones with zero average value and delta correlations in time, γ and T are the friction and temperature of the embedding fluid respectively ($k_B = 1$). Activity manifests itself through the propulsive force, having magnitude $F^{\text{A}} = \gamma v_0$ and direction along the particle vector n_i, defined by the orientation angle θ_i and randomised by rotational diffusion at rate D_{r}. Namely, we exclude both external torques or particle-particle alignment interactions affecting the orientational dynamics. Hydrodynamic fields can be defined from the microscopic dynamics by local ensemble averaging, which for simplicity of notation we denote, for any observable a_i by

$$\left\langle \sum_i a_i \right\rangle_r \equiv \left\langle \sum_i a_i \, \delta \left(x_i - r \right) \right\rangle. \qquad (6.2)$$

The average $\langle \cdot \rangle$ is taken with respect to the N-particle probability density function (PDF) $\rho_N(\{x_i, v_i, \theta_i\}_{i=1}^{N}, t)$. The relevant hydrodynamics fields are

- the fluid mass (or number) density, $\rho(r, t) \equiv \left\langle \sum_{i=1}^{N} 1 \right\rangle_r$,

- the flow momentum, $u(r, t) \rho(r, t) \equiv \left\langle \sum_{i=1}^{N} v_i \right\rangle_r$,

- the fluid polarisation $\mathcal{P}(r, t) \rho(r, t) \equiv \left\langle \sum_{i=1}^{N} n_i \right\rangle_r$, $\mathcal{P}(r, t) \in [0, 1]$.

For later convenience we introduce here the divergence of the Irving-Kirkwoord (IK) tensor

$$\nabla_r \cdot \sigma_{\text{IK}} \equiv \left\langle \sum_{i=1}^{N} F_i^{\text{int}} \right\rangle_r, \qquad (6.3)$$

which can be defined whenever $F_{ij}^{\text{int}} = -F_{ji}^{\text{int}}$ [239], irrespective of the functional dependence of F_{ij}^{int} [2]. The dynamical equations for these observables can be derived

---

[2]Noteworthy it remains valid even if the forces depend on the self-propulsion orientations, as long as they do not enter explicitly in the average value as for the observable $\langle \sum_{i=1}^{N} F_i^{\text{int}} n_i \rangle_r$.

from the formula $\partial_t \langle a \rangle = \langle \mathcal{L} a \rangle$, where

$$\mathcal{L} = \sum_{i=1}^{N} \left[v_i \cdot \nabla_{x_i} + (-\gamma v_i + F_i^{\text{int}} + F^{\text{A}} n_i + F_i^{\text{ext}}) \cdot \nabla_{v_i} + \gamma T \nabla_{v_i}^2 + D_{\text{r}} \partial_{\theta_i}^2 \right], \quad (6.4)$$

is the backward operator associated with (6.1), for any generic state observable a. For the density $\rho(r, t)$ we find the continuity equation

$$\partial_t \rho(r, t) + \nabla_r \cdot (u(r, t) \rho(r, t)) = 0. \tag{6.5}$$

For the polarisation density $\mathcal{P}(r, t) \rho(r, t)$ we obtain

$$\partial_t (\mathcal{P}(r, t) \rho(r, t)) = -D_{\text{r}} \mathcal{P}(r, t) \rho(r, t) - \nabla_r \cdot (\mathcal{C}_{nv}(r, t) \rho(r, t)), \tag{6.6}$$

in which we have introduced the correlation tensor

$$\mathcal{C}_{nv}(r, t) \rho(r, t) \equiv \left\langle \sum_{i=1}^{N} n_i v_i \right\rangle_r. \tag{6.7}$$

If the fluid is isotropic and homogeneous, (6.7) can be factorised into $\mathcal{C}_{nv} \rho = \mathcal{P} u \rho$. However, in many physical situations these symmetries are broken. Examples are cluster formation at high densities [244], and particle accumulation close to boundaries [59, 181]. In these cases $\mathcal{C}_{nv}$ plays an important role, as it keeps track of correlations between particle orientation and velocity. Note that, due to the first term on the RHS of (6.6), coming from the rotational diffusion, the polarisation is not a locally conserved field. Instead it is locally dissipated at rate D_{r}. For the momentum density $\rho u = \rho(r, t) u(r, t)$,

$$\partial_t (\rho u) + \nabla_r \cdot (\rho u u) = \nabla_r \cdot \sigma + F^{\text{A}} \mathcal{P} \rho - \gamma u \rho + F^{\text{ext}} \rho, \tag{6.8}$$

where we identified the full stress tensor $\sigma = \sigma_{\text{IK}} + \sigma_{\text{kin}}$. In the kinetic term,

$$\sigma_{\text{kin}} \equiv -\left\langle \sum_{i=1}^{N} (v_i - u)(v_i - u) \right\rangle_r \tag{6.9}$$

advective contributions have been subtracted. For completeness, we also note the dynamical equation for the kinetic tensor σ_{kin}, which represents the energy balance,

$$\frac{1}{2} \partial_t \sigma_{\text{kin}}(r, t) = -\nabla_r \cdot \left\langle \sum_{i=1}^{N} v_i (v_i - u)^2 \right\rangle_r + \left\langle \sum_{i=1}^{N} (-\gamma v_i + F^{\text{A}} n_i)(v_i - u) \right\rangle_r$$

$$+ \gamma T \rho(r, t) + \left\langle \sum_{i=1}^{N} (F_i^{\text{ext}} + F_i^{\text{int}})(v_i - u) \right\rangle_r \tag{6.10}$$

According to (6.8), activity behaves as an external force, on a par with F_i^{ext} [236]. In other words, it is responsible for local violations of momentum conservation and cannot be included in the stress tensor. Yet, if the time derivative of the polarisation is negligible, such local non-conservation of momentum can be neglected and the activity can be absorbed in the stress tensor. Indeed, the stationary solution of (6.6), $\nabla_r \cdot (\mathcal{C}_{nv}\rho) = -D_r \mathcal{P}\rho$, renders (6.8) in the form

$$\rho \frac{du}{dt} = \nabla_r \cdot \sigma_{\text{s}} - \gamma u \rho + F^{\text{ext}}\rho, \tag{6.11}$$

with

$$\sigma_{\text{s}} \equiv \sigma_{\text{IK}} + \sigma_{\text{kin}} - \frac{F^{\text{A}}}{D_r}\mathcal{C}_{nv}\rho. \tag{6.12}$$

entailing that local violations of momentum conservation are attributable to the friction and the external force only. We note that on the LHS of Eq. (6.11) we have introduced the material derivative, as usually done. Since the first summand on the RHS of (6.6) is a constant damping term, the condition $\partial_t (\mathcal{P}\rho) = 0$ may be guaranteed by a fast relaxation of the particle orientation in comparison with the shortest accessible time scale dt, i.e. $D_r\, dt \gg 1$. For particles of 1μm radius in water, $D_r \approx 10^{-1}$-$10^0\,\text{s}^{-1}$, which restricts the applicability of Eqs. (6.11)- (6.12) to considerations that do not resolve time scales below a minute, say. For a radius of $100\,\text{nm}$, the time resolution is about $10\,\text{ms}$. Large D_r corresponds to particles experiencing strong rotational diffusion, so that the persistence length of their paths is small in comparison with the mean particle distance and the characteristic system length and the only relevant effect of activity is an enhanced translational diffusion [75]. Formally, the system then behaves as a passive Brownian particle suspension maintained at an elevated effective temperature [181, 182, 189]. To sum up, in the fast rotation limit the polarisation can be written as the divergence of a tensor. If the external force represents the short-ranged interaction with a wall (and thus felt by the particles only in proximity of the wall itself), this result is valid both in the bulk where $F^{\text{ext}} = 0$ and close to the wall itself. Our model is valid for any sort of external force, even if explicitly depending on the self-propulsion orientation θ_i, while it is not if external torques, affecting the orientational dynamics, are taken into consideration. We will give some details regarding that in the following. Interestingly, if the features of the dynamics do not allows to neglect the time-derivative of the polarisation, the polarisation itself cannot be longer expressed as the divergence a tensor. Nonetheless, if we plug (6.6) into (6.8) and we sum and subtract the quantity $\frac{\gamma v_0}{D_r}\nabla_r \cdot (\rho\mathcal{P}u)$, we obtain an equation of motion for a new hybrid dynamic field involving both linear and angular momenta,

$$\rho \frac{d}{dt}\left(u + \frac{\gamma v_0 \mathcal{P}}{D_r}\right) = \nabla_r \cdot \left(\sigma + \frac{\gamma v_0}{D_r}\left(\mathcal{P}u - \mathcal{C}_{nv}\right)\rho\right) - \gamma\rho u + F^{\text{ext}}\rho \tag{6.13}$$

$$= \nabla_r \cdot \left(\sigma_{\text{s}} + \frac{\gamma v_0}{D_r}\mathcal{P}u\rho\right) - \gamma\rho u + F^{\text{ext}}\rho \tag{6.14}$$

As familiar from conventional hydrodynamics, the parenthesis in the divergence in (6.13) accounts for fluctuations, namely the fluctuation part of the tensor $\mathcal{C}_{nv}$. Eq. (6.13) (or equivalently (6.14)) is a continuity equation for a combination of linear momentum and polarisation. Interestingly it says that, even in the slow rotation regime, activity can be subsumed into a divergence, provided that momentum and polarisation are not investigated individually. On the other hand, no manipulation of (6.8) and (6.6) allows to write the friction as a divergence term. This plainly reveals the origin of dissipation for this model, in both the fast and slow rotational diffusion regime, with and without activity. In presence of activity the dissipation compensates the continuous source of momentum from the activity. In order to make the hydrodynamic description self-contained, we have to express the microscopic degrees of freedom, in terms of the hydrodynamic variables. To this end, we derive a suitable expression for the N-particle PDF valid in the limit of high-friction, in the next section.

6.3 Hydrodynamic equations in the high-friction limit

6.3.1 Multiple time scale theory

With typical suspensions of active colloidal particles in mind, we now consider the limit of large friction γ, where the particle velocity v_i relaxes rapidly in comparison with the position x_i. We can then treat the latter as adiabatically slow as compared to the former. The scale separation can formally be exploited by means of a multiple-time-scale theory [41]. With the aim of systematically performing the overdamped limit for the microscopic many-body PDF, we introduce a dimensionless bookkeeping parameter $\varepsilon \ll 1$, such that $\gamma = \varepsilon^{-1}\tilde{\gamma}$ with $\tilde{\gamma}$ an inverse natural time, e.g., the ratio of thermal speed and particle size. This permits the distinction of three time scales, namely, fast $\tau_0 = \varepsilon^{-1}t$, intermediate $\tau_1 = t$, and slow $\tau_2 = \varepsilon t$, and to expand the N-particle PDF $\rho_N(\{x_i, v_i, \theta_i\}_{i=1}^N, t)$ associated with (6.1) as

$$\rho_N = \rho_N^{(0)} + \varepsilon\rho_N^{(1)} + O(\varepsilon^2). \tag{6.15}$$

In the absence of activity, such multi-scale analysis leads to the overdamped FPE for a passive N-particle system with τ_0 and τ_2 associated to the velocity and position relaxation respectively, τ_1 being just a technical artefact. A standard derivation can be found, e.g., in [1, 42, 245]. As a byproduct, it yields a formal expression for ρ_N. While the Maxwell-Boltzmann distribution is *a priori* known to provide the stationary state for an equilibrium system, an explicit calculation is required for active and driven systems [246]. Our starting point is the FPE derivable from (6.4),

$$\left[\frac{\partial}{\partial t} + \sum_{i=1}^N v_i \cdot \nabla_{x_i} + \left(F_i^{\text{ext}} + F_i^{\text{int}}\right) \cdot \nabla_{v_i} - D_{\text{r}}\partial_{\theta_i}^2 - \gamma\nabla_{v_i} \cdot (v_i - v_0 n_i + T\nabla_{v_i})\right]\rho_N = 0 \tag{6.16}$$

in which the active force $\gamma v_0 n_i$ is seen to act like a negative friction along the particle orientation. Therefore, it contributes to the velocity relaxation, implying that the velocity PDF will depend on the orientation angle, differently from a passive system. Following the Supplemental Materials of Ref. [245], we derive the density ρ_N to the order ε in Appendix C.1. We merely summarise its results, here. Both terms in (6.15) involve a Gaussian weight for the correlations of velocities and orientations. Accordingly, we find the zero-order density

$$\rho_N^{(0)} = \Phi \frac{1}{2\pi T} \exp\left(-\frac{(v_i - v_0 n_i)^2}{2T}\right), \tag{6.17}$$

and the first correction

$$\rho_N^{(1)} = \frac{1}{\tilde{\gamma}} \left[\Psi - (v_i - v_0 n_i)\left(\frac{\partial}{\partial x_i} - \frac{F_i^{\text{int}} + F_i^{\text{ext}}}{T}\right)\Phi\right] \cdot \frac{1}{2\pi T} \exp\left(-\frac{(v_i - v_0 n_i)^2}{2T}\right), \tag{6.18}$$

where $\Phi(\{x_i, \theta_i\}_{i=1}^N, \tau_1, \tau_2)$ and $\Psi(\{x_i, \theta_i\}_{i=1}^N, \tau_1, \tau_2)$ are unknown N-particle functions independent of the fast time τ_0. Ignoring higher order contributions, they give the overdamped N-particle PDF

$$\int \prod_{i=1}^N dv_i \, \rho_N = \Phi + \frac{\varepsilon}{\tilde{\gamma}} \Psi + \mathcal{O}(\varepsilon^2). \tag{6.19}$$

By construction, this PDF satisfies the overdamped FPE [234], which can also directly be derived by ignoring the particle inertia in (6.1).

6.3.2   Momentum Equation

In the previous section we have seen that the large friction experienced by the particles allows for an expansion (6.15) of the N-particle PDF in powers of the friction γ. In the present section, we consistently make use of (6.15), together with (6.17) and (6.18), in order to expand the tensor

$$\sigma_{\text{kin}} = \sigma_{\text{kin}}^{(0)} + \varepsilon\, \sigma_{\text{kin}}^{(1)} + \mathcal{O}(\varepsilon^2). \tag{6.20}$$

The expansion of σ_{kin} utilises the notation of (6.15), e.g. $\sigma_{\text{kin}}^{(0)}$ involves only averaging over (6.17), namely,

$$-\sigma_{\text{kin}}^{(0)} = \sum_{i=1}^N \int dx_i d\theta_i \left[T\mathbb{I} + (v_0 n_i - u)^2\right] \delta(x_i - r)\Phi = T\rho^{(0)}\mathbb{I} + \left\langle \sum_{i=1}^N (v_0 n_i - u)^2 \right\rangle_r^{(0)} \tag{6.21}$$

Here, $\mathbb{I}$ is the identity matrix and $\langle\ldots\rangle^{(0)}$ denotes an average performed with $\rho_N^{(0)}$ given by (6.17), but marginalised with respect to velocities v_i, e.g. $\rho^{(0)} = \left\langle \sum_{i=1}^N 1 \right\rangle_r^{(0)}$.

With slight abuse of notation, we write $(v_0 n_i - u)^2$ for both the tensorial product in (6.21) and the scalar product in (6.17) and (6.18). From (6.21), it is clear that the active contribution prevents the velocity fluctuations from relaxing to the heat bath temperature on the fast time scale. The second-leading term, denoted by $\langle \ldots \rangle^{(1)}$, is found by using (6.18):

$$-\sigma_{\text{kin}}^{(1)} = \sum_{i=1}^{N} \int dx_i d\theta_i \ \left[T\mathbb{I} + (v_0 n_i - u)^2 \right] \delta\left(x_i - r\right) \frac{\Psi}{\tilde{\gamma}}$$

$$+ \frac{2}{\tilde{\gamma}} \int \prod_{i=1}^{N} dx_i d\theta_i \ \sum_{i=1}^{N} \delta\left(x_i - r\right) (v_0 n_i - u) \left(F_i^{\text{int}} + F_i^{\text{ext}}\right) \Phi$$

$$- \frac{2T}{\tilde{\gamma}} \int \prod_{i=1}^{N} dx_i d\theta_i \ \sum_{i=1}^{N} \delta\left(x_i - r\right) (v_0 n_i - u) \frac{\partial \Phi}{\partial x_i}. \tag{6.22}$$

With slight abuse of notation, here we denote by Ψ and Φ the functions in (6.17) and (6.18) integrated over the coordinates of the $N - 1$ particles $j \neq i$. According to (6.19), we identify the first term in the integral in (6.22) with $T\rho^{(1)}\mathbb{I}$. Integrating by parts in the third line and using the definition of $\rho^{(0)}$ we get

$$-\sigma_{\text{kin}}^{(1)} = T\rho^{(1)}\mathbb{I} + \left\langle \sum_{i=1}^{N} (v_0 n_i - u)^2 \right\rangle_r^{(1)} - \frac{2T}{\tilde{\gamma}} \nabla_r \left\langle \sum_{i=1}^{N} (v_0 n_i - u) \right\rangle_r^{(0)}$$

$$+ \frac{2}{\tilde{\gamma}} \left\langle \sum_{i=1}^{N} \left(F_i^{\text{int}} + F_i^{\text{ext}}\right) (v_0 n_i - u) \right\rangle_r^{(0)}. \tag{6.23}$$

The first two terms extend the leading contribution in (6.21) to the next order. The remaining terms constitute the non-equilibrium corrections to the kinetic tensor and they will be considered in the following. Reverting to the physical quantity γ, the sum of the kinetic tensors gives

$$-\sigma_{\text{kin}}^{(0)} - \varepsilon\, \sigma_{\text{kin}}^{(1)} \simeq T\rho\mathbb{I} + \left\langle \sum_{i=1}^{N} (v_0 n_i - u)^2 \right\rangle_r - \frac{2T}{\gamma} \nabla_r \left\langle \sum_{i=1}^{N} (v_0 n_i - u) \right\rangle_r$$

$$+ \frac{2}{\gamma} \left\langle \sum_{i=1}^{N} (v_0 n_i - u) \left(F_i^{\text{ext}} + F_i^{\text{int}}\right) \right\rangle_r \tag{6.24}$$

All the average values in (6.24) contain the hydrodynamic flow velocity u. In order to obtain a consistent expansion in powers of the friction γ, u must itself be expanded to order $\mathcal{O}(1/\gamma)$. Using the definition of the flow momentum together with the expansion (6.15), we obtain

$$\rho u = v_0 \mathcal{P}\rho - \frac{T}{\gamma} \nabla_r \rho + \frac{1}{\gamma} \left(\nabla_r \cdot \sigma_{\text{IK}} + F^{\text{ext}}\rho\right). \tag{6.25}$$

The physical interpretation is that the $O(\gamma^0)$ coherent velocity is an active streaming contribution $v_0 \mathcal{P}$, while the usual hydrodynamic streaming terms are damped by the factor γ^{-1}. In other words, they are smaller by a factor $TD_r/\gamma v_0^2 = \mathrm{Pe}^{-2}$ [68]. Plugging (6.25) into (6.24), we obtain for the kinetic tensor (6.20)

$$-\sigma_{\mathrm{kin}} = T\rho\mathbb{I} + v_0^2 \left(\mathcal{Q} - \mathcal{PP} \right) \rho - \frac{2v_0\mathcal{P}}{\gamma} \left(\nabla_r \cdot \sigma_{\mathrm{IK}} + F^{\mathrm{ext}}\rho \right)$$

$$+ \frac{2v_0}{\gamma} \left\langle \sum_{i=1}^{N} \left(F_i^{\mathrm{ext}} + F_i^{\mathrm{int}} \right) n_i \right\rangle_r + \mathcal{O}(1/\gamma^2) \tag{6.26}$$

where we defined the "nematic" tensor

$$\mathcal{Q}\left(r, t\right) \rho(r, t) \equiv \left\langle \sum_{i=1}^{N} n_i n_i \right\rangle_r , \tag{6.27}$$

in line with what we said about the order of the terms in (6.25) the $O(\gamma^0)$ correction to the equilibrium contribution to σ_{kin} is due to active noise, while the $O(1/\gamma)$ terms subtract the usual streaming contribution from it. If r is a point far from a boundary, and the density is low enough to prevent cluster or lanes formation [247], both $\mathcal{P}$ and the off-diagonal components of $\mathcal{Q}(r, t)$ are zero and the active noise term becomes $v_0^2 \mathbb{I}\rho$ divided by the space dimension. Together with the ordinary kinetic pressure it may then be identified as arising from an effective temperature. More generally, though, the temperature of an active fluid is, in principle, neither homogeneous nor isotropic. Nevertheless, since the entries of $\mathcal{Q}$ and $\mathcal{P}$ are bounded by one and, in typical experiments, $v_0 \lesssim 100\,\mu\mathrm{m/s}$, the active correction is much smaller than the thermal energy and can thus be neglected in practice.[3] In other words, the heating of an active particle system due to the activity itself (if not by its propulsion machinery) is usually minute. The remaining terms constitute the non-equilibrium corrections to the kinetic tensor, which evidently depend on the system's microscopic details. The correlation between F_i^{int} and n_i prevents an interpretation following the standard IK-tensor derivation. Indeed, due to activity, it is not possible to extract a gradient with respect to r from the expression in the second line of (6.23). Likewise, the external force contribution is not generally factorisable. We therefore define the local tensors

$$\mathcal{I}_1\left(r, t\right) \rho(r, t) = \left\langle \sum_{i=1}^{N} F_i^{\mathrm{ext}} n_i \right\rangle_r , \tag{6.28}$$

$$\mathcal{I}_2\left(r, t\right) \rho(r, t) = \left\langle \sum_{i=1}^{N} F_i^{\mathrm{int}} n_i \right\rangle_r , \tag{6.29}$$

---

[3]Indeed, in our equation we put $k_B = m_i = 1$, but in natural unity of measure, the first term in (6.26), would be $k_B T/m_i$. For 1-μm radius particle slightly denser than water at room temperature the average thermal velocity is $\sim 0,02\mathrm{m\,s}^{-1}$, much bigger than v_0.

that account for the correlations between the particle orientation and the external and internal forces, respectively. We recall that F^{ext} is considered to be a generic external force. If it represents the short-ranged interaction with a wall, the term $\mathcal{I}_1(r,t)\rho(r,t)$ describes the correlation among the wall force and the local polarisation – e.g., $\mathcal{I}_1 \simeq 0$ where particles swim parallel to a wall. When the integrated pressure is considered, this term can be neglected, either as a consequence of vanishing current [22,181,234] or invoking the thermodynamics limit in which it becomes a subdominant surface term [116]. However, when long-range correlations are induced by the external forces, or when $\mathcal{I}_1$ is considered locally near a wall or an obstacle, it is not negligible and may be responsible for such effects as wall accumulation or ratcheting. If relevant, these effects undermine attempts to interpret the pressure as a state function in the conventional (broad) sense [21]. Summing up, the balance equation for the momentum of the active fluid becomes

$$\rho \frac{du}{dt} = \nabla_r \cdot \sigma - \gamma \rho u + \gamma v_0 \mathcal{P} \rho + F^{\text{ext}} \rho, \tag{6.30}$$

with the stress tensor to order $\mathcal{O}(1/\gamma)$ given by

$$\sigma = -T\rho \mathbb{I} + \sigma_{\text{IK}} - \frac{2v_0}{\gamma}\left(\mathcal{I}_1 + \mathcal{I}_2\right)\rho + \frac{2v_0}{\gamma}\mathcal{P}\left(\nabla_r \cdot \sigma_{\text{IK}} + F^{\text{ext}}\rho\right). \tag{6.31}$$

Its negative trace, normalised by the space dimension, defines the local fluid pressure [239]. The last two terms can be understood as a nonequilibrium streaming contribution subtracted from the active stresses in the first line. Considering the limit $\gamma \to \infty$, (6.31) validates (and extends to interacting particles) a result by Speck and Jack [22], namely that pressure is independent of activity. Only for noninteracting particles in a homogeneous phase away from any boundaries the result remains valid even to $\mathcal{O}(1/\gamma)$. Under more general conditions, the pressure clearly differs from that of an equilibrium fluid. This should be expected, since static properties of a nonequilibrium system are known to depend on its dynamical parameters [248].

6.3.3   Density equation

From (6.30) we can derive a dynamical density equation for the number or mass density $\rho(r,t)$, making contact with previous works on density functional (field) theory for overdamped active particles. Neglecting the time derivative of the velocity in (6.30) in the case of steady flow, we find an expression for the stationary fluid velocity,

$$\gamma u \rho = \nabla_r \cdot \sigma + \gamma v_0 \mathcal{P} \rho + F^{\text{ext}} \rho \tag{6.32}$$

with which we can simplify the continuity equation (6.5) and the equation for the polarisation (6.6):

$$\partial_t \rho + \nabla_r \cdot J_\rho = 0 \qquad \partial_t\left(\mathcal{P}\rho\right) + \nabla_r \cdot \left(\mathcal{C}_{nv}\rho\right) = -D_r \mathcal{P} \rho.$$

Here we have introduced the particle flux

$$J_\rho = \frac{1}{\gamma}\left(\nabla_r \cdot \sigma + F^{\text{ext}}\rho\right) + v_0\mathcal{P}\rho, \tag{6.33}$$

and the polarisation flux, identified with the tensor $\mathcal{C}_{nv}\rho$. Similar equations have already been presented in Ref. [21, 244]. The former started from the FPE associated to the overdamped version of (6.1), and the latter considered phenomenological equations supported by numerical simulations. For consistency, also $\mathcal{C}_{nv}$ must be expanded in powers of γ^{-1}. Employing the very same procedure used above for σ_{kin}, an expression valid to order $\mathcal{O}(1/\gamma)$ is found,

$$\mathcal{C}_{nv}\rho = v_0\mathcal{Q}\rho + \frac{1}{\gamma}\left(\mathcal{I}_1\rho + \mathcal{I}_2\rho - T\nabla_r\left(\mathcal{P}\rho\right)\right). \tag{6.34}$$

As pointed out in Sec. 6.2, we can neglect the time variation of the polarisation in order to simplify J_ρ. Namely, setting $\partial_t\left(\mathcal{P}\rho\right) = 0$, we can replace the last term in J_ρ with $\mathcal{P}\rho = -\nabla_r \cdot \left(\mathcal{C}_{nv}\rho\right)/D_{\text{r}}$, and obtain

$$J_\rho = \frac{1}{\gamma}\nabla_r\cdot\left[\sigma - \frac{\gamma v_0^2}{D_{\text{r}}}\mathcal{Q}\rho + \frac{v_0 T}{D_{\text{r}}}\nabla_r\left(\mathcal{P}\rho\right)\right] - \frac{1}{\gamma}\nabla_r\cdot\left[\frac{v_0}{D_{\text{r}}}\mathcal{I}_1\rho + \frac{v_0}{D_{\text{r}}}\mathcal{I}_2\rho\right] + \frac{1}{\gamma}F^{\text{ext}}\rho. \tag{6.35}$$

Now we substitute the stress tensor (6.31) and neglect terms $\mathcal{O}\left(1/\gamma^2\right)$

$$J_\rho = \frac{1}{\gamma}\nabla_r\cdot\left[-T\rho\mathbb{I} + \sigma_{\text{IK}} - \frac{\gamma v_0^2}{D_{\text{r}}}\mathcal{Q}\rho + \frac{v_0 T}{D_{\text{r}}}\nabla_r(\mathcal{P}\rho)\right] - \frac{v_0}{\gamma D_{\text{r}}}\nabla_r\cdot(\mathcal{I}_1\rho + \mathcal{I}_2\rho) + \frac{1}{\gamma}F^{\text{ext}}\rho \tag{6.36}$$

For vanishing particle flux, the external force is balanced by the terms included in the divergence, inducing the definition of a stress tensor σ_{s} reliable in the regime of a stationary polarisation field, as pointed out in (6.12):

$$J_\rho = \frac{1}{\gamma}\nabla_r \cdot \sigma_{\text{s}} + \frac{1}{\gamma}F^{\text{ext}}\rho \tag{6.37}$$

Finally, we turn (6.37) into a sum of a purely diffusive flux plus a drift term arising from external forces, $J_\rho = -D_{\text{eff}}\nabla_r\rho + \frac{1}{\gamma}F^{\text{ext}}\rho$. This is done, like in equilibrium, relating the gradient diffusion matrix D_{eff} to the compressibility of the fluid. Using the chain rule, we can write

$$\frac{1}{\gamma}\nabla\cdot\sigma_{\text{s}} = \frac{1}{\gamma}\partial_\rho\sigma_{\text{s}}\cdot\nabla\rho \tag{6.38}$$

and then define the diffusion matrix D_{eff} by introducing the compressibility coefficients matrix κ_T^{ij} $(i, j = 1, 2)$,

$$\left(D_{\text{eff}}\right)_{ij} \equiv \frac{1}{\gamma\rho}(\kappa_T^{-1})_{ij}, \qquad \kappa_T^{ij} \equiv -\frac{1}{\rho}\left(\frac{\partial(\sigma_{\text{s}})_{ij}}{\partial\rho}\right)_T^{-1}. \tag{6.39}$$

The dependence of the stress tensor σ_{s} on density ρ is not straightforward, but a density-gradient-expansion ρ can be performed in a weakly inhomogeneous approximation as presented in Sec. 6.3.5.

6.3.4 Local fluid pressure and wall pressure

In the section 6.3.3 we have introduced the static stress tensor $\sigma_{\rm s}$. Equivalently, it can be derived from (6.11) by applying multiple-time-scale theory to (6.12), i.e. involving the dynamics characterised by a fast polarisation relaxation, $\partial_t(\mathcal{P}\rho) = 0$. Indeed, neglecting the time variation of the polarisation, the active contribution to the momentum balance is naturally included in the stress tensor through the correlating tensor $\mathcal{C}_{nv}$ that, up to order $\mathcal{O}(1/\gamma)$, is given by (6.34). If plugged into (6.12)

$$
\begin{aligned}
\sigma_{\rm s} = -T\rho\mathbb{I} + \sigma_{\rm IK} &- \frac{\gamma v_0^2}{D_{\rm r}}\mathcal{Q}\rho - \frac{2v_0}{\gamma}\left(1 + \frac{\gamma}{2D_{\rm r}}\right)\rho\left(\mathcal{I}_1 + \mathcal{I}_2\right) \\
&+ \frac{v_0 T}{D_{\rm r}}\nabla_r(\mathcal{P}\rho) + \frac{2v_0}{\gamma}\mathcal{P}\left(\nabla_r \cdot \sigma_{\rm IK} + F^{\rm ext}\rho\right)
\end{aligned}
\tag{6.40}
$$

We stress that the terms in the last parenthesis of (6.40) are a streaming contribution to some of the terms in the first line. So they are expected to be of the same order recalling that $\mathcal{P}$ is at maximum one, thus cannot change the order of magnitude. Note that some active contributions appearing in (6.31) now have a renormalised pre-factor. The typical friction for colloids of 1μm radius embedded in water is $\gamma \simeq 10^7\,{\rm s}^{-1}$ (assuming comparable solvent and particle densities), much larger than typical rotational diffusion coefficients $D_{\rm r} \simeq 10^{-1}$-$10^0\,{\rm s}^{-1}$. Namely, $\gamma \gg D_{\rm r}$, in agreement with the requirements for the employ of multiple-time-scale approach. Therefore we can neglect sub-leading terms to arrive at

$$
\sigma_{\rm s} = -T\rho\mathbb{I} + \sigma_{\rm IK} - \frac{\gamma v_0^2}{D_{\rm r}}\mathcal{Q}\rho + \frac{v_0}{D_{\rm r}}\left[T\nabla_r(\mathcal{P}\rho) - \rho\left(\mathcal{I}_1 + \mathcal{I}_2\right)\right].
\tag{6.41}
$$

We recall that the appended subscript "s" emphasises that (6.41) is valid only under the stationary condition $\partial_t\left(\mathcal{P}\rho\right) \simeq 0$, that is time scales larger than D_r^{-1}. In turn, for consistency with the assumption $\gamma \gg D_{\rm r}$, this implies that the hydrodynamic momentum density ρu is stationary as well, since it relaxes on time scales larger than γ^{-1}. If even $u = 0$ holds (i.e., under static conditions), the momentum balance equation takes the form

$$
F^{\rm ext}\rho = -\nabla_r \cdot \sigma_{\rm s}
\tag{6.42}
$$

which shows that $\sigma_{\rm s}$ is best suited to inspect the mechano-static equilibria of an active fluid. When $F^{\rm ext}$ is a confining wall force, $\sigma_{\rm s}$ gives the local force per unite area exerted by the active fluid on its container. It clearly differs from the local fluid pressure in (6.31), because the active force is already included in (6.40) and hence does not explicitly show up in (6.42). This becomes apparent when comparing (6.42) with the static limit of (6.30),

$$
F^{\rm ext}\rho + \gamma v_0 \mathcal{P}\rho = -\nabla_r \cdot \sigma.
\tag{6.43}
$$

It manifestly shows that the external forces F^{ext} are counterbalanced not only by the active pressure σ alone, but also by the *internal* body force $\gamma v_0 \mathcal{P}$ [22], legitimated to dissipate momentum only under non-stationary conditions. In the light of (6.42), we can define the local pressure exerted on a wall by taking the trace of (6.41). By construction, $\text{Tr } \mathcal{Q} = 1$, while the trace of the correlating tensors $\mathcal{I}_1$ and $\mathcal{I}_2$ reduces to the scalar product of the forces F_i^{int} and F_i^{ext} with the orientational angle n_i:

$$P^{\text{wall}}(r) = \rho T - \frac{1}{2} \text{Tr } \sigma_{\text{IK}} + \rho \frac{\gamma v_0}{2 D_{\text{r}}} v(r) + \frac{v_0 T}{2 D_{\text{r}}} \nabla_r \cdot (\mathcal{P}\rho). \qquad (6.44)$$

Here, we have introduced the density-dependent actual swim speed [76],

$$v(r) \equiv v_0 + \frac{1}{\gamma} \text{Tr } (\mathcal{I}_1(r) + \mathcal{I}_2(r)), \qquad (6.45)$$

in which the bare swim speed v_0 is renormalised by the effect of inter-particles interactions and external forces. In absence of external forces (6.45) reduces to the expression by Marchetti et al. [244]. Numerical simulations [24, 244, 249] show that, at high density, (the swim pressure and thus) the effective velocity of active particles is reduced due to self-caging effects [181,234], implying that the second term of (6.45) must turn negative, i.e. $\text{Tr}\mathcal{I}_2 < 0$. Intuitively, this happens when the particles are swimming oppositely to the mutual force they experience (regardless of the particular form of F^{int}) entailing that the pair distribution function, included implicitly in $\mathcal{I}_2$ as shown in Section 6.3.5, must be anisotropic [62]. This corresponds to trapped configurations as sketched in Fig. (6.1), broken and restored by the rotational diffusion. Hence, for hard-core interactions, the particle velocities point towards each other in the trapped state, but attractive interactions also allow for trapped configurations with outwards pointing velocities at small activities.

Note that the two terms in (6.44) are formally equivalent to the pressure of an equilibrium fluid, while the others represent the swim pressure P^{swim}, i.e. the explicit additional contribution due to self-propulsion. This expression (6.44) is consistent with the pressure derived by some of us in [116] through the virial theorem. The additional term in (6.44) depending on the divergence of the polarisation, does not appear in [116] since therein only the average pressure on a fluid container is considered, which requires an integration over the whole space. It plays a relevant role close to boundaries where, due to the wall-accumulation effect, the average polarisation can be nonzero, differently from the bulk. Also note that in many previous works, which consider only the overdamped version of (6.1), the swim pressure is defined as $F^{\text{A}} \langle n_i \cdot x_i \rangle$ [76, 181, 182, 234]. The (local version of this) definition is completely equivalent to ours based on tensors $\mathcal{I}_1$ and $\mathcal{I}_2$. In equation (30) of [116] this has been shown starting from microscopic overdamped dynamics. For underdamped dynamics, one can start from (6.4) and then make use of multiple-time-scale analysis. Namely, for a steady state, $\langle \mathcal{L} n_i x_i \rangle = 0$ entails $\langle v_i n_i \rangle = D_{\text{r}} \langle n_i x_i \rangle$. Averaging of $\langle v_i n_i \rangle$ can be performed with (6.17) and (6.18), to recover (the integral of) $P^{\text{swim}} = \rho \gamma v_0 v(r)/2 D_{\text{r}}$.
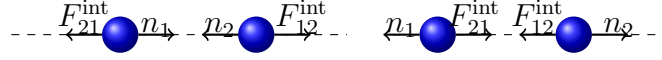
Figure 6.1: Trapped configurations of pairs of active particles with repulsive (left) and attractive (right) interactions.

6.3.5 Weakly inhomogeneous density approximation

Self-caging phenomena, as implied by the definition (6.45) of the actual velocity $v(r,t)$, are responsible also for the non-monotonic behaviour of the pressure as function of density. This becomes evident considering a gradient expansion of (6.44), in which the explicit density dependence, of the tensors σ_{IK}, $\mathcal{I}_1$, $\mathcal{I}_2$ is approximately resolved. Namely, the hydrodynamic fields are supposed to change slowly in space, so that gradient terms can be discarded. For simplicity, we suppose that the only external force is a hard-wall potential, and that inter-particle forces $F_{ij}^{\text{int}} = -\nabla_i U(|x_i - x_j|)$ derive from a central pair potential, here independent of the self-propulsion orientation. This assumption allows to neglect any term involving the short-ranged boundary force F^{ext}, when the average pressure is considered, since it amounts to a sub-leading contribution in the system size. We first consider the Irving-Kirkwood tensor,

$$\sigma_{\text{IK}} = \frac{\rho(r)}{2} \int dR \frac{RR}{|R|} U'(|R|) \rho(r+R) g_2(r,R). \tag{6.46}$$

The latter differs from the expression in [239] in the $g_2(r,R)$: it is a nonequilibrium angle-averaged pair distribution function. Namely $g_2(r,R) \equiv \int d\theta g_2(r,R,\theta)$, where $g_2(r,R,\theta)$ measures the probability of finding a particle in r with orientation θ and a particle in $r+R$ (with arbitrary orientation). With slight abuse of notation we use the same symbol to denote $g_2(r,R,\theta)$ and the angle-averaged $g_2(r,R)$ entering in (6.46). The θ-dependence contains information about possible anisotropies [250,251], with the contact probability increasing with an anti-alignment of the swim directions. Such an anisotropy is also responsible for the reduced actual velocity $v(r,t)$ as depicted in Fig. (6.1). The zero order in a gradient-expansion approximation, i.e., $\rho(r+R) \simeq \rho(r)$, yields $\sigma_{\text{IK}} \simeq -\rho^2 a$ with a slowly varying matrix

$$a(r) = -\frac{1}{2} \int dR \frac{RR}{|R|} U'(|R|) g_2(r,R). \tag{6.47}$$

We proceed similarly for the tensor $\mathcal{I}_2$, which involves a more complex dependence on θ. From the definition (6.29),

$$\mathcal{I}_2 \rho = \sum_{i,j \neq i}^{N} \int dx_i dx_j d\theta_i \delta(x_i - r) \rho_2(x_i, \theta_i, x_j) \times n(\theta_i) F_{ij}^{\text{int}}(x_i - x_j). \tag{6.48}$$

Here, ρ_2 is the two-body density distribution function to find a particle in x_i with orientation θ_i together with a particle at x_j (with arbitrary orientation). It decomposes into to one-body density distributions $\rho(r)$ and the pair correlation $g_2(r, R, \theta)$. The standard assumption of identical particles allows to drop the label i, namely,

$$\mathcal{I}_2\rho = \int dR d\theta\, n(\theta) F^{\text{int}}(R) \rho(r+R) \rho(r) g_2(r, R, \theta). \tag{6.49}$$

While in (6.46), the eventual anisotropies in the pair distribution function are averaged out, more interesting effect can emerge in (6.49). Hence, to a first approximation we obtain $\mathcal{I}_2\rho \simeq \rho^2 b$, where

$$b(r) = \int dR d\theta\, n(\theta) F^{\text{int}}(R) g_2(r, R, \theta). \tag{6.50}$$

If we plug (6.47) and (6.50) into (6.44) and take the trace, we get

$$P^{\text{wall}} = \left(T + \frac{\gamma v_0^2}{2D_{\text{r}}}\right)\rho + \frac{1}{2}\text{Tr}\left(a + \frac{v_0}{D_{\text{r}}}b\right)\rho^2. \tag{6.51}$$

Equation (6.51) is similar to the equilibrium virial equation of state, suggesting the definition of the effective temperature,

$$T_{\text{eff}} = T + \frac{\gamma v_0^2}{2D_{\text{r}}}. \tag{6.52}$$

due to the stochastic active motion [181, 182, 189]. The pressure arising from the interactions has a contribution $\text{Tr}a$ of the standard form known from equilibrium. It knows about the activity only through the nonequilibrium pair distribution g_2. The second term displays an explicit dependence on v_0 indicating its absence in equilibrium. The factor $\text{Tr}b$ can turn negative for self-trapping configurations, and leads to the aforementioned decrease of the actual velocity (6.45) as sketched in Fig. (6.1). Here we have found that the same phenomenon may cause a non-monotonic behaviour of the pressure for large enough values of the persistence length $v_0 D_{\text{r}}^{-1}$ compared to the mean particle distance $\rho^{-1/2}$ [236]. Similar conclusions have been drawn by Takatori et al. from a density expansion of the swim pressure [24] starting from microrheology results.

The weakly inhomogeneous density approximation (6.51) for P^{wall} and an equivalent expression for σ_{s} allow a simplification of the compressibility coefficient (6.39) introduced in the diffusion equation. Namely,

$$\frac{1}{2\rho}\text{Tr}(\kappa_T^{-1}) = T + \frac{\gamma v_0^2}{2D_{\text{r}}} + \text{Tr}\left(a + \frac{v_0}{D_{\text{r}}}b\right)\rho. \tag{6.53}$$

Generally, $(a)_{ij} > 0$ for systems with repulsive inter-particle potentials. Hence, at equilibrium we expect them to posses a reduced compressibility compared with an

ideal gas. Conversely, since $(b)_{ij}$ can be negative for active particles thanks to their self-caging properties, the compressibility can be increased even for purely repulsive inter-particle forces. In view of (6.39), an increasing compressibility entails a decreasing diffusivity, as usual.

6.3.6 Low density limit

For low densities ($\rho^{1/2}d \ll 1$, where d is the typical interaction length scale), g_2 can be evaluated by solving a two body problem, which yields the barometric equation at the effective temperature (6.52),

$$g_2\left(|R|\right) \sim \exp\left(-\frac{U\left(|R|\right)}{T_{\text{eff}}}\right). \tag{6.54}$$

Within this approximation, a simplified expression for (6.47), evaluated using polar coordinates $(|R|, \phi)$, can be found, namely

$$\text{Tr}\, a\left(r\right) = T_{\text{eff}} \int_0^\infty d|R|\, |R| \exp\left(-\frac{U\left(|R|\right)}{T_{\text{eff}}}\right). \tag{6.55}$$

If $U(R)$ is the hard-sphere potential, this reduces to $\text{Tr}\, a = T_{\text{eff}}d^2/2$, where here d denotes the particle diameter. The evaluation of $b(r)$ in Eq. (6.50) requires further considerations. Supposing a uniform distribution for θ, away from any boundaries, the approximation (6.54) implies $b = 0$. This clearly shows that an anisotropic pair distribution function must be considered for active fluids to unveil the genuine nonequilibrium contributions to the pressure beyond the effective temperature T_{eff} from Eq (6.54). In polar coordinates

$$b(r) = -\int d|R|d\theta d\phi\, n(\theta)n(\phi)U'(|R|)g_2(r,|R|,\theta,\phi), \tag{6.56}$$

where $n\left(\phi\right) \equiv R/|R|$ gives the direction of the force. As previously pointed out, particles with a net relative swim velocity towards each other give rise to an enhanced contact value. To make our point, we write

$$g_2\left(r,|R|,\theta,\phi\right) = \delta\left(\phi-\theta\right)\tilde{g}_2\left(r,|R|,\theta\right) \tag{6.57}$$

and we idealise the function δ, which will generally be peaked around zero, as the Dirac delta. We then find by integrating over ϕ,

$$b\left(r\right) = -\int d|R|d\theta\, n\left(\theta\right)n\left(\theta\right)U'\left(|R|\right)\tilde{g}_2\left(r,|R|,\theta\right). \tag{6.58}$$

Assuming a uniform distribution of $\theta \in [0, 2\pi]$ (which holds, e.g., in the bulk), leads to

$$\mathrm{Tr}\, b\,(r) = -2\pi T_{\mathrm{eff}} \int_0^\infty d|R|\, \exp\left(-\frac{U\,(|R|)}{T_{\mathrm{eff}}}\right) \tag{6.59}$$

and for hard spheres we obtain $\mathrm{Tr}\, b = -2\pi T_{\mathrm{eff}} d$. Plugging the result of a and b in (6.51)

$$P^{\mathrm{wall}} = \left(T + \frac{\gamma v_0^2}{2D_{\mathrm{r}}}\right)\rho + T_{\mathrm{eff}} d \left(\frac{d}{4} - \pi \frac{v_0}{D_{\mathrm{r}}}\right)\rho^2. \tag{6.60}$$

The magnitude of the persistence length $v_0 D_r^{-1}$ determines how the pressure behaves for high density. For parameter combinations v_0, D_{r} and d that guarantee a sufficient persistence of the swim direction between particle interactions, the second parenthesis in (6.60) is negative, leading to a non-monotonic behaviour of the swim pressure,

$$P^{\mathrm{swim}} = \frac{v_0}{D_{\mathrm{r}}}\left(\frac{\gamma v_0}{2}\rho - \pi T_{\mathrm{eff}} d\rho^2\right). \tag{6.61}$$

Similarly if we plug the result of a and b in (6.53) and (6.39) we obtain an expression for the effective diffusion coefficient D_{eff}

$$\frac{1}{2}\mathrm{Tr} D_{\mathrm{eff}} = \frac{T_{\mathrm{eff}}}{\gamma}\left[1 + \rho d\left(\frac{d}{2} - 2\pi\frac{v_0}{D_{\mathrm{r}}}\right)\right]. \tag{6.62}$$

6.4 Conclusion and Outlook

For a "dry" active system, we have derived balance equations for hydrodynamic observables starting from the underlying microscopic dynamics. Particularly, the equation for momentum balance univocally leads to a definition of the pressure via the stress tensor. Our expressions derived in the high-friction limit rationalise the features observed in active systems: violation of (local) momentum conservation due to the active swim force, reduced swim pressure due to self-trapping of the particles [234] (and adverse external forces) and the non-monotonic density-dependence of the pressure [181]. These phenomena, observed even if hydrodynamic interactions between the solvent and the active particles are neglected, are caused by active self-interactions of active particles contained in the tensor $\mathcal{I}_2$. Furthermore, our expression for the pressure shows manifestly the general lack of equivalence between the local pressure, defined via momentum exchange, and the mechanical pressure exerted on a wall for active systems, as previously argued [22]. Our theory clarifies the role of activity as responsible for this general violation of (local) momentum conservation, putting in evidence the regimes in which such violation can be neglected and the stress tensor actually counterbalances the force exerted on a wall.

The theory is still valid and leads to the same conclusion if the external force and the mutual active particles interaction depend on the self-propulsion orientation θ_i, as long as the orientational dynamics is still affected by rotational diffusion only. In this case the forces can induce some local imbalance in the polarisation, e.g. positive in some area and negative elsewhere according to the individual particles orientation. Nevertheless, the global polarisation must be conserved at zero, as long as the angular dynamics for each particle are decoupled by the others, so cannot lead to mean polarisation [4]. On the contrary the presence of torque affecting the orientational dynamics introduces new elements and requires further investigation. Needless to say, such an extension would be very interesting since it enables us to account for collective phenomena with aligning effects in the spirit of the well-known Vicsek model [252]. While the presence of a alignment interactions terms like in [21], e.g. $F_i^{\text{al}}(\theta_i, x_i) = F_{ij}^{\text{al}}(\theta_i - \theta_j, x_i, x_j)$, in the dynamics for the self-propulsion orientation would not change the density and the momentum balance equation, it would be responsible for an extra term into the polarisation equation (6.6), which in general cannot be expressed as the divergence of a tensor. Similar conclusion can be drawn for an external torque, depending on one particle orientation only. Consequently, even in the fast rotation limit, the polarisation cannot be included into the stress tensor, thus being necessarily responsible for local violation of momentum conservation, under such conditions. Those conclusion should be carefully adopted, since a rigorous microscopic derivation must consider the underdamped limit of the orientational dynamics endowed with the torques contributions as starting point for a multiple-time-scale approach and not just add a torque in the overdamped angular dynamics. Furthermore, it would be interesting to (approximately) implement the effect of hydrodynamic interactions mediated by the solvent [253, 254] in our theory, in order to elucidate its role for the collective dynamics and to eventually derive a comprehensive dynamical density functional theory for a "wet" active fluid. A first attempt would be the introduction of a position dependent active velocity in the microscopic Langevin equation. Finally, as an interesting application of our theory, its consequences for the important thermodynamic notion of surface tension should be studied [222, 249, 255].

---

[4]Private communication with Michael E. Cates from the University of Cambridge.

Appendix A

Chapter 4

A.1 Derivation of the Fourth Moment

From the solution of (4.24) we calculate the fourth moment,

$$\left\langle \mathbf{X}^4 \right\rangle = e^{-\frac{4K\mu}{N}t} \int_{-\infty}^{t} d\tau_1 \int_{-\infty}^{t} d\tau_2 \int_{-\infty}^{t} d\tau_3 \int_{-\infty}^{t} d\tau_4 e^{\frac{K\mu}{N}(\tau_1+\tau_2+\tau_3+\tau_4)} \mathcal{C}_\eta(\tau_1, \tau_2, \tau_3, \tau_4) \quad (A.1)$$

with $\mathcal{C}_\eta(\tau_1, \tau_2, \tau_3, \tau_4) = \langle \eta(\tau_1)\eta(\tau_2)\eta(\tau_3)\eta(\tau_4) \rangle$, four-time noise correlation, is made by three blocks of terms: one thermal, one active and one mixed. The thermal one involves four-times correlation of the Gaussian with noise and can be written as a sum of three two-times correlations. The mixed terms boils down to products of two-times correlations since thermal and active noise are assumed to be independent. Independence is supposed for different j-particles as well. Namely,

$$\mathcal{C}_\eta = \frac{v_0^4}{N^3} \langle \mathbf{n}(\tau_1)\mathbf{n}(\tau_2)\mathbf{n}(\tau_3)\mathbf{n}(\tau_4) \rangle + \frac{6\mu T}{N^2} \left[2\mu T \delta(\tau_1 - \tau_2) + v_0^2 e^{-D_r|\tau_1-\tau_2|} \right] \delta(\tau_3 - \tau_4) \quad (A.2)$$

The active noise cannot be factorised. From [256], for $\tau_1 > \tau_2 > \tau_3 > \tau_4$,

$$\langle \mathbf{n}(\tau_1)\mathbf{n}(\tau_2)\mathbf{n}(\tau_3)\mathbf{n}(\tau_4) \rangle = \frac{1}{4} e^{-D_r(\tau_1-\tau_2+\tau_3-\tau_4)} + \frac{1}{8} e^{-D_r(\tau_1+3\tau_2-3\tau_3-\tau_4)} \quad (A.3)$$

for cosine-cosine and sine-sine component and zero otherwise. Eq. (A.3) differs from Eq. (3.19) of [256] for the averaging over the initial angle. Eq. (A.3) gives the correlation of the orientations for a particular order of the times, but for each a similar expression is valid for any order of the times. The integrals in (A.1) can be split in 24 ordered integrals, as many as the number of orders of times. Each contribution weighs the same, therefore the evaluation of the integrals boils down to a combinatorial calculation. If we plug (A.2) into (A.1) we obtain (4.28).

A.2 Non-linear correction to $\mathbf{X}^2$

The first-order correction to the variance is given by the solution of (4.1) times (4.34) and it involves average values of the noise correlated with the perturbation F.

$$\langle \mathbf{X}_0 \mathbf{X}_1 \rangle = \sum_{j=1}^{N} \frac{1}{kN} \int_{-\infty}^{t} ds\, e^{-\frac{K\mu}{N}(t-s)} \left\langle \boldsymbol{\eta}(s) \mathbf{F}_0^j(t) \right\rangle$$

$$- \frac{K\mu}{kN^2} \sum_{j=1}^{N} \int_{-\infty}^{t} ds\, e^{-\frac{K\mu}{N}(t-s)} \int_{-\infty}^{t} d\tau\, e^{-\frac{K\mu}{N}(t-\tau)} \left\langle \boldsymbol{\eta}(s) \mathbf{F}_0^j(\tau) \right\rangle \tag{A.4}$$

Those can be simplified through the Novikov [50, 257] theorem within a Gaussian approximation for the active noise, reliable if the activity is not too strong ($K\mu < ND_r$). For non-Markov noise such that $\langle \xi(t) \xi(t') \rangle = \gamma(|t-t'|)$, Novikov theorem reads for any function ϕ,

$$\langle \xi(s) \phi(\xi(t)) \rangle = \int_{-\infty}^{t} dt'\, \gamma(|s-t'|) \left\langle \frac{\delta\phi(\xi(t))}{\delta\xi(t')} \right\rangle \tag{A.5}$$

It is convenient to separate the nonequilibrium source in the noise, i.e. $\boldsymbol{\eta}^j = \sqrt{2\mu T}\boldsymbol{\eta}_{\text{th}}^j + v_0 \boldsymbol{\eta}_{\text{act}}^j$, which satisfies (A.5) with $\gamma(|t-t'|) = 0.5 \exp\{-D_r |t-t'|\}$. Derivatives of the perturbation $\mathbf{F}_0$ with respect to the noise can be written as a function of the process with the chain rule. Namely the first order correction to variance becomes,

$$\langle \mathbf{X}_0 \mathbf{X}_1 \rangle = \frac{\sqrt{2\mu T}}{kN^2} \sum_{j,k=1}^{N} \int_{-\infty}^{t} ds\, e^{-\frac{K\mu}{N}(t-s)} \left\langle \frac{\partial \mathbf{r}_0^j(t)}{\partial \boldsymbol{\eta}_{\text{th}}^k(s)} \frac{\partial \mathbf{F}_0^j(t)}{\partial \mathbf{r}_0^j(t)} \right\rangle -$$

$$\frac{\sqrt{2\mu T}}{kN^2} \frac{K\mu}{N} \sum_{j,k=1}^{N} \int_{-\infty}^{t} ds\, e^{-\frac{K\mu}{N}(t-s)} \int_{s}^{t} d\tau\, e^{-\frac{K\mu}{N}(t-\tau)} \left\langle \frac{\partial \mathbf{r}_0^j(\tau)}{\partial \boldsymbol{\eta}_{\text{th}}^k(s)} \frac{\partial \mathbf{F}_0^j(\tau)}{\partial \mathbf{r}_0^j(\tau)} \right\rangle +$$

$$\frac{v_0}{2kN^2} \sum_{j,k=1}^{N} \int_{-\infty}^{t} ds\, e^{-\frac{K\mu}{N}(t-s)} \int_{-\infty}^{t} dt'\, e^{-D_r|s-t'|} \left\langle \frac{\partial \mathbf{r}_0^j(t)}{\partial \boldsymbol{\eta}_{\text{act}}^k(t')} \frac{\partial \mathbf{F}_0^j(t)}{\partial \mathbf{r}_0^j(t)} \right\rangle -$$

$$\frac{v_0}{2kN^2} \frac{K\mu}{N} \sum_{j,k=1}^{N} \int_{-\infty}^{t} ds\, e^{-\frac{K\mu}{N}(t-s)} \int_{-\infty}^{t} dt'\, e^{-D_r|s-t'|} \int_{s}^{t} d\tau\, e^{-\frac{K\mu}{N}(t-\tau)} \left\langle \frac{\partial \mathbf{r}_0^j(\tau)}{\partial \boldsymbol{\eta}_{\text{act}}^k(t')} \frac{\partial \mathbf{F}_0^j(\tau)}{\partial \mathbf{r}_0^j(\tau)} \right\rangle \tag{A.6}$$

The functional derivative in (A.6) can be easily solved from the unperturbed solution for the probe (4.24) and for the fluid (4.2), respectively. The functional derivative of the probe position with respect to the thermal noise

$$\frac{\partial \mathbf{X}_0(t)}{\partial \eta_{\text{th}}^k(s)} = \frac{\partial}{\partial \eta_{\text{th}}^k(s)} \int_{-\infty}^{t} dt'\, e^{-\frac{K\mu}{N}(t-t')} \frac{1}{N} \sum_{j=1}^{N} \left(v_0 \eta_{\text{act}}^j(t') + \sqrt{2\mu T} \eta_{\text{th}}^j(t') \right) \tag{A.7}$$

$$= \sqrt{2\mu T} \int_{-\infty}^{t} dt'\, e^{-\frac{K\mu}{N}(t-t')} \frac{1}{N} \sum_{j=1}^{N} \delta_{jk} \frac{\partial \eta_{\text{th}}^j(t')}{\partial \eta_{\text{th}}^k(s)} = \Theta(t-s) \frac{\sqrt{2\mu T}}{2N} e^{-\frac{K\mu}{N}(t-s)} \tag{A.8}$$

since the equilibrium and the active noise are independent. The functional derivative of the probe position with respect to the active noise

$$\frac{\partial \mathbf{X}_0(t)}{\partial \eta_{\text{act}}^k(s)} = \frac{\partial}{\partial \eta_{\text{act}}^k(s)} \int_{-\infty}^t dt' \, e^{-\frac{K\mu}{N}(t-t')} \frac{1}{N} \sum_{j=1}^N \left(v_0 \eta_{\text{act}}^j(t') + \sqrt{2\mu T} \eta_{\text{th}}^j(t') \right) \quad (A.9)$$

$$= \frac{v_0}{N} \int_s^t dt' \, e^{-\frac{K\mu}{N}(t-t')} \sum_{j=1}^N \delta_{jk} \frac{\partial \eta_{\text{act}}^j(t')}{\partial \eta_{\text{act}}^k(s)} = \Theta(t-s) \frac{v_0}{2N} e^{-\frac{K\mu}{N}(t-s)} \quad (A.10)$$

The derivative of the active noise with respect to itself gives a $\delta(t'-s)$ [50], from (A.5)

$$\left\langle \boldsymbol{\eta}_{\text{act}}^k(s) \boldsymbol{\eta}_{\text{act}}^j(t) \right\rangle = \frac{1}{2} \int_{-\infty}^t dt' \, e^{-D_r|s-t'|} \left\langle \frac{\partial \boldsymbol{\eta}_{\text{act}}^j(t)}{\partial \boldsymbol{\eta}_{\text{act}}^k(t')} \right\rangle$$

$$= \frac{1}{2} e^{-D_r(t-s)} \quad \Longleftrightarrow \quad \left\langle \frac{\partial \boldsymbol{\eta}_{\text{act}}^j(t)}{\partial \boldsymbol{\eta}_{\text{act}}^k(t')} \right\rangle = \delta(t-t'). \quad (A.11)$$

The functional derivative of the particles position with respect to the thermal noise

$$\frac{\partial \mathbf{x}_0^j(t)}{\partial \eta_{\text{th}}^k(s)} = \sqrt{2\mu T} \int_s^t dt' \, e^{-\frac{k\mu}{N}(t-t')} \frac{\partial \eta_{\text{th}}^j(t')}{\partial \eta_{\text{th}}^k(s)} + \frac{k\mu}{N} \int_s^t dt' \, e^{-\frac{k\mu}{N}(t-t')} \frac{\partial \mathbf{X}_0(t')}{\partial \eta_{\text{th}}^k(s)} \quad (A.12)$$

$$= \frac{\sqrt{2\mu T}}{2} \left[e^{-\frac{k\mu}{N}(t-s)} \delta_{jk} \Theta(t-s) + \frac{1}{N} \frac{k\mu}{N} \int_s^t dt' \, e^{-\frac{k\mu}{N}(t-t')} e^{-\frac{K\mu}{N}(t'-s)} \right] \quad (A.13)$$

Noteworthy, here replacing $k\mu \exp(-k\mu\tau/N)/N$ with $\delta(\tau)$ in the limit $k\mu/N \to \infty$ requires to assume that $k \gg K$ and leads to

$$\frac{\partial \mathbf{x}_0^j(t)}{\partial \eta_{\text{th}}^k(s)} \underset{K \ll k}{=} \frac{\sqrt{2\mu T}}{2} \left(e^{-\frac{k\mu}{N}(t-s)} \delta_{jk} + \frac{1}{N} e^{-\frac{K\mu}{N}(t-s)} \right) \Theta(t-s). \quad (A.14)$$

While replacing $K\mu \exp(-K\mu\tau/N)/N$ necessarily leads to the regime $K \gg k$ in which

$$\frac{\partial \mathbf{x}_0^j(t)}{\partial \eta_{\text{th}}^k(s)} \underset{K \gg k}{=} \frac{\sqrt{2\mu T}}{2} \left(\delta_{jk} + \frac{1}{N} \frac{k}{K} \right) e^{-\frac{k\mu}{N}(t-s)} \Theta(t-s) \approx \frac{\sqrt{2\mu T}}{2} \delta_{jk} e^{-\frac{k\mu}{N}(t-s)} \Theta(t-s) \quad (A.15)$$

the second term is negligible. It is important to stress that if we consider the regime $K \gg k$ the overdamped limit we performed for $\mathbf{X}_1$ is no longer valid since we used $k\mu \exp(-k\mu\tau/N)/N$ to replace the exponential with the δ. To obtain the solution of $\mathbf{X}_1$ we must proceed in another way. Namely we start from (4.33) and we neglect the inertia,

$$k \int_{-\infty}^t ds \, e^{-\frac{k\mu}{N}(t-s)} \dot{\mathbf{X}}_1(s) = -K\mathbf{X}_1 + \frac{1}{N} \sum_{j=1}^N \int_{-\infty}^t ds \, e^{-\frac{k\mu}{N}(t-s)} \dot{\mathbf{F}}_0^j(s) \quad (A.16)$$

and we take a time derivative

$$(k+K)\dot{\mathbf{X}}_1 = \frac{k\mu}{N}\int_{-\infty}^{t} ds\, e^{-\frac{k\mu}{N}(t-s)}\dot{\mathbf{X}}_1(s) + \frac{1}{N}\sum_{j=1}^{N}\left[\dot{\mathbf{F}}_0^j - \frac{k\mu}{N}\int_{-\infty}^{t} ds\, e^{-\frac{k\mu}{N}(t-s)}\dot{\mathbf{F}}_0^j(s)\right] \quad (A.17)$$

then we substitute (A.16) into (A.17) so that some terms cancel out and we obtain

$$\dot{\mathbf{X}}_1 = -\frac{K}{k+K}\frac{k\mu}{N}\mathbf{X}_1 + \frac{1}{k+K}\frac{1}{N}\sum_{j=1}^{N}\dot{\mathbf{F}}_0^j \quad (A.18)$$

First we use that $K \gg k$ and then we solve the equation obtaining,

$$\mathbf{X}_1 = \frac{1}{NK}\sum_{j=1}^{N}\left[\mathbf{F}_0^j - \frac{k\mu}{N}\int_{-\infty}^{t} e^{-\frac{k\mu}{N}(t-s)}\mathbf{F}_0^j(s)\right] \quad (A.19)$$

which is different from (4.34). In this regime we cannot replace the exponential of $\frac{k\mu}{N}$ with the δ-function. As explained in Sec. 4.5.1, the interesting regime is the latter, since in the former the non-linear correction becomes negligible. The functional derivative of the particles with respect to the active noise,

$$\frac{\partial \mathbf{x}_0^j(t)}{\partial \eta_{\text{act}}^k(s)}\bigg|_{K \ll k} = \frac{v_0}{2}\left(e^{-\frac{k\mu}{N}(t-s)}\delta_{jk} + \frac{1}{N}e^{-\frac{K\mu}{N}(t-s)}\right)\Theta(t-s) \quad (A.20)$$

$$\frac{\partial \mathbf{x}_0^j(t)}{\partial \eta_{\text{act}}^k(s)}\bigg|_{K \gg k} = \frac{v_0}{2}\left(\delta_{jk} + \frac{1}{N}\frac{k}{K}\right)e^{-\frac{k\mu}{N}(t-s)}\Theta(t-s) \approx \frac{v_0}{2}\delta_{jk}e^{-\frac{k\mu}{N}(t-s)}\Theta(t-s) \quad (A.21)$$

If we plug the functional derivatives into (A.6) we have to fix in advance the ratio K/k. If $K \ll k$ we need to use (A.14) and (A.20), while if $K \gg k$ we need to use (A.15) and (A.21). Since we are more interested in the second regime,

$$\langle \mathbf{X}_0(t)\,\mathbf{X}_1(t)\rangle = \frac{\mu T}{N}\frac{1}{KN}\int_{-\infty}^{t} ds\, e^{-\frac{2K\mu}{N}(t-s)}\left\langle\sum_{j=1}^{N}\frac{\partial \mathbf{F}_0(t)}{\partial \mathbf{r}_0^j(t)}\right\rangle$$

$$-\frac{\mu T}{N}\frac{1}{KN}\int_{-\infty}^{t} ds\, e^{-\frac{K\mu}{N}(t-s)}e^{-\frac{k\mu}{N}(t-s)}\left\langle\sum_{j=1}^{N}\frac{\partial \mathbf{F}_0(t)}{\partial \mathbf{r}_0^j(t)}\right\rangle$$

$$+\frac{v_0^2}{4N}\frac{1}{KN}\int_{-\infty}^{t} ds\, e^{-\frac{K\mu}{N}(t-s)}\int_{-\infty}^{t} dt'\, e^{-D_r|s-t'|}e^{-\frac{K\mu}{N}(t-t')}\left\langle\sum_{j=1}^{N}\frac{\partial \mathbf{F}_0(t)}{\partial \mathbf{r}_0^j(t)}\right\rangle$$

$$-\frac{v_0^2}{4N}\frac{1}{KN}\int_{-\infty}^{t} ds\, e^{-\frac{K\mu}{N}(t-s)}\int_{-\infty}^{t} dt'\, e^{-D_r|s-t'|}e^{-\frac{k\mu}{N}(t-t')}\left\langle\sum_{j=1}^{N}\frac{\partial \mathbf{F}_0(t)}{\partial \mathbf{r}_0^j(t)}\right\rangle \quad (A.22)$$

and we assume that the average is taken over the steady state so that they can now be taken out from the integrals, which can be exactly solved leading to the first

correction in ε to the variance (4.36). Indeed one obtains from (A.22)

$$\langle \mathbf{X}_0 \mathbf{X}_1 \rangle = - \left(\frac{T}{2K^2 N} + \frac{v_0^2}{4\mu} \frac{1}{K^2 N} \left(\frac{1}{\frac{k\mu}{N} + D_r} - \frac{N}{2K\mu} \right) \right) \left\langle \sum_{j=1}^{N} \frac{\partial \mathbf{F}_0 (t)}{\partial \mathbf{r}_0^j (t)} \right\rangle \quad (A.23)$$

but for consistency the second active term in the derivation is negligible. The solution is thus in the regime $K \gg k$, but the solution in the opposite regime, $K \ll k$, can be similarly derived using (A.14) and (A.20) into (A.19) and it is (4.37). As a last remark we point out that the Gaussian approximation in (A.5) used to calculate the first-order non-linear correction is not necessary if we consider an infinite expansion in correlations function of the noise $\boldsymbol{\eta}$ [258, 259].

$$\langle \xi (s) \phi (\xi (t)) \rangle = \sum_{n=1}^{\infty} \frac{1}{n!} \int_{-\infty}^{t} ds_1 \ldots ds_n \, C_{n+1} (t, s_1, \ldots, s_n) \left\langle \frac{\delta^n \phi (\xi (t))}{\delta \xi (s_1) \ldots \delta \xi (s_n)} \right\rangle \quad (A.24)$$

For to the symmetry of the process, the n-odd are the only nonzero contributions. The first, being Gaussian, gives the term already calculated, so the first non-Gaussian correction comes from the third term, i.e. $\mathcal{C}_\eta^{\mathrm{act}}$ in (A.2). Due to the complexity of estimating the correlation of the active noise for $n > 4$, the expansion must be truncated, unless the function ϕ is a power of the process $\mathbf{X}$. Indeed, for the quartic potential an truncation is not necessary and the non-Gaussian correction can be exactly calculated and added up to the correction in the Gaussian approximation. We have calculated it for (4.41) in the $k \gg K$ regime, but the derivation is equivalent, although more complicated in the opposite regime. Indeed, given that

$$\left\langle \frac{\partial^3 \left(\mathbf{r}_0^j (t) \right)^3}{\partial \eta_{\mathrm{act}}^k (s_1) \, \partial \eta_{\mathrm{act}}^k (s_2) \, \partial \eta_{\mathrm{act}}^k (s_3)} \right\rangle = 6 \frac{\partial \mathbf{r}_0^j (t)}{\partial \eta_{\mathrm{act}}^k (s_1)} \frac{\partial \mathbf{r}_0^j (t)}{\partial \eta_{\mathrm{act}}^k (s_2)} \frac{\partial \mathbf{r}_0^j (t)}{\partial \eta_{\mathrm{act}}^k (s_3)}$$

$$= -\frac{v_0^3}{8} e^{-\frac{k\mu}{N} (3t - s_1 - s_2 - s_3)} \quad (A.25)$$

where in the last passage we use the (A.14) and (A.20), the non-Gaussian correction is given by the integrals,

$$\langle \mathbf{X}_0 \mathbf{X}_1 \rangle_{\mathrm{nG}} = -\frac{v_0^4}{8} \frac{\alpha}{kN} e^{-\frac{\mu}{N} (3k + K) t} \int_{-\infty}^{t} ds \prod_{i=1}^{3} \int_{-\infty}^{t} ds_i \, \mathcal{C}_\eta^{\mathrm{act}} \, e^{\frac{\mu}{N} \left(Ks + k \sum_{i=1}^{3} s_i \right)} +$$

$$\frac{v_0^4}{8} \frac{\alpha}{kN} \frac{K\mu}{N} e^{-\frac{2K\mu}{N} t} \int_{-\infty}^{t} ds \int_{s}^{t} d\tau \, e^{-\frac{K\mu}{N} (s + \tau)} \prod_{i=1}^{3} \int_{-\infty}^{\tau} ds_i \, \mathcal{C}_\eta^{\mathrm{act}} \, e^{-\frac{k\mu}{N} \left(3\tau - \sum_{i=1}^{3} s_i \right)} \quad (A.26)$$

with $\mathcal{C}_\eta^{\mathrm{act}} = C_4 (s, s_1, s_2, s_3)$. Its analytical expression is not very enlightening and thus here not reported. A graphic analysis of its behaviour as a function of K, v_0, D_r confirms that its contribution to (4.41) is small and not able to spoil the behaviour of the dominant Gaussian part. This has been checked also in the regime $K \gg k$.

Appendix B

Chapter 5

B.1   Analytical solution for variance

The x-component Langevin of Eq. (5.2) for particle position with the parabolic potential can be formally solved with the result

$$x(t) = x_0 e^{-K(t,t_0)} + \int_{t_0}^{t} dt'\, \eta_x(t') e^{-K(t',t_0)}, \tag{B.1}$$

where $\eta_x(t) = \sqrt{2D(t)}\xi_x(t) + v(t)\cos\theta$ and x_0 denotes the initial position of the particle. Multiplying the formula (5.2) by $2x$ we obtain the formula $dx^2/dt = -2\mu k(t)x^2 + 2\eta_x x$. Inserting the solution (B.1) into the last expression, taking the average with respect to the noise and using the noise correlation function, we get the following dynamic equation for the variance $\sigma = \langle x^2 \rangle + \langle y^2 \rangle$:

$$\dot{\sigma} + 2\mu k\sigma = 4\langle x_0 \eta_x(t)\rangle\, e^{-K(t,t_0)} + 4D(t) + 2v(t)\int_{t_0}^{t} dt'\, v(t') e^{-K(t,t')-F(t,t')}. \tag{B.2}$$

In order to evaluate thermodynamics of the active heat engine described in Sec. 5.2, we need the solution of Eq. (B.2) in the time periodic regime which is attained by the system at long times after a relaxation period. This can be obtained by taking the limit $t_0 \to -\infty$ in the formal solution to Eq. (B.2). This way we obtain the formula

$$\sigma(t) = 2\lim_{t_0 \to -\infty} \int_{t_0}^{t} dt'[2D(t') + v(t')H(t')]e^{-2K(t,t')} \tag{B.3}$$

with

$$H(t) = \lim_{t_0 \to -\infty} \int_{t_0}^{t} dt'\, v(t') e^{-K(t,t')-F(t,t')}, \tag{B.4}$$

$$K(t,t_0) = \mu \int_{t_0}^{t} dt'\, k(t'), \tag{B.5}$$

$$F(t,t_0) = \int_{t_0}^{t} dt'\, D_{\mathrm{r}}(t'). \tag{B.6}$$

For the numerical evaluation of Eq. (B.3) it is useful to note that $H(t)$ is a t_p-periodical function. Furthermore, it is favourable to rewrite $K(t, t_0)$ as

$$K(t, t_0) = \lfloor (t - t_0)/t_p \rfloor K(t_p, 0) + K(t, t_0 + \lfloor (t - t_0)/t_p \rfloor t_p) \tag{B.7}$$

using the t_p-periodicity of $k(t)$ (the symbol $\lfloor x \rfloor$ denotes the floor operation) and similarly for $F(t, t_0)$. For memoryless dynamics, one can find the time-periodic solution without considering the limit $t_0 \to -\infty$ [209, 210] which is inconvenient for numerical evaluation of the solution. Interestingly, using a simple trick, one can do the same in the present model. The key is to note that not only the function σ, but also H fulfils certain differential equation which can be obtained by taking time derivative of Eq. (B.4). The resulting formula and the time-periodic solution is given in the main text in Sec. 5.2.4.

B.2 Slow driving limit of variance

For slowly varying driving functions $k(t)$, $D(t)$, $D_r(t)$ and $v(t)$ the variance (B.3) can be approximated using a simple formula which follows from the Laplace type approximation of the integral [260, 261]

$$\int_{t_0}^{t} dt\, f(t') e^{\int_{t'}^{t} dt'' g(t'')} = \int_{t_0}^{t} dt\, f(t') e^{t_p \int_{t'/t_p}^{t/t_p} dt'' g(t_p t'')} = \tag{B.8}$$

$$= \frac{f(t)}{g(t)} - \frac{1}{g^2(t)} \left(\dot{v}(t) - v(t) \frac{\dot{g}(t)}{g(t)} \right) + o(\dot{f}, \dot{g}). \tag{B.9}$$

Applying this approximation first on the function $H(t)$ (B.4) and then on the variance $\sigma(t)$ (B.3) we obtain the approximate formula (for space saving reasons we omit explicit writing of time arguments)

$$\sigma(t) = \sigma_\infty - \frac{v^2}{k\mu\kappa^2} \left(\frac{\dot{v}}{v} - \frac{\dot{\kappa}}{\kappa} \right) - \frac{D}{k^2\mu^2} \left(\frac{\dot{D}}{D} - \frac{\dot{k}}{k} \right) \tag{B.10}$$

$$- \frac{v^2}{2k^2\mu^2\kappa} \left(2\frac{\dot{v}}{v} - \frac{\dot{\kappa}}{\kappa} - \frac{\dot{k}}{k} \right) + o(\dot{v}, \dot{D}, \dot{k}, \dot{\kappa}). \tag{B.11}$$

Here σ_∞ is the variance for infinitely slow driving given in Eq. (5.15) and $\kappa = \kappa(t) = k\mu + D_r$. The zero order solution σ_∞ is discontinuous for discontinuous driving, the first order correction (B.11) is discontinuous if the first derivatives of the driving functions exhibit jumps. In such a case, however, the assumption on smallness of the derivatives used for derivation of Eq. (B.11) is not valid. In accord with the discussion below Eq. (B.15), Eqs. (B.11) reveal that the corrections caused by the active term $v \cos \theta$ are at least of the second order in active velocity.
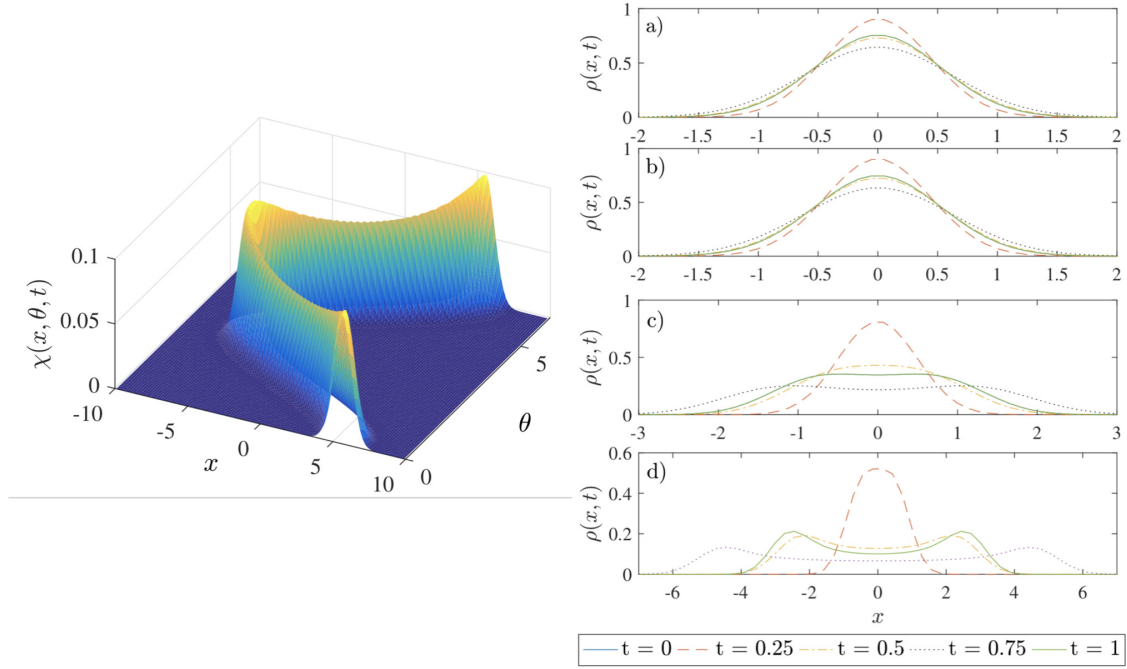
Figure B.1: Left Panel. Probability distribution χ for particle position x and orientation θ at the end of the hot isotherm ($t = t_p/3$, see Fig. 5.1). We take $v_+ = 30$ and $t_p = 10^4$. Other parameters are the same as in Fig. 5.1.

Right Panel. Marginal distribution ρ for the particle position x at the end of the individual branches of the cycle for different values of the maximum active velocity a) $v_+ = 0$, b) $v_+ = 1$, c) $v_+ = 10$, and d) $v_+ = 30$. We set $t_p = 1$. The other parameters are the same as in Fig. 5.1. Note that the curves at $t = 0$ and $t = 1$ are equal, in accord with the fact that the system sets in a time periodic steady state.

B.3   Probability distributions

Although the components x and y of the Langevin equation (5.1) are not coupled, the steady probability distribution (PDF) to find the particle with orientation θ at position (x, y), solution of the Fokker-Planck equation associated to (5.1), cannot be written in the separated form $p(x, y, \theta) = \chi(x, \theta)\rho(y, \theta)$. Namely, the latter does not solve the steady state Fokker-Planck equation (5.24), since it produces an extra term for the rotational diffusion of the form $2D_r\partial_\theta\left(\chi(x, \theta)\partial_\theta\rho(y, \theta)\right)$. Nevertheless, one can still reduce the system to just two degrees of freedom introducing polar coordinates $x = r\cos\phi$, $y = \sin\phi$ such that (5.1) becomes,

$$\dot{r} = -kr + v\cos(\theta - \phi) + \sqrt{2D_r}\eta_r, \quad \dot{\phi} = \frac{v}{r}\sin(\theta - \phi) + \sqrt{\frac{2D}{r^2}}\eta_\phi \qquad \text{(B.12)}$$

while the equation for θ is not changed. Noises η_r and η_ϕ are still gaussian and delta-correlated. Since (B.12) does depend only on the difference $\theta - \phi$, we introduce a new angle $\psi = \theta - \phi$ such that,

$$\dot{r} = -kr + v\cos\psi + \sqrt{2D_{\mathrm{r}}}\eta_r, \quad \dot{\psi} = -\frac{v}{r}\sin\psi + \sqrt{2\left(\frac{D}{r^2} + D\right)}\eta_\psi \qquad \text{(B.13)}$$

The Fokker-Planck associated to (B.13) for $\rho = \rho(r, \psi, t)$ can be easily derived [46]

$$\partial_t\rho = \left[D\partial_r^2 + \left(\frac{D}{r} + D_{\mathrm{r}}\right)\partial_\psi^2\right]\rho - \cos\psi\partial_r(v\rho) - D\partial_r\left(\frac{\rho}{r}\right) + k\partial_r(r\rho) + \frac{v}{r}\partial_\psi(\sin\psi\rho) \quad \text{(B.14)}$$

This consideration is not necessary if the phase space is (x, θ) since the probability distribution (PDF) $\chi = \chi(x, \theta, t)$ to find the particle at time t with orientation θ at position x is given by

$$\partial_t\chi = \left[D\partial_x^2 + D_{\mathrm{r}}\partial_\theta^2 + \partial_x\left(\mu\partial_x V - v\cos\theta\right)\right]\chi. \qquad \text{(B.15)}$$

In general, both equations (B.14) and (B.15) can not be solved analytically and thus we solved it using the numerical method proposed in [223]. In the left panel of Fig. B.1 we show the snapshot of the PDF $\chi(x, \theta, t)$, solution of (B.15), at the end of the third branch of a quasi-static cycle (hot "isotherm"). The figure shows the typical shape of the PDF χ with two global maxima located at $\theta = 0$ and π obtained even for a finite driving. Physically, the shape of the PDF can be understood as follows: 1) It can be expected that for any fixed orientation angle θ, the distribution have a maximum at the position where the active velocity (which acts in the Langevin Eq. (5.1) as a force $v\cos\theta/\mu$) is balanced by the force kx exerted by the parabolic potential. 2) The cosine of the angle in the velocity changes slowest around its extrema (0 and π) and thus most trajectories contribute to the surroundings of these points, making the extrema for 0 and π largest. In the right panel of Fig. B.1 we show the marginal PDF for position $\rho(x, t) = \int d\theta\chi(x, \theta, t)$ at the beginning of the individual branches of the cycle introduced in Sec. 5.2.2 for four values of maximum active velocity v_+. With increasing v_+, the resulting PDFs become increasingly non-Gaussian and finally even exhibit two separated peaks. Physically, this behaviour can be understood as a competition between the wall accumulation effect [59, 60, 74] leading to the double peak and the effect of the potential trying to localise the particle in its minimum. Qualitatively the same results are obtained also in quasi-static limit. See [77, 262] for similar PDFs.

To get some intuition about these results on analytical grounds, we now present several approximate solutions to Eq. (B.15), but valid also for (B.14). Different from passive diffusion ($v = 0$) in an external potential, the quasi-static ($\partial_t\chi = 0$) solution of the Fokker-Planck equation (B.15) is not given by the Boltzmann distribution. This is because one cannot subsume the activity into a generalised potential $\tilde{V}$ which would rule the dynamics of x and θ. Nevertheless, there are

several limiting situations where the Boltzmann form $\chi \propto \exp(-\beta \tilde{V})$, with $\beta = T^{-1}$, is still a useful approximation.

The best analytical insight in the described qualitative properties of the presented numerical solutions to Eq. (B.15) with time-dependent parameters is obtained for diffusion coefficient D_{r} much smaller than $k\mu$ (parameter R from Sec. 5.6 large). Then, the direction of the active velocity can be treated as constant and one can describe the particle dynamics by a generalised potential $\tilde{V} kx^2/2 - vx\cos\theta/\mu$. The corresponding quasi-static solution of Eq. (B.15) thus reads

$$\chi = \frac{1}{Z_\chi} \exp\left[-\beta\left(\frac{kx^2}{2} - \frac{vx\cos\theta}{\mu}\right)\right]. \tag{B.16}$$

Here Z_χ is a normalisation constant. For each fixed value of the angle θ, the distribution is Gaussian with maximum value $\exp[\beta v^2\cos^2\theta/(2\mu^2 k)]/Z_\chi$ located at the position $v\cos\theta/(\mu k)$. The distribution thus posses two global maxima located at $x = \pm v/(\mu k)$, $\theta = 0$ and π and is qualitatively similar to the distribution shown in the left panel of Fig. B.1. The marginal distribution for position obtained from the PDF (B.17) reads

$$\rho(x,t) = \int d\theta \chi = \frac{1}{Z_\rho} \exp\left(-\frac{\beta kx^2}{2}\right) I_0\left(\frac{\beta vx}{\mu}\right). \tag{B.17}$$

Here, the function $I_0(x)$ denotes the modified Bessel function of the first kind and Z_ρ is a normalisation constant. The marginal PDF is Gaussian for $v = 0$ and becomes more and more non-Gaussian with increasing $v/(\mu k)$, while for large values of $v/(\mu k)$, it can even become bimodal. This behaviour can be traced back to the shifting of the maxima of the distribution ρ with increasing $v/(\mu k)$. For small $v/(\mu k)$, the two maxima overlap substantially and the integration over the angle θ yields a single peak which is nearly Gaussian. For large values of $v/(\mu k)$, the two peaks do not overlap any more and the marginal distribution thus exhibits two peaks. The behaviour of the marginal PDF obtained in the limit $D_{kr} \ll \mu$ thus shows qualitatively the same behaviour as the actual solution of Eq. (B.15) shown in the left panel of Fig. B.1. For D_{r} much larger than $k\mu$ (parameter R from Sec. 5.6 small), the quasi-static PDF is given by $\chi \propto \exp(-\beta_{\mathrm{eff}} V)$, This is because the particles rotates so fast that the non-equilibrium bath becomes an effective equilibrium one with the temperature $1/\beta_{\mathrm{eff}} = T + v^2/(2\mu D_{\mathrm{r}})$.

Another situation where Eq. (B.15) can be solved is the case of quasi-static driving and small active velocity. Then the quasi-static PDF ρ can be approximated by the McLennan type formula $\chi \approx \exp(-\beta U)[1 - W(x)]$ [263–267]. Without going into the details, the function $W(x)$ is in general proportional to the (average) dissipation in the driven system [265] and thus to the product of the active "force" $\mu^{-1}v\cos\theta$ and the particle velocity $\dot{x}$. Since the average over the angle θ of the active force is zero, the correction $W(x)$ vanishes and thus the effect of the active velocity on the particle distribution is at least of the second order in v.

Appendix C

Chapter 6

C.1 Multiple time scale analysis

In this section we sketch the systematic expansion in the high-friction limit by which we obtain the contributions to zero order (6.17) and to first order (6.18), as reported in the main text. We rewrite the microscopic FPE (6.16) with the help of a multiple-time-scale analysis, introducing the small dimensionless bookkeeping parameter ε to label the expansion of the FP density (as in the main text $\tilde{\gamma} = \varepsilon\gamma$). The derivation follows that for a passive Langevin system [245] and extends it to active systems, with slight manipulations. Just an important remark concerning the rotational diffusion. Depending on its nature it can act on a faster or slower time scale and thus influence the overdamped Fokker-Planck equation. In the following we suppose that rotational diffusion is a thermal effect, $D_{\rm r} = T/(8\pi\eta R^3) = T/(\alpha\gamma)$ with $\gamma = 6\pi\eta R$ and $\alpha = 4R^2/3$. An expansion of the N-particle PDF is obtained comparing the terms in the FPE order by order. For this purpose, the three time scales defined in the main text are introduced on the LHS of the FPE through the chain rule relation for the times,

$$\frac{\partial}{\partial t} = \varepsilon^{-1}\frac{\partial}{\partial \tau_0} + \frac{\partial}{\partial \tau_1} + \varepsilon\frac{\partial}{\partial \tau_2} \tag{C.1}$$

Since the active force is proportional to γ via the definition $F^{\rm A} = \gamma v_0$, the zero order or fast time scale, corresponding to the terms proportional to ε^{-1}, is given by

$$\frac{\partial \rho^{(0)}}{\partial \tau_0} = \mathcal{L}_{\rm FP}\rho^{(0)}, \quad \mathcal{L}_{\rm FP} = \tilde{\gamma}\frac{\partial}{\partial v_i}\left(v_i - v_0 n_i + T\frac{\partial}{\partial v_i}\right) \tag{C.2}$$

where the summation convention for repeated indices is adopted. After a transient, (C.2) describes the fast time scale τ_0 a relaxation the solution of $\mathcal{L}_{\rm FP}\rho^{(0)} = 0$, namely,

$$\rho^{(0)} = \Phi\left(x_i, \theta_i, \tau_1, \tau_2\right)\mathcal{W}, \quad \mathcal{W} = \frac{1}{2\pi T}\exp\left(-\frac{(v_i - v_0 n_i)^2}{2T}\right). \tag{C.3}$$

To this order, the local swim velocity is the only contribution to the hydrodynamic flow velocity. Note that $\mathcal{W}$ is for a $D = 2$ system, but an extension to higher dimensions is straightforward.

First-order corrections can be found comparing the terms proportional to ε^0 in the FPE, and using that the operator $\mathcal{L}_{\mathrm{FP}}$ acts only on $\rho^{(1)}$. For simplicity we denote by $\mathcal{F}$ all forces appearing in the FPE apart from the active one,

$$\frac{\partial \rho^{(1)}}{\partial \tau_0} + \frac{\partial \rho^{(0)}}{\partial \tau_1} + v_i \frac{\partial \rho^{(0)}}{\partial x_i} + \mathcal{F}_i \frac{\partial \rho^{(0)}}{\partial v_i} = \mathcal{L}_{\mathrm{FP}} \rho^{(1)} \tag{C.4}$$

On the fast timescale τ_0, the solution $\rho^{(1)}$ relaxes to the solution of

$$\frac{\partial \rho^{(0)}}{\partial \tau_1} + v_i \frac{\partial \rho^{(0)}}{\partial x_i} + \mathcal{F}_i \frac{\partial \rho^{(0)}}{\partial v_i} = \mathcal{L}_{\mathrm{FP}} \rho^{(1)}. \tag{C.5}$$

An integration over velocities eliminates the still unknown dependence of $\rho^{(1)}$ and leads to a solvability equation for Φ

$$\frac{\partial \Phi}{\partial \tau_1} + v_0 n_i \frac{\partial \Phi}{\partial x_i} = 0. \tag{C.6}$$

In the derivation for passive systems [42], the solvability condition imposes $\partial_{\tau_1} \Phi = 0$, while from (C.6) one sees that activity implies a dependence on τ_1. In other words, for passive systems the intermediate time τ_1 is only a formal expedient, here it is physically meaningful. Introducing (C.6) in (C.5) and noting that

$$\mathcal{L}_{\mathrm{FP}} \left[(v_i - v_0 n_i) \, \mathcal{W} \right] = -\tilde{\gamma} \, (v_i - v_0 n_i) \, \mathcal{W} \tag{C.7}$$

the expression for $\rho^{(1)}$ can be obtained,

$$\rho^{(1)} = -\frac{1}{\tilde{\gamma}} \, (v_i - v_0 n_i) \left(\frac{\partial \Phi}{\partial x_i} - \frac{\mathcal{F}_i \, (x)}{T} \Phi \right) \mathcal{W} + \frac{1}{\tilde{\gamma}} \Psi \mathcal{W}. \tag{C.8}$$

where $\Psi \, (x_i, \theta_i, \tau_1, \tau_2)$ is still unknown.

Second-order corrections can be found comparing the terms proportional to ε in the FPE, and using that the operator $\mathcal{L}_{\mathrm{FP}}$ acts only on $\rho^{(2)}$.

$$\frac{\partial \rho^{(2)}}{\partial \tau_0} + \frac{\partial \rho^{(1)}}{\partial \tau_1} + \frac{\partial \rho^{(0)}}{\partial \tau_2} + v_i \frac{\partial \rho^{(1)}}{\partial x_i} + \mathcal{F}_i \, (x) \frac{\partial \rho^{(1)}}{\partial v_i} - \frac{T}{\alpha \tilde{\gamma}} \frac{\partial^2 \rho^{(0)}}{\partial \theta^2} = \mathcal{L}_{FP} \rho^{(2)} \tag{C.9}$$

On the fast timescale τ_0, the solution $\rho^{(1)}$ relaxes to the solution of

$$\frac{\partial \rho^{(1)}}{\partial \tau_1} + \frac{\partial \rho^{(0)}}{\partial \tau_2} + v_i \frac{\partial \rho^{(1)}}{\partial x_i} + \mathcal{F}_i \, (x) \frac{\partial \rho^{(1)}}{\partial v_i} - \frac{T}{\alpha \tilde{\gamma}} \frac{\partial^2 \rho^{(0)}}{\partial \theta^2} = \mathcal{L}_{FP} \rho^{(2)} \tag{C.10}$$

Given the expression for $\rho^{(1)}$ (C.8) we calculate its derivates, we plug into (C.10) and then we integrate over the velocities. Many terms cancel out employing

$$\frac{\partial \Phi}{\partial \tau_2} = -\frac{1}{\tilde{\gamma}} \left(\frac{\partial}{\partial \tau_1} + v_0 n_i \frac{\partial}{\partial x_i} \right) \Psi + \frac{T}{\alpha \tilde{\gamma}} \frac{\partial^2 \Phi}{\partial \theta^2} - \frac{T}{\tilde{\gamma}} \frac{\partial}{\partial x_i} \left(\frac{\mathcal{F}_i(x)}{T} \Phi - \frac{\partial \Phi}{\partial x_i} \right) \qquad \text{(C.11)}$$

Eq.(C.11) is the solvability equation for Φ at time τ_2 as well as (C.6) was the equation for time τ_1. Given $\rho = \rho^{(0)} + \varepsilon \rho^{(1)} + \ldots$, we plug (C.3) and (C.8) and we integrate over the velocities such that, $\rho(x, \theta, t) = (\Phi + \varepsilon \Psi / \tilde{\gamma})$. If we take a time derivative and we use (C.1) we obtain an equation for $\rho = \rho(x, \theta, t)$

$$\frac{\partial \rho}{\partial t} = \left(\varepsilon^{-1} \frac{\partial}{\partial \tau_0} + \frac{\partial}{\partial \tau_1} + \varepsilon \frac{\partial}{\partial \tau_2} \right) \left(\Phi + \frac{\varepsilon}{\tilde{\gamma}} \Psi \right) \qquad \text{(C.12)}$$

Neglecting the derivative with respect to τ_0 and using (C.6) and (C.11), (C.12) becomes

$$\frac{\partial \rho}{\partial t} = -v_0 n_i \frac{\partial \rho}{\partial x_i} + \varepsilon \left[\frac{T}{\alpha \tilde{\gamma}} \frac{\partial^2 \Phi}{\partial \theta^2} - \frac{T}{\tilde{\gamma}} \frac{\partial}{\partial x_i} \left(\frac{\mathcal{F}_i(x)}{T} \Phi - \frac{\partial \Phi}{\partial x_i} \right) \right] \qquad \text{(C.13)}$$

Given that $\rho = \Phi + \mathcal{O}(\varepsilon)$ we obtain the final overdamped equation reintroducing the real friction $\tilde{\gamma} = \varepsilon \gamma$ and the rotational diffusion coefficient,

$$\frac{\partial \rho}{\partial t} + \frac{\partial}{\partial x_i} \left(\frac{\mathcal{F}_i(x)}{\gamma} + v_0 n_i \right) \rho = \frac{T}{\gamma} \frac{\partial^2 \rho}{\partial x_i^2} + D_r \frac{\partial^2 \rho}{\partial \theta^2} \qquad \text{(C.14)}$$

If the rotational diffusion is not a thermal effect and for example is independent of γ, the high-friction limit of (6.16) leads to another overdamped Langevin equation,

$$\frac{\partial \rho}{\partial t} + \frac{\partial}{\partial x_i} \left(\frac{\mathcal{F}_i(x)}{\gamma} + v_0 n_i + 2v_0 \frac{D_r}{\gamma} \frac{\partial n_i}{\partial \theta} \frac{\partial}{\partial \theta} \right) \rho = \frac{T}{\gamma} \frac{\partial^2 \rho}{\partial x_i^2} + D_r \frac{\partial^2 \rho}{\partial \theta^2} \qquad \text{(C.15)}$$

An extra term appears with respect to (C.14). Noteworthy it is multiplied by a small pre-factor D_r / γ, such that it can be neglected. Similar for the $\rho^{(1)}$,

$$\rho^{(1)} = -\frac{1}{\tilde{\gamma}} (v_i - v_0 n_i) \left(\frac{\partial \Phi}{\partial x_i} - \frac{\mathcal{F}_i(x)}{T} \Phi - \frac{2D_r v_0}{T} \frac{\partial n_i}{\partial \theta} \frac{\partial \Phi}{\partial \theta} \right) \mathcal{W} + \frac{1}{\tilde{\gamma}} \Psi \mathcal{W}$$

$$- \frac{D_r}{2\tilde{\gamma}} \Phi \left(\frac{\partial n_i}{\partial \theta} \right)^2 \frac{v_0^2}{T} \left[1 - \frac{(v_i - v_0 n_i)^2}{T} \right] \mathcal{W} \qquad \text{(C.16)}$$

Bibliography

[1] NG Van Kampen. *Stochastic processes in physics and chemistry*, volume 1. Elsevier, 1992.

[2] Mark Haw. *Middle World: The Restless Heart of Matter and Life*. Springer, 2016.

[3] Mehran Kardar. *Statistical physics of particles*. Cambridge University Press, 2007.

[4] K Huang. Statistical mechanics, 2nd. *Edition (New York: John Wiley & Sons)*, 1987.

[5] Denis J Evans and Debra J Searles. The fluctuation theorem. *Advances in Physics*, 51(7):1529–1585, 2002.

[6] U. Seifert. Stochastic thermodynamics, fluctuation theorems and molecular machines. *Rep. Prog. Phys.*, 75:126001, 2012.

[7] G. Crooks. Entropy production fluctuation theorem and the nonequilibrium work relation for free energy differences. *Phys. Rev. E*, 60:2721 (1999), 1999.

[8] C. Jarzynski. Nonequilibrium equality for free energy differences. *Phys. Rev. Lett.*, 78:2690, 1997.

[9] Ken Sekimoto and Shin ichi Sasa. Complementarity relation for irreversible process derived from stochastic energetics. *J. Phys. Soc. Jpn.*, 66(11):3326–3328, 1997.

[10] U. Seifert. Entropy production along a stochastic trajectory and an integral fluctuation theorem. *Phys. Rev. Lett.*, 95:040602, 2005.

[11] Hugo Touchette. The large deviation approach to statistical mechanics. *Physics Reports*, 478(1-3):1–69, 2009.

[12] Angelo Vulpiani, Fabio Cecconi, Massimo Cencini, Andrea Puglisi, and Davide Vergni. Large deviations in physics. *The Legacy of the Law of Large Numbers (Berlin: Springer)*, 2014.

[13] C. Maes and K. Netočný. Time-reversal and entropy. *J. Stat. Phys.*, 110:269–310, 2003.

[14] Andreas M Menzel. Tuned, driven, and active soft matter. *Phys. Rep.*, 554:1–45, 2015.

[15] Christian Maes and Stefano Steffenoni. Friction and noise for a probe in a nonequilibrium fluid. *Phys. Rev. E*, 91(2):022128, 2015.

[16] Stefano Steffenoni, Klaus Kroy, and Gianmaria Falasco. Interacting brownian dynamics in a nonequilibrium particle bath. *Phys. Rev. E*, 94(6):062139, 2016.

[17] S. Steffenoni, G. Falasco, and K. Kroy. Colloid in an active particle bath. in preparation.

[18] S. Steffenoni, V. Holubec, G. Falasco, and K. Kroy. Active brownian heat engine: Dynamics and average thermodynamics. in preparation.

[19] Viktor Holubec, Klaus Kroy, and Stefano Steffenoni. Efficient numerical solver for time-dependent fokker-planck equations. *arXiv preprint arXiv:1804.01285*, 2018.

[20] Stefano Steffenoni, Gianmaria Falasco, and Klaus Kroy. Microscopic derivation of the hydrodynamics of active-brownian-particle suspensions. *Phys. Rev. E*, 95(5):052142, 2017.

[21] A. P. Solon, Y. Fily, A. Baskaran, M. E. Cates, Y. Kafri, M. Kardar, and J. Tailleur. Pressure is not a state function for generic active fluids. *Nat. Phys.*, 11:3377, 2015.

[22] Thomas Speck and Robert L Jack. Ideal bulk pressure of active brownian particles. *Phys. Rev. E*, 93(6):062605, 2016.

[23] Umberto Marini Bettolo Marconi, Claudio Maggi, and Simone Melchionna. Pressure and surface tension of an active simple liquid: a comparison between kinetic, mechanical and free-energy based approaches. *Soft Matter*, 12(26):5727–5738, 2016.

[24] Sho C Takatori, Wen Yan, and John F Brady. Swim pressure: stress generation in active matter. *Phys. Rev. Lett.*, 113(2):028103, 2014.

[25] Albert Einstein. Über die von der molekularkinetischen theorie der wärme geforderte bewegung von in ruhenden flüssigkeiten suspendierten teilchen. *Ann. Phys.*, 4, 1905.

[26] Louis Bachelier. *Théorie de la spéculation.* Gauthier-Villars, 1900.

[27] JB Perrin. Discontinuous structure of matter, nobel lecture 1926. *Nobel Lectures*, 1926.

[28] Paul Langevin. *On the theory of Brownian motion.* 1908.

[29] LS Ornstein. On the brownian motion. In *Proc. Amst*, volume 21, pages 96–108, 1919.

[30] Leonard Salomon Ornstein. On the theory of the brownian motion. *Phys. Rev.*, 36:823–841, 1930.

[31] NG Van Kampen and I Oppenheim. Brownian motion as a problem of eliminating fast variables. *Physica A*, 138(1-2):231–248, 1986.

[32] K. Sekimoto. *Stochastic Energetics*, volume 799 of *Lecture Notes in Physics*. Springer, 2010.

[33] Daniel T Gillespie. The mathematics of brownian motion and johnson noise. *American Journal of Physics*, 64(3):225–240, 1996.

[34] Daniel T Gillespie. *Markov processes: an introduction for physical scientists*. Elsevier, 1991.

[35] Ryōgo Kubo, Morikadzu Toda, and Natsuki Hashitsume. *Statistical physics II*. Springer, 1992.

[36] Ryōgo Kubo. The fluctuation-dissipation theorem. *Rep Progr. Phys.*, 29(1):255, 1966.

[37] William T. Coffey, Yu. P. Kalmykov, and J. T. Waldron. *The Langevin equation.* World Scientific, 2004.

[38] Takeshi Kuroiwa and Kunimasa Miyazaki. Brownian motion with multiplicative noises revisited. *J. Phys. A*, 47(1):012001, 2013.

[39] JM Sancho. Brownian colloidal particles: Ito, stratonovich, or a different stochastic interpretation. *Phys. Rev. E*, 84(6):062102, 2011.

[40] NG Van Kampen. Itô versus stratonovich. *J. of Stat. Phys.*, 24(1):175–187, 1981.

[41] Mark H Holmes. *Introduction to perturbation methods*, volume 20. Springer Science & Business Media, 2012.

[42] Lydéric Bocquet. High friction limit of the kramers equation: The multiple time-scale approach. *Am. J. Phys.*, 65(2):140–144, 1997.

[43] JM Sancho, M San Miguel, and D Dürr. Adiabatic elimination for systems of brownian particles with nonconstant damping coefficients. *J. of Stat. Phys.*, 28(2):291–305, 1982.

[44] C. W. Gardiner. *Handbook of stochastic methods for physics, chemistry and the natural sciences*, volume 13 of *Springer Series in Synergetics*. Springer-Verlag, Berlin, third edition, 2004.

[45] Jorge Kurchan. Six out of equilibrium lectures. *arXiv preprint arXiv:0901.1271*, 2009.

[46] Hannes Risken. Fokker-planck equation. In *The Fokker-Planck Equation*, pages 63–95. Springer, 1996.

[47] Hugo Touchette. Introduction to dynamical large deviations of markov processes. *Physica A: Statistical Mechanics and its Applications*, 504:5–19, 2018.

[48] James R Norris. *Markov chains*. Number 2. Cambridge university press, 1998.

[49] David S Dean. Langevin equation for the density of a system of interacting langevin processes. *Journal of Physics A: Mathematical and General*, 29(24):L613, 1996.

[50] José M Sancho, M San Miguel, SL Katz, and JD Gunton. Analytical and numerical studies of multiplicative noise. *Phys. Rev. A*, 26(3):1589, 1982.

[51] Christian Maes, Karel Netočný, Bidzina Shergelashvili, et al. A selection of nonequilibrium issues. In *Methods of contemporary mathematical statistical physics*, pages 1–60. Springer, 2009.

[52] T. Harada and S.-i. Sasa. Energy dissipation and violation of the fluctuation-response relation in nonequilibrium Langevin systems. *Phys. Rev. E*, 73:026131, 2006.

[53] JL Lebowitz. Stationary nonequilibrium gibbsian ensembles. *Physical Review*, 114(5):1192, 1959.

[54] Sheldon Katz, Joel L. Lebowitz, and H. Spohn. Phase transitions in stationary nonequilibrium states of model lattice systems. *Phys. Rev. B*, 28:1655–1658, Aug 1983.

[55] M. Baiesi, C. Maes, and B. Wynants. The modified Sutherland-Einstein relation for diffusive non-equilibria. *Proc. Royal Soc. A*, 467:2792–2809, 2011.

[56] V. Blickle, T. Speck, C. Lutz, U. Seifert, and C. Bechinger. Einstein relation generalized to nonequilibrium. *Phys. Rev. Lett.*, 98:210601, 2007.

[57] Ilya Prigogine. Introduction to thermodynamics of irreversible processes. *New York: Interscience, 1967, 3rd ed.*, 1967.

[58] Jens Elgeti and Gerhard Gompper. Wall accumulation of self-propelled spheres. *EPL*, 101(4):48003, 2013.

[59] H. H. Wensink and H. Löwen. Aggregation of self-propelled colloidal rods near confining walls. *Phys. Rev. E*, 78:031409, Sep 2008.

[60] Yaouen Fily, Aparna Baskaran, and Michael F. Hagan. Dynamics of self-propelled particles under strong confinement. *Soft Matter*, 10:5609–5617, 2014.

[61] Yaouen Fily and M Cristina Marchetti. Athermal phase separation of self-propelled particles with no alignment. *Phys. Rev. Lett.*, 108(23):235702, 2012.

[62] Ivo Buttinoni, Julian Bialké, Felix Kümmel, Hartmut Löwen, Clemens Bechinger, and Thomas Speck. Dynamical clustering and phase separation in suspensions of self-propelled colloidal particles. *Phys. Rev. Lett.*, 110(23):238301, 2013.

[63] JG Kirkwood. Phase transformations in solids, 1951.

[64] BJ Alder and TEf Wainwright. Phase transition for a hard sphere system. *J. Chem. Phys*, 27(5):1208–1209, 1957.

[65] ME Cates. Diffusive transport without detailed balance in motile bacteria: does microbiology need statistical physics? *Rep. Prog. Phys*, 75(4):042601, 2012.

[66] Ran Ni, Martien A Cohen Stuart, and Peter G Bolhuis. Tunable long range forces mediated by self-propelled colloidal hard spheres. *Phys. Rev. Lett.*, 114(1):018302, 2015.

[67] J. Harder, S. A. Mallory, C. Tung, C. Valeriani, and A. Cacciuto. The role of particle shape in active depletion. *J. Chem. Phys.*, 141(19), 2014.

[68] Clemens Bechinger, Roberto Di Leonardo, Hartmut Löwen, Charles Reichhardt, Giorgio Volpe, and Giovanni Volpe. Active particles in complex and crowded environments. *Rev. Mod. Phys.*, 88(4):045006, 2016.

[69] Pawel Romanczuk, Markus Bär, Werner Ebeling, Benjamin Lindner, and Lutz Schimansky-Geier. Active brownian particles. *The European Physical Journal Special Topics*, 202(1):1–162, 2012.

[70] Andreas Zöttl and Holger Stark. Emergent behavior in active colloids. *Journal of Physics: Condensed Matter*, 28(25):253001, 2016.

[71] Iain D Couzin, Jens Krause, Nigel R Franks, and Simon A Levin. Effective leadership and decision-making in animal groups on the move. *Nature*, 433(7025):513, 2005.

[72] Vishwesha Guttal and Iain D Couzin. Social interactions, information use, and the evolution of collective migration. *Proc. Natl. Acad. Sci. U S A*, 107(37):16172–16177, 2010.

[73] Howard C Berg. *E. coli in Motion.* Springer Science & Business Media, 2008.

[74] R. Nosrati, P. J. Graham, Q. Liu, and D. Sinton. Predominance of sperm motion in corners. *Scientific Reports*, 6:26669, 2016.

[75] Eric Lauga. Enhanced diffusion by reciprocal swimming. *Phys. Rev. Lett.*, 106(17):178101, 2011.

[76] Roland G Winkler, Adam Wysocki, and Gerhard Gompper. Virial pressure in systems of spherical active brownian particles. *Soft Matter*, 11(33):6680–6691, 2015.

[77] Xu Zheng, Borge ten Hagen, Andreas Kaiser, Meiling Wu, Haihang Cui, Zhanhua Silber-Li, and Hartmut Löwen. Non-gaussian statistics for the motion of self-propelled janus particles: Experiment versus theory. *Phys. Rev. E*, 88(3):032304, 2013.

[78] Grzegorz Szamel. Self-propelled particle in an external potential: Existence of an effective temperature. *Phys. Rev. E*, 90:012111, Jul 2014.

[79] M. C. Marchetti, J. F. Joanny, S. Ramaswamy, T. B. Liverpool, J. Prost, Madan Rao, and R. Aditi Simha. Hydrodynamics of soft active matter. *Rev. Mod. Phys.*, 85:1143, 2013.

[80] J Tailleur and ME Cates. Statistical mechanics of interacting run-and-tumble bacteria. *Phys. Rev. Lett.*, 100(21):218103, 2008.

[81] AP Solon, ME Cates, and J Tailleur. Active brownian particles and run-and-tumble particles: A comparative study. *EPJ ST*, 224(7):1231–1262, 2015.

[82] Chiu Fan Lee. Active particles under confinement: aggregation at the wall and gradient formation inside a channel. *New Journal of Physics*, 15(5):055007, 2013.

[83] Étienne Fodor, Cesare Nardini, Michael E. Cates, Julien Tailleur, Paolo Visco, and Frédéric van Wijland. How far from equilibrium is active matter? *Phys. Rev. Lett.*, 117:038103, Jul 2016.

[84] Norbert Wiener. The average value of a functional. *Proceedings of the London Mathematical Society*, 2(1):454–467, 1924.

[85] Richard Phillips Feynman. A relativistic cut-off for classical electrodynamics. *Physical Review*, 74(8):939, 1948.

[86] Markus F Weber and Erwin Frey. Master equations and the theory of stochastic path integrals. *Reports on Progress in Physics*, 80(4):046601, 2017.

[87] Peter Häunggi and Peter Jung. Colored noise in dynamical systems. *Advances in chemical physics*, 89:239–326, 1994.

[88] L Pesquera, MA Rodriguez, and E Santos. Path integrals for non-markovian processes. *Physics Letters A*, 94(6-7):287–289, 1983.

[89] Horacio S Wio, P Colet, M San Miguel, L Pesquera, and MA Rodriguez. Path-integral formulation for stochastic processes driven by colored noise. *Phys. Rev. A*, 40(12):7312, 1989.

[90] A. W. C. Lau and T. C. Lubensky. State-dependent diffusion: Thermodynamic consistency and its path integral formulation. *Phys. Rev. E*, 76:011123, Jul 2007.

[91] Leticia F Cugliandolo and Vivien Lecomte. Rules of calculus in the path integral representation of white noise langevin equations: the onsager–machlup approach. *Journal of Physics A: Mathematical and Theoretical*, 50(34):345001, 2017.

[92] Lars Onsager and S Machlup. Fluctuations and irreversible processes. *Phys. Rev.*, 91(6):1505, 1953.

[93] Christian Maes. Fluctuations and response out-of-equilibrium. *Progress of Theoretical Physics-Supplement*, (184):318, 2010.

[94] Richard S Ellis. *Entropy, large deviations, and statistical mechanics*. Springer, 2007.

[95] C. Maes. The fluctuation theorem as a Gibbs property. *J. Stat. Phys.*, 95:367–392, 1999.

[96] C. Maes, F. Redig, and A. Van Moffaert. On the definition of entropy production, via examples. *J. Mat. Phys.*, 41:1528–1554, 2000.

[97] Christian Maes, Frank Redig, and Michel Verschuere. From global to local fluctuation theorems. *Moscow Mathematical Journal*, 1(3):421–438, 2001.

[98] Christian Maes and Frank Redig. Positivity of entropy production. *Journal of statistical physics*, 101(1-2):3–15, 2000.

[99] Lars Onsager. Reciprocal relations in irreversible processes. i. *Phys. Rev.*, 37:405–426, Feb 1931.

[100] Ryogo Kubo. Statistical-mechanical theory of irreversible processes. i. general theory and simple applications to magnetic and conduction problems. *J. Phys. Soc. Jpn.*, 12(6):570–586, 1957.

[101] NG Van Kampen. *Phys. Norv.*, 5:10, 1971.

[102] R Kubo. A general expression for the conductivity tensor. *Canadian Journal of Physics*, 34(12A):1274–1277, 1956.

[103] Gary P Morriss and Denis J Evans. *Statistical Mechanics of Nonequilbrium Liquids*. ANU Press, 2013.

[104] S. Lepri, R. Livi, and A. Politi. Thermal conduction in classical low-dimensional lattices. *Phys. Rep.*, 377:1–80, 2003.

[105] P Baert, U Basu, C Maes, and S Safaverdi. Frenetic origin of negative differential response. *Phys. Rev. E*, 88:052109, 2013.

[106] M. Baiesi, C. Maes, and B. Wynants. Fluctuations and response of nonequilibrium states. *Phys. Rev. Lett.*, 103:010602, 2009.

[107] M. Baiesi and C. Maes. An update on the nonequilibrium linear response. *New J. Phys.*, 15:013004, 2013.

[108] T. Harada and S.-i. Sasa. Equality connecting energy dissipation with violation of fluctuation-response relation. *Phys. Rev. Lett.*, 95:130602, 2005.

[109] E. Lippiello, M. Baiesi, and A. Sarracino. Nonequilibrium fluctuation-dissipation theorem and heat production. *Phys. Rev. Lett.*, 112:140602, 2014.

[110] C. Maes, S. Safaverdi, P. Visco, and F. van Wijland. Fluctuation-response relations for nonequilibrium diffusions with memory. *Phys. Rev. E*, 87:022125, 2013.

[111] M. Baiesi, E. Boksenbojm, C. Maes, and B. Wynants. Linear response of nonequilibrium states, II: inertial dynamics. *J. Stat. Phys.*, 139:492–505, 2010.

[112] M. Baiesi, C. Maes, and B. Wynants. Nonequilibrium linear response for Markov dynamics, I: Jump processes and overdamped diffusions. *J. Stat. Phys.*, 137:1094–1116, 2009.

[113] J. R. Gomez-Solano, A. Petrosyan, S. Ciliberto, and C. Maes. Fluctuations and response in a non-equilibrium micron-sized system. *J. Stat. Mech.*, page P01008, 2011.

[114] Robert Zwanzig. Nonlinear generalized langevin equations. *J. Stat. Phys.*, 9(3):215–220, 1973.

[115] Kyozi Kawasaki. Simple derivations of generalized linear and nonlinear langevin equations. *J. Phys. A*, 6(9):1289, 1973.

[116] Gianmaria Falasco, Fulvio Baldovin, Klaus Kroy, and Marco Baiesi. Mesoscopic virial equation for nonequilibrium statistical mechanics. *New J. Phys.*, 18(9):093043, 2016.

[117] Urna Basu, Christian Maes, and Karel Netočný. How statistical forces depend on the thermodynamics and kinetics of driven media. *Phys. Rev. Lett.*, 114:250601, Jun 2015.

[118] A. V. Ivlev, J. Bartnick, M. Heinen, C.-R. Du, V. Nosenko, and H. Löwen. Statistical mechanics where newton's third law is broken. *Phys. Rev. X*, 5:011035, Mar 2015.

[119] J Dzubiella, H Löwen, and CN Likos. Depletion forces in nonequilibrium. *Phys. Rev. Lett.*, 91(24):248301, 2003.

[120] R. Candelier and O. Dauchot. Creep motion of an intruder within a granular glass close to jamming. *Phys. Rev. Lett.*, 103:128001, Sep 2009.

[121] Bérengère Abou and Francois Gallet. Probing a nonequilibrium einstein relation in an aging colloidal glass. *Phys. Rev. Lett.*, 93:160603, Oct 2004.

[122] D. T. N. Chen, A. W. C. Lau, L. A. Hough, M. F. Islam, M. Goulian, T. C. Lubensky, and A. G. Yodh. Fluctuations and rheology in active bacterial suspensions. *Phys. Rev. Lett.*, 99:148302, Oct 2007.

[123] A. W. C. Lau, B. D. Hoffman, A. Davies, J. C. Crocker, and T. C. Lubensky. Microrheology, stress fluctuations, and active behavior of living cells. *Phys. Rev. Lett.*, 91:198101, Nov 2003.

[124] Herbert Spohn. *Large scale dynamics of interacting particles*. Springer Science & Business Media, 2012.

[125] Nicolaas Godfried Van Kampen. Elimination of fast variables. *Phys. Rep.*, 124(2):69–160, 1985.

[126] T. Nakamura and S.-i. Sasa. A fluctuation-response relation of many Brownian particles under non-equilibrium conditions. *Phys. Rev. E*, 77:021108, 2008.

[127] R. Chetrite, G. Falkovich, and K. Gawędzki. Fluctuation relations in simple examples of non-equilibrium steady states. *J. Stat. Mech.*, page P08005, 2008.

[128] T. Speck and U. Seifert. Extended fluctuation-dissipation theorem for soft matter in stationary flow. *Phys. Rev. E*, 79:040102, 2009.

[129] U. Seifert and T. Speck. Fluctuation-dissipation theorem in nonequilibrium steady states. *Europhys. Lett.*, 89:10007, 2010.

[130] J. Prost, J.-F. Joanny, and J. M. Parrondo. Generalized fluctuation-dissipation theorem for steady-state systems. *Phys. Rev. Lett.*, 103:090601, 2009.

[131] G. Verley, K. Mallick, and D. Lacoste. Modified fluctuation-dissipation theorem for non-equilibrium steady states and applications to molecular motors. *Europhys. Lett.*, 93:10002, 2011.

[132] E. Lippiello, F. Corberi, and M. Zannetti. Off-equilibrium generalization of the fluctuation dissipation theorem for Ising spins and measurement of the linear response function. *Phys. Rev. E*, 71:036104, 2005.

[133] Christian Maes. On the second fluctuation–dissipation theorem for nonequilibrium baths. *Journal of Statistical Physics*, 154(3):705–722, 2014.

[134] Indira Sriram and Eric M Furst. Out-of-equilibrium forces between colloids. *Soft Matter*, 8(12):3335–3341, 2012.

[135] V. Lecomte, C. Appert-Rolland, and F. van Wijland. Chaotic properties of systems with Markov dynamics. *Phys. Rev. Lett.*, 95:010601, 2005.

[136] M. Merolle, J. P. Garrahan, and D. Chandler. Space-time thermodynampics of the glass transition. *Proc. Natl. Acad. Sci.*, 102:10837–10840, 2005.

[137] J. P. Garrahan, R. L. Jack, V. Lecomte, E. Pitard, K. van Duijvendijk, and F. van Wijland. First-order dynamical phase transition in models of glasses: an approach based on ensembles of histories. *J. Phys. A: Math. Gen*, 42:075007, 2009.

[138] C. J. Fullerton and R. L. Jack. Dynamical phase transitions in supercooled liquids: Interpreting measurements of dynamical activity. *J. Chem. Phys.*, 138:224506, 2013.

[139] Kumiko Hayashi and Shin-ichi Sasa. The law of action and reaction for the effective force in a non-equilibrium colloidal system. *J. Phys. Condens. Matter*, 18(10):2825, 2006.

[140] Pascal R Buenzli and Rodrigo Soto. Violation of the action-reaction principle and self-forces induced by nonequilibrium fluctuations. *Phys. Rev. E*, 78(2):020102, 2008.

[141] Urna Basu, Christian Maes, and Karel Netočnỳ. Statistical forces from close-to-equilibrium media. *New Journal of Physics*, 17(11):115006, 2015.

[142] Caterina De Bacco, Fulvio Baldovin, Enzo Orlandini, and Ken Sekimoto. Nonequilibrium statistical mechanics of the heat bath for two brownian particles. *Phys. Rev. Lett.*, 112(18):180605, 2014.

[143] V. Blickle, T. Speck, U. Seifert, and C. Bechinger. Characterizing potentials by a generalized Boltzmann factor. *Phys. Rev. E*, 75:060101(R), 2007.

[144] Christopher Battle, Chase P. Broedersz, Nikta Fakhri, Veikko F. Geyer, Jonathon Howard, Christoph F. Schmidt, and Fred C. MacKintosh. Broken detailed balance at mesoscopic scales in active biological systems. *Science*, 352(6285):604–607, 2016.

[145] Jakob Mehl, Boris Lander, Clemens Bechinger, Valentin Blickle, and Udo Seifert. Role of hidden slow degrees of freedom in the fluctuation theorem. *Phys. Rev. Lett.*, 108(22):220601, 2012.

[146] B. Lander, J. Mehl, V. Blickle, C. Bechinger, and U. Seifert. Noninvasive measurement of dissipation in colloidal systems. *Phys. Rev. E*, 86:030401, Sep 2012.

[147] J. R. Gomez-Solano, A. Petrosyan, S. Ciliberto, R. Chetrite, , and K. Gawędzki. Experimental verification of a modified fluctuation-dissipation relation for a micron-sized particle in a non-equilibrium steady state. *Phys. Rev. Lett.*, 103:040601, 2009.

[148] G. Verley, R. Chétrite, and D. Lacoste. Modified fluctuation-dissipation theorem near non-equilibrium states and applications to the Glauber-Ising chain. *J. Stat. Mech.*, page P10025, 2011.

[149] Marco Baiesi, Sergio Ciliberto, Gianmaria Falasco, and Cem Yolcu. Thermal response of nonequilibrium r c circuits. *Phys. Rev. E*, 94(2):022144, 2016.

[150] T. Speck and U. Seifert. Restoring a fluctuation-dissipation theorem in a nonequilibrium steady state. *Europhys. Lett.*, 74:391–396, 2006.

[151] C. Maes and K. Netočný. A nonequilibrium extension of the Clausius heat theorem. *J. Stat. Phys.*, 154:188–203, 2014.

[152] Tamás Sándor Biró. *Is there a temperature?: conceptual challenges at high energy, acceleration and complexity*, volume 171. Springer Science & Business Media, 2011.

[153] A Puglisi, A Sarracino, and A Vulpiani. Temperature in and out of equilibrium: A review of concepts, tools and attempts. *Physics Reports*, 2017.

[154] Christian Maes and Karel Netocny. Non-reactive forces and pattern formation induced by a nonequilibrium medium. *arXiv preprint arXiv:1711.05168*, 2017.

[155] Peter Reimann. Brownian motors: noisy transport far from equilibrium. *Phys. Rep.*, 361(2-4):57–265, 2002.

[156] R. Eichhorn, P. Reimann, and P. Hänggi. Brownian motion exhibiting absolute negative mobility. *Phys. Rev. Lett.*, 88:190601, 2002.

[157] Alexandra Ros, Ralf Eichhorn, Jan Regtmeier, Thanh Tu Duong, Peter Reimann, and Dario Anselmetti. Brownian motion: absolute negative particle mobility. *Nature*, 436(7053):928, 2005.

[158] L. Machura, M. Kostur, P. Talkner, J. Łuczka, and P. Hänggi. Absolute negative mobility induced by thermal equilibrium fluctuations. *Phys. Rev. Lett.*, 98:040601, 2007.

[159] P. K. Ghosh, P. Hänggi, F. Marchesoni, and F. Nori. Giant negative mobility of janus particles in a corrugated channel. *Phys. Rev. E*, 89:062115, 2014.

[160] Raphaël Chetrite and Hugo Touchette. Nonequilibrium markov processes conditioned on large deviations. In *Annales Henri Poincaré*, volume 16, pages 2005–2057. Springer, 2015.

[161] G. Falasco and K. Kroy. Nonisothermal fluctuating hydrodynamics and brownian motion. *Phys. Rev. E*, 93:032150, Mar 2016.

[162] G. Falasco, M. V. Gnann, D. Rings, and K. Kroy. Effective temperatures of hot brownian motion. *Phys. Rev. E*, 90:032131, Sep 2014.

[163] Udo Seifert. First and second law of thermodynamics at strong coupling. *Phys. Rev. Lett.*, 116(2):020601, 2016.

[164] Matthias Krüger and Christian Maes. The modified langevin description for probes in a nonlinear medium. *arXiv preprint arXiv:1607.08790*, 2016.

[165] Juan Ruben Gomez-Solano and Clemens Bechinger. Transient dynamics of a colloidal particle driven through a viscoelastic fluid. *New J. Phys.*, 17(10):103032, 2015.

[166] Oliver Otto, Sebastian Sturm, Nadanai Laohakunakorn, Ulrich F Keyser, and Klaus Kroy. Rapid internal contraction boosts dna friction. *Nat. Commun.*, 4:1780, 2013.

[167] R. Di Leonardo, L. Angelani, D. Dell'Arciprete, G. Ruocco, V. Iebba, S. Schippa, MP. Conte, F. Mecarini, F. De Angelis, and E. Di Fabrizio. Bacterial ratchet motors. *Proc. Natl. Acad. Sci.*, 107(21):9541–9545, 2010.

[168] Carlos Mejia-Monasterio and Gleb Oshanin. Bias- and bath-mediated pairing of particles driven through a quiescent medium. *Soft Matter*, 7:993–1000, 2011.

[169] Lukas Holzer, Jochen Bammert, Roland Rzehak, and Walter Zimmermann. Dynamics of a trapped brownian particle in shear flows. *Phys. Rev. E*, 81:041124, Apr 2010.

[170] L. Angelani, C. Maggi, M. L. Bernardini, A. Rizzo, and R. Di Leonardo. Effective interactions between colloidal particles suspended in a bath of swimming cells. *Phys. Rev. Lett.*, 107:138302, Sep 2011.

[171] L. R. Leite, D. Lucena, F. Q. Potiguar, and W. P. Ferreira. Depletion forces on circular and elliptical obstacles induced by active matter. *Phys. Rev. E*, 94:062602, Dec 2016.

[172] D. Ray, C. Reichhardt, and C. J. Olson Reichhardt. Casimir effect in active matter systems. *Phys. Rev. E*, 90:013019, Jul 2014.

[173] T. F. F. Farage, P. Krinninger, and J. M. Brader. Effective interactions in active brownian suspensions. *Phys. Rev. E*, 91:042310, Apr 2015.

[174] Xiao-Lun Wu and Albert Libchaber. Particle diffusion in a quasi-two-dimensional bacterial bath. *Phys. Rev. Lett.*, 84(13):3017, 2000.

[175] Gastón Miño, Thomas E. Mallouk, Thierry Darnige, Mauricio Hoyos, Jeremi Dauchet, Jocelyn Dunstan, Rodrigo Soto, Yang Wang, Annie Rousselet, and Eric Clement. Enhanced diffusion due to active swimmers at a solid surface. *Phys. Rev. Lett.*, 106:048102, Jan 2011.

[176] Kyriacos C. Leptos, Jeffrey S. Guasto, J. P. Gollub, Adriana I. Pesci, and Raymond E. Goldstein. Dynamics of enhanced tracer diffusion in suspensions of swimming eukaryotic microorganisms. *Phys. Rev. Lett.*, 103:198103, Nov 2009.

[177] Aykut Argun, Ali-Reza Moradi, Erça ğ Pinçe, Gokhan Baris Bagci, Alberto Imparato, and Giovanni Volpe. Non-boltzmann stationary distributions and nonequilibrium relations in active baths. *Phys. Rev. E*, 94:062150, Dec 2016.

[178] Jean-Luc Thiffeault. Distribution of particle displacements due to swimming microorganisms. *Phys. Rev. E*, 92(2):023023, 2015.

[179] Urna Basu, Satya N. Majumdar, and Alberto Rosso andGregory Schehr. Active brownian motion in two dimensions. *arXiv:1804.09027*, 2018.

[180] L. F. Cugliandolo. The effective temperature. *J. Phys. A: Math. Gen*, 44:483001, 2011.

[181] Xingbo Yang, M Lisa Manning, and M Cristina Marchetti. Aggregation and segregation of confined active particles. *Soft Matter*, 10(34):6477–6484, 2014.

[182] Sho C Takatori and John F Brady. A theory for the phase behavior of mixtures of active particles. *Soft Matter*, 11(40):7920–7931, 2015.

[183] Robert Wulfert, Michael Oechsle, Thomas Speck, and Udo Seifert. Driven brownian particle as a paradigm for a nonequilibrium heat bath: Effective temperature and cyclic work extraction. *Phys. Rev. E*, 95(5):050103, 2017.

[184] Leticia F Cugliandolo, Jorge Kurchan, and Luca Peliti. Energy flow, partial equilibration, and effective temperatures in systems with slow dynamics. *Phys. Rev. E*, 55(4):3898, 1997.

[185] Ken Sekimoto. Microscopic heat from the energetics of stochastic phenomena. *Phys. Rev. E*, 76(6):060103, 2007.

[186] Claudio Maggi, Matteo Paoluzzi, Luca Angelani, and Roberto Di Leonardo. Memory-less response and violation of the fluctuation-dissipation theorem in colloids suspended in an active bath. *Sci. Rep.*, 7(1):17588, 2017.

[187] Claudio Maggi, Matteo Paoluzzi, Nicola Pellicciotta, Alessia Lepore, Luca Angelani, and Roberto Di Leonardo. Generalized energy equipartition in harmonic oscillators driven by active baths. *Phys. Rev. Lett.*, 113:238303, Dec 2014.

[188] Ruben Zakine, Alexandre Solon, Todd Gingrich, and Frédéric van Wijland. Stochastic stirling engine operating in contact with active baths. *Entropy*, 19(5):193, 2017.

[189] Jérémie Palacci, Cécile Cottin-Bizonne, Christophe Ybert, and Lydéric Bocquet. Sedimentation and effective temperature of active colloidal suspensions. *Phys. Rev. Lett.*, 105:088304, Aug 2010.

[190] Samuel Sánchez, Lluís Soler, and Jaideep Katuri. Chemically powered micro- and nanomotors. *Angewandte Chemie International Edition*, 54(5):1414–1444, 2015.

[191] Peter Hänggi and Fabio Marchesoni. Artificial brownian motors: Controlling transport on the nanoscale. *Reviews of Modern Physics*, 81(1):387, 2009.

[192] Geoffrey A Ozin, Ian Manners, Sébastien Fournier-Bidoz, and André Arsenault. Dream nanomachines. *Advanced Materials*, 17(24):3011–3018, 2005.

[193] James R. Baylis, Ju Hun Yeon, Max H. Thomson, Amir Kazerooni, Xu Wang, Alex E. St. John, Esther B. Lim, Diana Chien, Anna Lee, Jesse Q. Zhang, James M. Piret, Lindsay S. Machan, Thomas F. Burke, Nathan J. White, and Christian J. Kastrup. Self-propelled particles that transport cargo through flowing blood and halt hemorrhage. *Sci. Adv.*, 1(9), 2015.

[194] Massimiliano Esposito, Upendra Harbola, and Shaul Mukamel. Nonequilibrium fluctuations, fluctuation theorems, and counting statistics in quantum systems. *Reviews of modern physics*, 81(4):1665, 2009.

[195] O. Abah, J. Roßnagel, G. Jacob, S. Deffner, F. Schmidt-Kaler, K. Singer, and E. Lutz. Single-ion heat engine at maximum power. *Phys. Rev. Lett.*, 109:203006, Nov 2012.

[196] Johannes Roßnagel, Samuel T. Dawkins, Karl N. Tolazzi, Obinna Abah, Eric Lutz, Ferdinand Schmidt-Kaler, and Kilian Singer. A single-atom heat engine. *Science*, 352(6283):325–329, 2016.

[197] Jean-Philippe Brantut, Charles Grenier, Jakob Meineke, David Stadler, Sebastian Krinner, Corinna Kollath, Tilman Esslinger, and Antoine Georges. A thermoelectric heat engine with ultracold atoms. *Science*, 342(6159):713–715, 2013.

[198] Valentin Blickle and Clemens Bechinger. Realization of a micrometre-sized stochastic heat engine. *Nat Phys*, 8, 2011.

[199] I.A. Martinez, É. Roldán, L. Dinis, D. Petrov, J.M.R Parrondo, and Rica. R.A. Brownian carnot engine. *Nat Phys*, 12(2):67–70, 2015.

[200] Ignacio A. Martinez, Edgar Roldan, Luis Dinis, and Raul A. Rica. Colloidal heat engines: a review. *Soft Matter*, 13:22–36, 2017.

[201] Massimiliano Esposito, Ryoichi Kawai, Katja Lindenberg, and Christian Van den Broeck. Quantum-dot carnot engine at maximum power. *Phys. Rev. E*, 81:041106, Apr 2010.

[202] Gatien Verley, Massimiliano Esposito, Tim Willaert, and Christian Van den Broeck. The unlikely carnot efficiency. *Nature Communications*, 5, 2014.

[203] Konstantin E. Dorfman, Dmitri V. Voronine, Shaul Mukamel, and Marlan O. Scully. Photosynthetic reaction center as a quantum heat engine. *Proceedings of the National Academy of Sciences*, 110(8):2746–2751, 2013.

[204] Viktor Holubec and Artem Ryabov. Work and power fluctuations in a critical heat engine. *Phys. Rev. E*, 96:030102, Sep 2017.

[205] Michele Campisi and Rosario Fazio. The power of a critical heat engine. *Nat. comm.*, 7:11895, 2016.

[206] Petr Chvosta, Mario Einax, Viktor Holubec, Artem Ryabov, and Philipp Maass. Energetics and performance of a microscopic heat engine based on exact calculations of work and heat distributions. *J. Stat. Mech: Theory Exp.*, 2010(03):P03002, 2010.

[207] Ronnie Kosloff and Yair Rezek. The quantum harmonic otto cycle. *Entropy*, 19(4):136, 2017.

[208] Robert S. Whitney. Most efficient quantum thermoelectric at finite power output. *Phys. Rev. Lett.*, 112:130601, 2014.

[209] T. Schmiedl and U. Seifert. Efficiency at maximum power: An analytically solvable model for stochastic heat engines. *EPL*, 81(2):20003, 2008.

[210] Viktor Holubec. An exactly solvable model of a stochastic heat engine: optimization of power, power fluctuations and efficiency. *J. Stat. Mech: Theory Exp.*, 2014(5):P05022, 2014.

[211] Jordan M Horowitz and Juan MR Parrondo. Thermodynamics: a stirling effort. *Nat. Phys.*, 8(2):108, 2012.

[212] Sudeesh Krishnamurthy, Subho Ghosh, Dipankar Chatterji, Rajesh Ganapathy, and A. K. Sood. A micrometre-sized heat engine operating between bacterial reservoirs. *Nat Phys*, 12, 2016.

[213] D Martin, C Nardini, ME Cates, and É Fodor. Extracting maximum power from active colloidal heat engines. *arXiv preprint arXiv:1803.01620*, 2018.

[214] Xi Zhao, Krishna K. Dey, Selva Jeganathan, Peter J. Butler, Ubaldo M. Córdova-Figueroa, and Ayusman Sen. Enhanced diffusion of passive tracers in active enzyme solutions. *Nano Letters*, 17(8):4807–4812, 2017. PMID: 28726415.

[215] Viktor Holubec and Artem Ryabov. Maximum efficiency of low-dissipation heat engines at arbitrary power. *J. Stat. Mech. Theory Exp.*, 2016(7):073204, 2016.

[216] Viktor Holubec and Artem Ryabov. Diverging, but negligible power at carnot efficiency: Theory and experiment. *Phys. Rev. E*, 96:062107, Dec 2017.

[217] T. Hatano and S.-i. Sasa. Steady-state thermodynamics of langevin systems. *PRL*, 86, 2001.

[218] Todd R. Gingrich, Jordan M. Horowitz, Nikolay Perunov, and Jeremy L. England. Dissipation bounds all steady-state current fluctuations. *Phys. Rev. Lett.*, 116:120601, Mar 2016.

[219] Karel Proesmans and Christian Van den Broeck. Discrete-time thermodynamic uncertainty relation. *EPL*, 119(2):20001, 2017.

[220] Patrick Pietzonka and Udo Seifert. Universal trade-off between power, efficiency and constancy in steady-state heat engines. *arXiv preprint arXiv:1705.05817*, 2017.

[221] David Luposchainsky and Haye Hinrichsen. Entropy production in continuous phase space systems. *Journal of Statistical Physics*, 153(5):828–841, Dec 2013.

[222] Thomas Speck. Stochastic thermodynamics for active matter. *EPL (Europhysics Letters)*, 114(3):30006, 2016.

[223] Viktor Holubec and Artem Ryabov. Cycling tames power fluctuations near optimum efficiency. *Phys. Rev. Lett.*, 121:120601, Sep 2018.

[224] Debasish Chaudhuri. Entropy production by active particles: Coupling of odd and even functions of velocity. *Phys. Rev. E*, 94:032603, Sep 2016.

[225] Patrick Pietzonka and Udo Seifert. Entropy production of active particles and for particles in active baths. *J. of Phys. A: Mathematical and Theoretical*, 51(1):01LT01, 2017.

[226] Massimiliano Esposito. Stochastic thermodynamics under coarse graining. *Phys. Rev. E*, 85(4):041125, 2012.

[227] Takahiro Nemoto, Étienne Fodor, Michael E Cates, Robert L Jack, and Julien Tailleur. Optimizing active work: dynamical phase transitions, collective motion and jamming. *arXiv preprint arXiv:1805.02887*, 2018.

[228] Rémi Dreyfus, Jean Baudry, Marcus L Roper, Marc Fermigier, Howard A Stone, and Jérôme Bibette. Microscopic artificial swimmers. *Nature*, 437(7060):862–865, 2005.

[229] Peter Friedl and Darren Gilmour. Collective cell migration in morphogenesis, regeneration and cancer. *Nat. Rev. Mol. Cell Biol.*, 10(7):445–457, 2009.

[230] Michele Ballerini, Nicola Cabibbo, Raphael Candelier, Andrea Cavagna, Evaristo Cisbani, Irene Giardina, Vivien Lecomte, Alberto Orlandi, Giorgio Parisi, Andrea Procaccini, et al. Interaction ruling animal collective behavior depends on topological rather than metric distance: Evidence from a field study. *Proc. Natl. Acad. Sci.*, 105(4):1232–1237, 2008.

[231] Mariana Medina-Sánchez, Lukas Schwarz, Anne K Meyer, Franziska Hebenstreit, and Oliver G Schmidt. Cellular cargo delivery: toward assisted fertilization by sperm-carrying micromotors. *Nano Lett.*, 16(1):555–561, 2015.

[232] SA Mallory, C Valeriani, and A Cacciuto. Curvature-induced activation of a passive tracer in an active bath. *Phys. Rev. E*, 90(3):032309, 2014.

[233] CJ Olson Reichhardt and Charles Reichhardt. Ratchet effects in active matter systems. *Annu. Rev. Condens. Matter Phys.*, (0), 2016.

[234] Alexandre P Solon, Joakim Stenhammar, Raphael Wittkowski, Mehran Kardar, Yariv Kafri, Michael E Cates, and Julien Tailleur. Pressure and phase equilibria in interacting active brownian spheres. *Phys. Rev. Lett.*, 114(19):198301, 2015.

[235] Umberto Marini Bettolo Marconi and Claudio Maggi. Towards a statistical mechanical theory of active fluids. *Soft Matter*, 11(45):8768–8781, 2015.

[236] Wen Yan and John F Brady. The swim force as a body force. *Soft Matter*, 11(31):6235–6244, 2015.

[237] Frank Smallenburg and Hartmut Löwen. Swim pressure on walls with curves and corners. *Phys. Rev. E*, 92(3):032304, 2015.

[238] Nikolai Nikola, Alexandre P. Solon, Yariv Kafri, Mehran Kardar, Julien Tailleur, and Raphaël Voituriez. Active particles with soft and curved walls: Equation of state, ratchets, and instabilities. *Phys. Rev. Lett.*, 117:098001, Aug 2016.

[239] JH Irving and John G Kirkwood. The statistical mechanical theory of transport processes. iv. the equations of hydrodynamics. *J. Chem. Phys*, 18(6):817–829, 1950.

[240] John Toner and Yuhai Tu. Long-range order in a two-dimensional dynamical xy model: how birds fly together. *Phys. Rev. Lett.*, 75(23):4326, 1995.

[241] Yashodhan Hatwalne, Sriram Ramaswamy, Madan Rao, and R Aditi Simha. Rheology of active-particle suspensions. *Phys. Rev. Lett.*, 92(11):118101, 2004.

[242] Sriram Ramaswamy. The mechanics and statistics of active matter. *Annu. Rev. Condens. Matter Phys.*, 1(1):323–345, 2010.

[243] Eric Bertin, Michel Droz, and Guillaume Grégoire. Hydrodynamic equations for self-propelled particles: microscopic derivation and stability analysis. *J. Phys. A*, 42(44):445001, 2009.

[244] M. Cristina Marchetti, Yaouen Fily, Silke Henkes, Adam Patch, and David Yllanes. Minimal model of active colloids highlights the role of mechanical interactions in controlling the emergent behavior of active matter. *Curr. Opin. Colloid Interface Sci.*, 21:34 – 43, 2016.

[245] Antonio Celani, Stefano Bo, Ralf Eichhorn, and Erik Aurell. Anomalous thermodynamics at the microscale. *Phys. Rev. Lett.*, 109:260603, Dec 2012.

[246] Joseph M Brader, Th Voigtmann, Michael E Cates, and Matthias Fuchs. Dense colloidal suspensions under time-dependent shear. *Phys. Rev. Lett.*, 98(5):058301, 2007.

[247] Andreas M Menzel. Unidirectional laning and migrating cluster crystals in confined self-propelled particle systems. *J. Phys. Condens. Matter*, 25(50):505103, 2013.

[248] R K P Zia and B Schmittmann. Probability currents as principal characteristics in the statistical mechanics of non-equilibrium steady states. *J. Stat. Mech. Theor. Exp.*, 2007(07):P07012, 2007.

[249] Demian Levis, Joan Codina, and Ignacio Pagonabarraga. Active brownian equation of state: metastability and phase coexistence. *arXiv preprint arXiv:1703.02412*, 2017.

[250] Julian Bialké, Hartmut Löwen, and Thomas Speck. Microscopic theory for the phase separation of self-propelled repulsive disks. *EPL*, 103(3):30008, 2013.

[251] Vishwajeet Mehandia and Prabhu R Nott. The collective dynamics of self-propelled particles. *J. Fluid Mech.*, 595:239–264, 2008.

[252] Tamás Vicsek, András Czirók, Eshel Ben-Jacob, Inon Cohen, and Ofer Shochet. Novel type of phase transition in a system of self-driven particles. *Phys. Rev. Lett.*, 75(6):1226, 1995.

[253] Andreas Zöttl and Holger Stark. Hydrodynamics determines collective motion and phase behavior of active colloids in quasi-two-dimensional confinement. *Phys. Rev. Lett.*, 112(11):118101, 2014.

[254] Saverio E. Spagnolie and Eric Lauga. Hydrodynamics of self-propulsion near a boundary: predictions and accuracy of far-field approximations. *J. Fluid Mech.*, 700:105–147, 006 2012.

[255] Julian Bialké, Jonathan T Siebert, Hartmut Löwen, and Thomas Speck. Negative interfacial tension in phase-separated active brownian particles. *Phys. Rev. Lett.*, 115(9):098301, 2015.

[256] B. ten Hagen, S. van Teeffelen, and H. Löwen. Non-gaussian behaviour of a self-propelled particle on a substrate. *Cond. Matt. Phys.*, 12:725–738, 2009.

[257] Evgenii A Novikov. Functionals and the random-force method in turbulence theory. *Sov. Phys. JETP*, 20(5):1290–1294, 1965.

[258] P Hänggi. Correlation functions and masterequations of generalized (non-markovian) langevin equations. *Z. Phys. B*, 31:407, 1978.

[259] Kiyoshi Kanazawa, Takahiro Sagawa, and Hisao Hayakawa. Stochastic energetics for non-gaussian processes. *Phys. Rev. Lett*, 108(21):210601, 2012.

[260] Norman Bleistein and Richard A Handelsman. *Asymptotic expansions of integrals*. Courier Corporation, 1975.

[261] Gergo Nemes. Asymptotic expansions for integrals. Master's thesis, Loránd Eötvös University, 2012.

[262] Jaeoh Shin, Andrey G. Cherstvy, Won Kyu Kim, and Vasily Zaburdaev. Elasticity-based polymer sorting in active fluids: a brownian dynamics study. *Phys. Chem. Chem. Phys.*, 19:18338–18347, 2017.

[263] James A. McLennan. Statistical mechanics of the steady state. *Phys. Rev.*, 115:1405–1409, Sep 1959.

[264] T. S. Komatsu and N. Nakagawa. Expression for the stationary distribution in nonequilibrium steady states. *Phys. Rev. Lett.*, 100:030601, 2008.

[265] Christian Maes and Karel Netočný. Rigorous meaning of mclennan ensembles. *Journal of Mathematical Physics*, 51(1):015219, 2010.

[266] David A. Sivak and Gavin E. Crooks. Near-equilibrium measurements of nonequilibrium free energy. *Phys. Rev. Lett.*, 108:150601, Apr 2012.

[267] Naoko Nakagawa and Shin-ichi Sasa. Work relations for time-dependent states. *Phys. Rev. E*, 87:022109, Feb 2013.

Acknowledgements

Many people have supported me, either directly or indirectly, and helped me during PhD, for which I want to use the opportunity to express my sincerest gratitude. Firstly, I would like to thank my advisor, Prof. Dr. Klaus Kroy which introduced me into a stimulating research topic and at the same time gave me the freedom to pursue my own interest. He was always a source of promising solutions if I needed assistance and his keen insight into the physics at hand helped me to spot the weak points in my arguments. Secondly, I would like to thank Prof. Dr. Felix Otto, director of the Max Planck Institute for the Mathematics in the Science in Leipzig and the IMPRS (international Max Planck research schools) for granting me not only a three years and an half scholarship, but also the opportunity and the honour to be a member of the Max Planck society. A special thanks goes to my collaborators Dr. Gianmaria Falasco and Dr. Viktor Holubec, which have helped me so many times, correcting my mistakes and addressing me in the right direction. To follow, the other members of my research group at the Institute for Theoretical Physics of Leipzig through the years, Sven, Anne, Marc and Constantin and Jacob for their pleasant company and their help. A special thanks goes to my dear friends in the Max Planck Institute. We have shared a lot of great, mostly non-scientific, moments that have made my life in Leipzig never boring: Renan Assimos Martin, Gianluca Lauteri, Arianna Giunti, Ramon Urquijo Novella, Kostantinos Zemas, Souhayl Sadik, Kostantinos Dareiotis, Caio Teodoro, Marcello Carioni, Niccolò Pederzani, Paolo Perrone (Vasileios Barlakas and Gabriele Benedetti should be part of this list even though they were never affiliated to the Max Planck Institute) and Giovanni Andrea Frigeri. Among them an even more special thanks goes to Giovanni, mate of conferences and of every working day, of countless pleasant and refreshing "water" breaks, holidays and unforgettable evenings, and trusted friend. As promised (to him), I would like to thank Davide Colì for his decisive help to improve my numerical skills with just few commands. Without his advises, probably my simulations would still be running. And I thank my parents for their everlasting and unconditioned support. Last but not least, I express my gratitude to Irene Resmi. It is not easy to endure and support at the same time a PhD student and his/her continuous complaints about everything that does not work (and so everything), but she did with an unshakable constancy and the sweetest empathy.

Curriculum vitae

Personal information

Name:	Stefano Steffenoni
Date and place of birth:	October 9th 1990 in Venice, Italy
Nationality:	Italian

Education

07.2018- PhD candidate at the University of Leipzig, Germany.

01.2015-06.2018 PhD candidate at Max Planck Institute for Mathematics in the Science of Leipzig, Germany.

03.-09.2014 Erasmus Program at the Katholieke Universiteit Leuven, Belgium.

09.2009-09.2014 Bachelor and Master of Science in Physics at the University of Padova, Italy.

09.2004-06.2009 Diploma of Humanistic High School at Liceo Classico Marco Polo.

Original publications

1 C. Maes, and S. S. "Friction and noise for a probe in a nonequilibrium fluid". PRE 91 (2015)

2 S.S, K. Kroy, and G. Falasco. "Interacting Brownian dynamics in a nonequilibrium particle bath". PRE 94 (2016)

3 S.S, G. Falasco, and K. Kroy. "Microscopic derivation of the hydrodynamics of active-Brownian-particle suspensions". PRE 95 (2017)

4 Viktor Holubec, Klaus Kroy and "S.S. Efficient numerical solver for time-dependent Fokker-Planck equations". arXiv:1804.01285

5 S.S., Viktor Holubec, G. Falasco and Klaus Kroy. "Active Brownian heat engine: Dynamics and average thermodynamics". In preparation

6 S.S. G. Falasco and Klaus Kroy. "Colloid in an active particle bath". In preparation